EFFECTS OF EXERCISE AND OBESITY ON SKELETAL MUSCLE DAMAGE AND REPAIR

by

Brian Sullivan

A Dissertation

Submitted to the Faculty of Purdue University

In Partial Fulfillment of the Requirements for the degree of

Doctor of Philosophy

Department of Health and Kinesiology

West Lafayette, Indiana

August 2021

THE PURDUE UNIVERSITY GRADUATE SCHOOL

STATEMENT OF COMMITTEE APPROVAL

Dr. Timothy P. Gavin, Chair

Department of Health and Kinesiology

Dr. Monica J. Hubal

Department of Health and Kinesiology

Dr. Bruno T. Roseguini

Department of Health and Kinesiology

Dr. Shihuan Kuang

Department of Animal Science

Approved by:

Dr. David B. Klenosky

ACKNOWLEDGMENTS

I would like to thank my advisor Dr. Tim Gavin for his excellent mentorship. This document would not have been completed without his limitless support, guidance and encouragement.

I would also like to thank my committee members, Dr. Bruno Roseguini, Dr. Shihuan Kuang and Dr. Monica Hubal for their support, guidance and critical insight.

I would like to acknowledge my colleagues, Chris Kargl, Lundon Burton, Michael Belbis, Michael Holmes, Jacob Monroe, Dr. Kyoungrae Kim, Dr. Ron Garner, Dr. Shivam Patel, Dr. Yaohui Nie and Dr. Feng Yue for their friendship and willingness to collaborate, instruct and aid one another and myself.

I would like to acknowledge Ann Hazelgrove, Michelle Scott and Christy Daugherty for their academic guidance and scheduling assistance.

Finally, I would like to thank my family for their unconditional love and unwavering support throughout this PhD journey. Most importantly I would like to thank Ellie for always believing in me even when I didn’t, without you none of this would be possible.

TABLE OF CONTENTS

LIST OF TABLES

LIST OF FIGURES

ABSTRACT

Obesity is associated with an increase in low grade systemic inflammation. Skeletal muscle of individuals with obesity undergo numerous biochemical and morphological alterations including an increase in ectopic lipid accumulation in skeletal muscle and increased macrophage infiltration. Increased intermuscular adipose tissue and macrophages contribute to skeletal muscle inflammation and insulin resistance by secreting elevated proinflammatory cytokines and lipids. This also contributes to reduction in skeletal muscle quality, increasing the susceptibility of muscle to damage and impairing the regenerative response to muscle. Exercise training can reduce inflammation and improve skeletal muscle quality. Importantly reductions in inflammation occur without change in adiposity. Peroxisome proliferator activated receptor γ coactivator 1-α (PGC-1α) exerts protective effects on skeletal muscle against damaging insults and may improve muscle regeneration.

The primary aim of my dissertation was to determine the mechanisms that lead to deficits in skeletal muscle integrity and regeneration in persons with obesity. In Chapter 1, an introduction to the various physiological, pathological, and clinical topics is provided. In Chapter 2, we investigated how exercise training and obesity independently alter skeletal muscle extracellular vesicle (EV) miRNA (miR) content. We found that obesity alters EV miR content indicative of altered anabolic signaling, while exercise training altered EV miR content in a manner indicative of reduced inflammation. In Chapter 3, we report that overexpression of PGC-1α reduces cardiotoxin induced damage of primary human myotubes but limits the ability of undifferentiated cells to reenter the cell cycle and produce progeny that could aid in the restoration of myotubes. In Chapter 4, we demonstrate that exposure to an obesogenic environment increases cardiotoxin induced damage of primary human myotubes from obese donors. In this study we also found that the restoration of myotube fusion index was reduced in lean and obese subjects when incubated with obesogenic media. In Chapter 5 is a review and summary of the outcomes described in Chapters 2-4, a discussion of the limitations of these experiments, and a discussion of future directions.

CHAPTER 1. REVIEW OF THE LITERATURE

Obesity

Obesity (BMI ≥ 30 kg/m^2), poses a significant public health concern. In 2008, the cost of obesity was estimated to be $147 billion (1) and despite concerted efforts to combat obesity, rates are continuing to rise; as of 2018, 42.4% of the U.S. adult population was considered obese, up from 30.5% in 2000 (2). Obesity is associated with numerous chronic diseases such as insulin resistance, Type 2 Diabetes mellitus, metabolic syndrome, cardiovascular disease and numerous cancers. Skeletal muscle comprises approximately 40% of body mass, is the largest secretory organ in lean humans (3) and accounts for approximately 80% of insulin stimulated glucose disposal under normal conditions (4).

Obesity has been associated with numerous biochemical and morphological changes in skeletal muscle. Skeletal muscle of individuals with obesity is associated with an increase in macrophage infiltration and ectopic lipid accumulation (5, 6). Young humans with obesity have increased skeletal muscle fiber cross sectional area (FCSA) (7), which is more pronounced in type II, glycolytic fibers, suggesting that obesity causes a hypertrophic response within type II fibers (7). Despite larger muscle FCSA, muscle quality is reduced in obese individuals, characterized by reduced whole muscle and fascicle strength, an increased likelihood of functional limitations (8, 9) and reduced skeletal muscle fiber membrane integrity, increasing the susceptibility and extent of muscle damage (10). The regenerative capacity of obese skeletal muscle is impaired as well (11, 12), which can be attributed to reduced satellite cell (SC) proliferation and altered cell signaling pathways governing the regenerative response (13-17).

Inflammation

Obesity is characterized by a heightened and sustained inflammatory response, altering cell signaling and morphology and contributing to the development of chronic disease (3, 18, 19). The obese inflammatory phenotype is associated with an increase in circulating inflammatory cytokines such as interleukin-6 (IL-6), tumor necrosis factor α (TNF-α) and C-reactive protein (CRP) and an increase in skeletal muscle and adipose tissue macrophage number and activity (20, 21). Adipose tissue oxygen levels are reduced, due to reduced angiogenic stimuli, increased vasoconstriction, or decreased total blood flow in obesity (22). It is unclear if the hypoxic state of adipose tissue directly contributes to chronic inflammation in obesity,

however hypoxia may be responsible for the increased macrophage infiltration in adipose tissue (23). The increase in inflammatory cells in adipose tissue is directly correlated with the hypertrophy of adipocytes, contributing to increased secretion of circulating cytokines (21).

Similar to adipose tissue, macrophage infiltration into skeletal muscle of subjects with obesity is greater (24-26). Increased macrophage infiltration is related to the rise in ectopic intramuscular lipid accumulation in skeletal muscle of persons with obesity as macrophages tend to cluster around these lipid droplets (25). Obesity also alters the skeletal muscle secretome in a manner consistent with increased inflammatory signaling. The expression of IL-6 is reduced and TNF-α is increased in the skeletal muscle of humans with obesity (27). In contrast to most cytokines secreted from adipocytes and inflammatory cells, cytokines produced by skeletal muscle, termed myokines, are regulated via exercise, exert predominantly anti-inflammatory effects and can improve glucose disposal and lipid metabolism (3). Skeletal muscle is unique from other tissues in that it can produce IL-6 in a TNF independent manner, indicating that muscle produced IL-6 contributes to metabolic improvements (28). Skeletal muscle derived IL-6 exerts beneficial effects on whole body metabolism via the activation of AMP protein kinase (AMPK) (29). IL-6 also exerts inhibitory effects on TNF-α and IL-1 production (30).

Peroxisome proliferator-activated receptor γ coactivator 1α (PGC-1α) is a transcriptional coactivator that regulates the expression of genes involved in energy metabolism and is considered to be the master regulator of mitochondrial biogenesis (31). Increasing PGC-1α increases mitochondrial density, metabolic enzymes integral for β-oxidation and lipolysis, and promotes an oxidative, slow twitch muscular phenotype (32, 33). The expression of PGC-1α is reduced in obese subjects, which is associated with an increase in the proportion of type II fibers, impairments in substrate metabolism, and contributes to the chronic inflammatory response that accompanies obesity (34). PGC-1α promotes an anti-inflammatory environment in skeletal muscle and may play a key role in regulating the polarization of M2 macrophages (35, 36). As a result of these factors, PGC-1α is a promising therapeutic target to prevent the progression of chronic disease associated with obesity.

Skeletal Muscle Regeneration

Skeletal muscle is a post-mitotic tissue with high stability and minimal nuclei turnover. Minor skeletal muscle damage occurs as a result of normal daily activities resulting in a very

slow turnover of nuclei in affected muscle fibers; it is estimated that only 1-2% of myonuclei are replaced every week (37). However, mammalian skeletal muscle is capable of an extensive and rapid regeneration process that occurs in response to muscle damage (38). SCs are a major group of resident stem cells located between the basal lamina and sarcolemma (39, 40). SCs are usually mitotically quiescent with few mitochondria and a large nuclear to cytoplasmic ratio (41). Quiescent SCs are typically characterized by their expression of paired box 7 (Pax7) but not myoblast determination protein 1 (MyoD) or Myogenin (42). SCs are the source of nuclei in skeletal muscle and are vital for the regeneration of adult skeletal muscle (43, 44).

Muscle injury that leads to fiber necrosis will result in a myogenic/regeneration response consisting of SC activation, proliferation, differentiation, fusion and ultimately the regrowth of muscle fibers to their original size within three weeks (38, 45). Fiber necrosis is caused by disruptions in the myofiber sarcolemma which results in an increase in the permeability of the myofiber membrane. Disruptions in the myofiber membrane are often reflected by an increase in serum levels of muscle proteins such as creatine kinase, however, this is not always indicative of true myofiber damage (46, 47).

The acute inflammatory response is a crucial aspect of the early response to muscle damage. Firstly, neutrophils invade the injury site, promoting inflammation by releasing cytokines that may attract additional inflammatory cells (38, 48, 49). Pro-inflammatory M1 macrophages then infiltrate the damaged fibers and clear debris through phagocytosis, while augmenting the inflammatory response by secreting inflammatory cytokines such as TNF-α (50). Following resolution of the initial pro-inflammatory response to muscle damage, M1 macrophages will polarize to anti-inflammatory M2 macrophages. M2 macrophages play a critical role later in muscle regeneration, secreting anti-inflammatory cytokines and other molecules that stimulate SC differentiation and extracellular matrix (ECM) remodeling (51). Effective transition from pro-inflammatory M1 macrophages to anti-inflammatory M2 macrophages is vital for proper muscle regeneration (51). Prolonged expression of pro-inflammatory macrophages can exacerbate muscle damage and delay functional recovery (51, 52).

Following damage to the sarcolemma and the SC niche, the influx of calcium and growth factors from the ECM, lead to the mobilization and activation of SCs (40, 53, 54). SCs are capable of extreme motility; localized damage at one end of the muscle fiber stimulates SC

migration to the regeneration site from all along the fiber (55). Activated SCs or myoblasts, are characterized by rapid expression of the myogenic transcription factors, MyoD and myogenic factor 5 (Myf5) (56, 57). SCs are able to upregulate MyoD and Myf5 independently of one another, suggesting that these two transcription factors have different functions in adult myogenesis (41). MyoD is important for the differentiation of SCs. MyoD deficient mice exhibit reduced muscle mass and an impaired muscle regeneration response (58). Interestingly, Myf5 deficient mice display a hypertrophied phenotype and reduced myoblast proliferation (59, 60). Therefore, it appears that a predominance of Myf5 expression directs the SC towards enhanced proliferation and delayed differentiation, and a predominance of MyoD drives the myoblast toward early differentiation. This is exemplified by the differential expression of MyoD and Myf5 during different stages in the cell cycle; MyoD expression peaks in G_1 while Myf5 expression peaks at the G_0 and G_2 phases (61). Increased expression of MyoD does not always lead to differentiation of myoblasts. Pax7 decreases the transcriptional ability of MyoD, making the ratio of Pax7 to MyoD vital for the determination of SC fate (62). This regulation of SC fate by MyoD and Myf5 captures one of the unique features of SCs, the ability to self-renew through symmetric and asymmetric cell division. Asymmetric cell division gives rise to two different daughter cells, one stem cell and one cell destined for differentiation; symmetric cell division gives rise to two daughter stem cells (41, 63).

SCs that enter the myogenic differentiation program, either fuse to the damaged muscle fibers or to one another, forming new myofibers. The myogenic differentiation program is an irreversible process that is driven by the sequential expression of key transcription factors, including Myogenin and myogenic factor 6 (MRF4), that upregulate muscle-specific structural and contractile genes, such as myosin, actin and troponin (42, 64, 65). The expression of these muscle-specific genes is vital for the proper formation and function of regenerating skeletal muscle. Upon exiting the cell cycle, SC fusion occurs in two stages. First, differentiated SCs fuse to one another or the damaged fiber, second, additional myoblasts are incorporated into the nascent myofiber, resulting in a mature myofiber with many nuclei, and contractile proteins (41).

Regulation of Skeletal Muscle Regeneration

The janus kinase (JAK)/ signal transducer and activator of transcription (STAT) pathway plays a critical role in muscle regeneration regulating the expression of myogenic factors via

cytokine receptor activation. In SCs, increases in IL-6 result in an increase in MyoD and STAT3, leading to early differentiation and reduced proliferation of SCs (66). Chronic elevations of IL-6 and STAT3 are associated with muscle wasting which may be due to exhaustion of the SC pool (66, 67). Further, the inhibition of the JAK/STAT pathway results in increased SC function and muscle regeneration following cardiotoxin injury (68). However, local and transient production of IL-6 appears to be necessary during muscle regeneration. In IL-6 knockout mice, muscle hypertrophy of the plantaris is blunted following surgical section of the distal tendon of the lateral and medial gastrocnemius. This blunted hypertrophic response appears to occur due to reductions in STAT3 activation and was further confirmed in SCs *in vitro* (69). Therefore, it appears that of effects IL-6 exerts during muscle regeneration are due to the tissue of origin and transience of expression.

The Wingless/ Integrated (Wnt) signaling pathway has diverse effects on the proliferation and differentiation of SCs during skeletal muscle regeneration (70, 71). Wnt signaling promotes myogenic commitment and terminal differentiation in adult myogenesis. Treatment of regenerating muscle and cultured myoblasts with Wnt3a, increases desmin expression and the size of newly formed tubes *in vivo* and *in vitro* (72). The opposite effect is observed when secreted frizzled-related protein 3 (sFRP3), an inhibitor of Wnt signaling, is administered (72). β-catenin directly interacts with MyoD to enhance the transcriptional binding capacity of MyoD, making β-catenin necessary for MyoD function (73). The Wnt ligands have also been proposed to induce SC proliferation. The activation of Wnt ligands promotes SC proliferation during muscle regeneration, whereas inhibitory Wnt ligands reduce proliferation by sequestering β-catenin in the cytoplasm (71). Axis inhibition protein 2 (Axin2) is essential for the differentiation of myoblasts to occur, due to its role in sequestering β-catenin in the cytoplasm (70). Therefore, Wnt signaling is a key component of skeletal muscle regeneration, due to its effects on the proliferation and differentiation ability of SCs.

Obesity and Skeletal Muscle Regeneration

Mounting evidence from models of obesity and type II diabetes indicate that muscle regeneration and muscle fiber integrity are diminished in these conditions (10-12, 15, 74). Critically, these models suggests that SC function is compromised in obesity (52). In obese Zucker rats, SC proliferation is reduced, and so is the size of the plantaris and soleus muscles.

However, SC proliferation appears to be restored with loading, leading to hypertrophy of the muscle fibers in obese Zucker rats. Despite the hypertrophic response, the muscle weights of obese rats are still lower than lean rats following loading (75). Following mechanical load induced muscle damage, obese rodents display greater membrane disruptions than lean rodents (10). The disruptions in fiber integrity in obese skeletal muscle may be due to increased intramuscular lipids, inflammatory cells and fibrosis among other factors (5, 6, 76).

Obesity dysregulates the acute inflammatory response following muscle damage, which may exacerbate muscle damage and blunt the regeneration process. Obese mice present with reduced skeletal muscle IL-6 and MyoD mRNA compared to lean mice (15). Three days following cardiotoxin injury, lean mice exhibit 14-fold, 4-fold and 5-fold increases in TNF-a mRNA, p-STAT3, and phosphorylated protein kinase B (AKT) respectively. However, there are no observed differences in the obese injured mice (15). These results suggest that the acute inflammatory response to muscle damage is diminished in obese animals despite chronic inflammation.

Wnt signaling is proposed to play a critical role in the regulation of skeletal muscle of insulin-resistant individuals (13, 14). There is evidence that Wnt signaling is dysregulated during obesity, which may cause impairments in muscle regeneration. In obesity prone rodents, the Wnt ligands and downstream target genes, c-myelocytomatosis (c-Myc), Insulin receptor substrate 1 (IRS-1), Myf5 and MyoD are reduced compared to obesity resistant rodents when both are fed a high fat diet. Nuclear β-Catenin, IRS-1 and phosphorylated AKT are all decreased in obesity prone rodents as well (14). Whether a decrease in Wnt signaling is associated with reduced skeletal muscle regenerative capacity in obese humans remains unclear.

Mitochondrial biogenesis is a crucial regulatory event during muscle regeneration (77), that is accompanied by an increase in PGC-1 signaling and oxidative capacity (78). Blocking PGC-1α expression results in incomplete regeneration, characterized by smaller muscle FCSA and an increase in fibrotic tissue formation (79). Lower PGC-1α in obese humans may contribute to impairments in the myogenic response via blunted mitochondrial biogenesis.

Extracellular Vesicles and Intercellular Communication

Skeletal muscle is the largest secretory organ in lean humans. Myokines secreted from skeletal muscle exert potent autocrine, paracrine and endocrine effects. Recently, the method

through which skeletal muscle can communicate with distal tissues has been expanded to include extracellular vesicles (EVs). EVs are membrane bound particles that are secreted by cells and are currently divided into 3 subtypes: exosomes, microvesicles and apoptotic bodies (80). Currently, the lack of consensus regarding distinct markers for EV subtypes and the associated difficulty validating the efficacy of EV isolation methods to yield pure subpopulations, necessitates the use of the term 'EVs' for all isolated extracellular vesicles (81). Following secretion, EVs enter the extracellular fluid and can be up took by neighboring cells or enter the circulation and be endocytosed by a distant cell (82-84). EVs have a bilayer lipid membrane and contain a variety of molecules including microRNA, mRNA and proteins (83, 84). EV contents can be reflective of their original cell source but often are enriched in certain protein, lipids and RNAs, which suggests that EVs are assembled to transport unique molecules for a specific purpose (82).

MicroRNAs (miR) are a family of evolutionarily conserved, short (20-22 nucleotide), single-stranded, non-coding RNAs that post transcriptionally regulate gene expression (85). miRs are transcribed by RNA Polymerase II, forming a primary miR transcript (pri-miR) (86, 87). The RNase III ribonuclease, Drosha, is a regulator of miR formation and executes the initiation step in miR processing, resulting in the formation of a precursor miR (pre-miR) (88). The nucleocytoplasmic shuttler protein, exportin-5, transports the pre-miR into the cytoplasm (89). In the cytoplasm, the endonuclease, Dicer cleaves the pre-miR to produce a 20-22 nucleotide double stranded RNA molecule where one strand is incorporated into the RNA-induced silencing complex and the other is marked for degradation (90). The mature miR binds through imperfect base pairing to its target mRNA, resulting in the inhibition of translation or the degradation of the targeted mRNA (85, 87, 91). miRs bind to their target mRNA through imperfect base pairing granting miRs the unique ability to target numerous mRNAs (92).

miRs are expressed in a tissue specific manner; consequently, miR that are expressed in only skeletal muscle are referred to as myomiR. The myomiR family (miR-1, -133a, -206, -208a, -486, and -499) is heavily implicated in the maintenance, repair and homeostasis of skeletal muscle (87, 93). Increased expression of miR-1, -206 and -486 reduces the proliferative potential of myoblasts, but enhances myogenic differentiation *in vitro* (94, 95), whereas increased expression of miR-133a promotes the opposite effect (96). The myomiRs appear to be vital for the proper functioning of skeletal muscle; miR-133a knockout in mice leads to impaired exercise tolerance, mitochondrial biogenesis and muscle fiber maintenance (97).

Exercise Training

Reducing chronic inflammation is the most important factor for the prevention of insulin resistance and diabetes in obese subjects. Lifestyle interventions that combine exercise and dietary changes are the most effective at reversing obesity and reducing chronic inflammation. Exercise training alone has been demonstrated to reduce both local and systemic inflammation in patients with type II diabetes. However, it appears that the greatest reductions in chronic inflammation occur as a result of concurrent (aerobic and resistance) exercise training (98-100). Importantly, exercise training mediated reductions in inflammation occur independent of weight loss or changes in adiposity (101).

Exercise training also exerts a protective effect on skeletal muscle against future damaging insults, known as exercise preconditioning (102). The exercise preconditioning effect can be attributed in part to the exercise dependent increase in PGC-1α, increasing mitochondrial density and associated mitochondrial antioxidant capacity (31). Increased PGC-1α that accompanies exercise training may also exert beneficial effects on muscle regeneration in obese subjects. Overexpressing PGC-1α in mice accelerates the resolution of necrosis and the early inflammatory response by increasing the polarization of pro inflammatory, M1 macrophages to anti-inflammatory, M2 macrophages (103). Exercise training also increases the number and function of SCs, accelerating SC response to injury and enhancing muscle regeneration (104). PGC-1α appears to mediate some of the beneficial effects of exercise training on SC function. Overexpression of PGC-1α remodels the SC niche, improving the proliferative potential of SCs (105), and the knockdown of PGC-1α in myoblasts completely inhibits myotube formation (106). Together this indicates the vital role that PGC-1α has on regulating muscle damage and regeneration.

Within the field of EV biology it is hypothesized that skeletal muscle EVs modulate the beneficial systemic effects of physical exercise. At the onset of exercise, there is a rapid release of EVs into the circulation that slowly returns to resting levels within 90 to 180 minutes following exercise termination (107); suggesting that EVs released as a result of physical exercise can be up took by various target cells. EVs are released from skeletal muscle during and following exercise and are likely contributors to the post exercise increase in circulating EVs (82, 108, 109). Previously we have demonstrated that skeletal muscle EVs are capable of

exerting potent paracrine effects on cells within the skeletal muscle compartment (110); however, the endocrine effects of skeletal muscle EVs are not certain. The impact that exercise and disease have on skeletal muscle EV contents is unclear and little work has been performed that examines these differences.

References

1. Finkelstein EA, Trogdon JG, Cohen JW, Dietz W. Annual medical spending attributable to obesity: payer-and service-specific estimates. *Health Aff (Millwood)*. 2009;28(5):w822-31.
2. Hales CMC, M.D.; Fryar, C.D.; Ogden, C.L. Prevalence of obesity among adults and youth: United States 2017-2018. *NCHS Data Brief*. 2020;no. 360.
3. Pedersen BK, Febbraio MA. Muscles, exercise and obesity: skeletal muscle as a secretory organ. *Nat Rev Endocrinol*. 2012;8(8):457-65.
4. DeFronzo RA, Tripathy D. Skeletal muscle insulin resistance is the primary defect in type 2 diabetes. *Diabetes Care*. 2009;32 Suppl 2:S157-63.
5. Collins KH, Hart DA, Reimer RA et al. High-fat high-sucrose diet leads to dynamic structural and inflammatory alterations in the rat vastus lateralis muscle. *J Orthop Res*. 2016;34(12):2069-78.
6. Collins KH, Paul HA, Hart DA et al. A High-Fat High-Sucrose Diet Rapidly Alters Muscle Integrity, Inflammation and Gut Microbiota in Male Rats. *Sci Rep*. 2016;6:37278.
7. Gavin TP, Stallings HW, 3rd, Zwetsloot KA et al. Lower capillary density but no difference in VEGF expression in obese vs. lean young skeletal muscle in humans. *J Appl Physiol (1985)*. 2005;98(1):315-21.
8. Tomlinson DJ, Erskine RM, Morse CI, Winwood K, Onambele-Pearson G. The impact of obesity on skeletal muscle strength and structure through adolescence to old age. *Biogerontology*. 2016;17(3):467-83.
9. Tomlinson DJ, Erskine RM, Winwood K, Morse CI, Onambele GL. Obesity decreases both whole muscle and fascicle strength in young females but only exacerbates the aging-related whole muscle level asthenia. *Physiol Rep*. 2014;2(6).
10. Knoblauch MA, O'Connor DP, Clarke MS. Obese mice incur greater myofiber membrane disruption in response to mechanical load compared with lean mice. *Obesity (Silver Spring)*. 2013;21(1):135-43.
11. D'Souza DM, Trajcevski KE, Al-Sajee D et al. Diet-induced obesity impairs muscle satellite cell activation and muscle repair through alterations in hepatocyte growth factor signaling. *Physiol Rep*. 2015;3(8).

12. Fu X, Zhu M, Zhang S, Foretz M, Viollet B, Du M. Obesity Impairs Skeletal Muscle Regeneration Through Inhibition of AMPK. *Diabetes*. 2016;65(1):188-200.
13. Laudes M. Role of WNT signalling in the determination of human mesenchymal stem cells into preadipocytes. *J Mol Endocrinol*. 2011;46(2):R65-72.
14. Zhou D, Strakovsky RS, Zhang X, Pan YX. The skeletal muscle Wnt pathway may modulate insulin resistance and muscle development in a diet-induced obese rat model. *Obesity (Silver Spring)*. 2012;20(8):1577-84.
15. Brown LA, Lee DE, Patton JF et al. Diet-induced obesity alters anabolic signalling in mice at the onset of skeletal muscle regeneration. *Acta Physiol (Oxf)*. 2015;215(1):46-57.
16. Paturi S, Gutta AK, Kakarla SK et al. Impaired overload-induced hypertrophy in obese Zucker rat slow-twitch skeletal muscle. *J Appl Physiol (1985)*. 2010;108(1):7-13.
17. Sullivan BP, Weiss JA, Nie Y et al. Skeletal muscle IGF-1 is lower at rest and after resistance exercise in humans with obesity. *European Journal of Applied Physiology*. 2020.
18. Haddad F, Zaldivar F, Cooper DM, Adams GR. IL-6-induced skeletal muscle atrophy. *J Appl Physiol (1985)*. 2005;98(3):911-7.
19. Lackey DE, Olefsky JM. Regulation of metabolism by the innate immune system. *Nat Rev Endocrinol*. 2016;12(1):15-28.
20. Kawasaki N, Asada R, Saito A, Kanemoto S, Imaizumi K. Obesity-induced endoplasmic reticulum stress causes chronic inflammation in adipose tissue. *Sci Rep*. 2012;2:799.
21. Weisberg LA. "Stroke and struck": protecting the brain from cerebrovascular disease. *South Med J*. 2003;96(4):331.
22. Ye J. Emerging role of adipose tissue hypoxia in obesity and insulin resistance. *Int J Obes (Lond)*. 2009;33(1):54-66.
23. Rausch ME, Weisberg S, Vardhana P, Tortoriello DV. Obesity in C57BL/6J mice is characterized by adipose tissue hypoxia and cytotoxic T-cell infiltration. *International Journal Of Obesity*. 2007;32:451.
24. Patsouris D, Cao JJ, Vial G et al. Insulin resistance is associated with MCP1-mediated macrophage accumulation in skeletal muscle in mice and humans. *PLoS One*. 2014;9(10):e110653.

25. Khan IM, Perrard XY, Brunner G et al. Intermuscular and perimuscular fat expansion in obesity correlates with skeletal muscle T cell and macrophage infiltration and insulin resistance. *Int J Obes (Lond)*. 2015;39(11):1607-18.
26. Fink LN, Oberbach A, Costford SR et al. Expression of anti-inflammatory macrophage genes within skeletal muscle correlates with insulin sensitivity in human obesity and type 2 diabetes. *Diabetologia*. 2013;56(7):1623-8.
27. Wu H, Ballantyne CM. Skeletal muscle inflammation and insulin resistance in obesity. *J Clin Invest*. 2017;127(1):43-54.
28. Keller C, Hellsten Y, Steensberg A, Pedersen BK. Differential regulation of IL-6 and TNF-alpha via calcineurin in human skeletal muscle cells. *Cytokine*. 2006;36(3-4):141-7.
29. Carey AL, Steinberg GR, Macaulay SL et al. Interleukin-6 increases insulin-stimulated glucose disposal in humans and glucose uptake and fatty acid oxidation in vitro via AMP-activated protein kinase. *Diabetes*. 2006;55(10):2688-97.
30. Petersen AM, Pedersen BK. The anti-inflammatory effect of exercise. *J Appl Physiol (1985)*. 2005;98(4):1154-62.
31. Lira VA, Benton CR, Yan Z, Bonen A. PGC-1alpha regulation by exercise training and its influences on muscle function and insulin sensitivity. *Am J Physiol Endocrinol Metab*. 2010;299(2):E145-61.
32. Lin J, Wu H, Tarr PT et al. Transcriptional co-activator PGC-1 alpha drives the formation of slow-twitch muscle fibres. *Nature*. 2002;418(6899):797-801.
33. Huang TY, Zheng D, Houmard JA, Brault JJ, Hickner RC, Cortright RN. Overexpression of PGC-1alpha increases peroxisomal activity and mitochondrial fatty acid oxidation in human primary myotubes. *Am J Physiol Endocrinol Metab*. 2017;312(4):E253-E63.
34. Tanner CJ, Barakat HA, Dohm GL et al. Muscle fiber type is associated with obesity and weight loss. *Am J Physiol Endocrinol Metab*. 2002;282(6):E1191-6.
35. Eisele PS, Furrer R, Beer M, Handschin C. The PGC-1 coactivators promote an anti-inflammatory environment in skeletal muscle in vivo. *Biochem Biophys Res Commun*. 2015;464(3):692-7.
36. Yakeu G, Butcher L, Isa S et al. Low-intensity exercise enhances expression of markers of alternative activation in circulating leukocytes: roles of PPARgamma and Th2 cytokines. *Atherosclerosis*. 2010;212(2):668-73.

37. Schmalbruch H, Lewis DM. Dynamics of nuclei of muscle fibers and connective tissue cells in normal and denervated rat muscles. *Muscle Nerve*. 2000;23(4):617-26.
38. Charge SB, Rudnicki MA. Cellular and molecular regulation of muscle regeneration. *Physiol Rev*. 2004;84(1):209-38.
39. Mauro A. Satellite cell of skeletal muscle fibers. *J Biophys Biochem Cytol*. 1961;9:493-5.
40. Fu X, Wang H, Hu P. Stem cell activation in skeletal muscle regeneration. *Cell Mol Life Sci*. 2015;72(9):1663-77.
41. Yin H, Price F, Rudnicki MA. Satellite cells and the muscle stem cell niche. *Physiol Rev*. 2013;93(1):23-67.
42. Cornelison DD, Wold BJ. Single-cell analysis of regulatory gene expression in quiescent and activated mouse skeletal muscle satellite cells. *Dev Biol*. 1997;191(2):270-83.
43. Moss FP, Leblond CP. Satellite cells as the source of nuclei in muscles of growing rats. *Anat Rec*. 1971;170(4):421-35.
44. Lepper C, Partridge TA, Fan CM. An absolute requirement for Pax7-positive satellite cells in acute injury-induced skeletal muscle regeneration. *Development*. 2011;138(17):3639-46.
45. Mackey AL, Kjaer M. The breaking and making of healthy adult human skeletal muscle in vivo. *Skelet Muscle*. 2017;7(1):24.
46. Crameri RM, Aagaard P, Qvortrup K, Langberg H, Olesen J, Kjaer M. Myofibre damage in human skeletal muscle: effects of electrical stimulation versus voluntary contraction. *J Physiol*. 2007;583(Pt 1):365-80.
47. Morooka S, Asano N, Kobayashi M, Nosaka S. Volume loading inhibits baroreflex vagal bradycardia in rats. *Auton Neurosci*. 2002;95(1-2):97-102.
48. Fielding RA, Manfredi TJ, Ding W, Fiatarone MA, Evans WJ, Cannon JG. Acute phase response in exercise. III. Neutrophil and IL-1 beta accumulation in skeletal muscle. *Am J Physiol*. 1993;265(1 Pt 2):R166-72.
49. Toumi H, F'Guyer S, Best TM. The role of neutrophils in injury and repair following muscle stretch. *J Anat*. 2006;208(4):459-70.
50. Tidball JG. Inflammatory cell response to acute muscle injury. *Med Sci Sports Exerc*. 1995;27(7):1022-32.

51. Saclier M, Yacoub-Youssef H, Mackey AL et al. Differentially activated macrophages orchestrate myogenic precursor cell fate during human skeletal muscle regeneration. *Stem Cells*. 2013;31(2):384-96.
52. Akhmedov D, Berdeaux R. The effects of obesity on skeletal muscle regeneration. *Front Physiol*. 2013;4:371.
53. Allen RE, Sheehan SM, Taylor RG, Kendall TL, Rice GM. Hepatocyte growth factor activates quiescent skeletal muscle satellite cells in vitro. *J Cell Physiol*. 1995;165(2):307-12.
54. Sheehan SM, Tatsumi R, Temm-Grove CJ, Allen RE. HGF is an autocrine growth factor for skeletal muscle satellite cells in vitro. *Muscle Nerve*. 2000;23(2):239-45.
55. Schultz E, Jaryszak DL, Valliere CR. Response of satellite cells to focal skeletal muscle injury. *Muscle Nerve*. 1985;8(3):217-22.
56. Fuchtbauer EM, Westphal H. MyoD and myogenin are coexpressed in regenerating skeletal muscle of the mouse. *Dev Dyn*. 1992;193(1):34-9.
57. Cooper RN, Tajbakhsh S, Mouly V, Cossu G, Buckingham M, Butler-Browne GS. In vivo satellite cell activation via Myf5 and MyoD in regenerating mouse skeletal muscle. *J Cell Sci*. 1999;112 (Pt 17):2895-901.
58. Megeney LA, Kablar B, Garrett K, Anderson JE, Rudnicki MA. MyoD is required for myogenic stem cell function in adult skeletal muscle. *Genes Dev*. 1996;10(10):1173-83.
59. Ustanina S, Carvajal J, Rigby P, Braun T. The myogenic factor Myf5 supports efficient skeletal muscle regeneration by enabling transient myoblast amplification. *Stem Cells*. 2007;25(8):2006-16.
60. Gayraud-Morel B, Chretien F, Flamant P, Gomes D, Zammit PS, Tajbakhsh S. A role for the myogenic determination gene Myf5 in adult regenerative myogenesis. *Dev Biol*. 2007;312(1):13-28.
61. Kitzmann M, Carnac G, Vandromme M, Primig M, Lamb NJ, Fernandez A. The muscle regulatory factors MyoD and myf-5 undergo distinct cell cycle-specific expression in muscle cells. *J Cell Biol*. 1998;142(6):1447-59.
62. Olguin HC, Yang Z, Tapscott SJ, Olwin BB. Reciprocal inhibition between Pax7 and muscle regulatory factors modulates myogenic cell fate determination. *J Cell Biol*. 2007;177(5):769-79.

63. Kuang S, Kuroda K, Le Grand F, Rudnicki MA. Asymmetric self-renewal and commitment of satellite stem cells in muscle. *Cell*. 2007;129(5):999-1010.
64. Penn BH, Bergstrom DA, Dilworth FJ, Bengal E, Tapscott SJ. A MyoD-generated feed-forward circuit temporally patterns gene expression during skeletal muscle differentiation. *Genes Dev*. 2004;18(19):2348-53.
65. Smith CK, 2nd, Janney MJ, Allen RE. Temporal expression of myogenic regulatory genes during activation, proliferation, and differentiation of rat skeletal muscle satellite cells. *J Cell Physiol*. 1994;159(2):379-85.
66. Tierney MT, Aydogdu T, Sala D et al. STAT3 signaling controls satellite cell expansion and skeletal muscle repair. *Nat Med*. 2014;20(10):1182-6.
67. Bonetto A, Aydogdu T, Jin X et al. JAK/STAT3 pathway inhibition blocks skeletal muscle wasting downstream of IL-6 and in experimental cancer cachexia. *Am J Physiol Endocrinol Metab*. 2012;303(3):E410-21.
68. Price FD, von Maltzahn J, Bentzinger CF et al. Inhibition of JAK-STAT signaling stimulates adult satellite cell function. *Nat Med*. 2014;20(10):1174-81.
69. Serrano AL, Baeza-Raja B, Perdiguero E, Jardi M, Munoz-Canoves P. Interleukin-6 is an essential regulator of satellite cell-mediated skeletal muscle hypertrophy. *Cell Metab*. 2008;7(1):33-44.
70. Huraskin D, Eiber N, Reichel M et al. Wnt/beta-catenin signaling via Axin2 is required for myogenesis and, together with YAP/Taz and Tead1, active in IIa/IIx muscle fibers. *Development*. 2016;143(17):3128-42.
71. Otto A, Schmidt C, Luke G et al. Canonical Wnt signalling induces satellite-cell proliferation during adult skeletal muscle regeneration. *J Cell Sci*. 2008;121(Pt 17):2939-50.
72. Brack AS, Conboy IM, Conboy MJ, Shen J, Rando TA. A temporal switch from notch to Wnt signaling in muscle stem cells is necessary for normal adult myogenesis. *Cell Stem Cell*. 2008;2(1):50-9.
73. Kim CH, Neiswender H, Baik EJ, Xiong WC, Mei L. Beta-catenin interacts with MyoD and regulates its transcription activity. *Mol Cell Biol*. 2008;28(9):2941-51.
74. Nguyen MH, Cheng M, Koh TJ. Impaired muscle regeneration in ob/ob and db/db mice. *ScientificWorldJournal*. 2011;11:1525-35.

75. Peterson JM, Bryner RW, Alway SE. Satellite cell proliferation is reduced in muscles of obese Zucker rats but restored with loading. *Am J Physiol Cell Physiol*. 2008;295(2):C521-8.
76. Fink LN, Costford SR, Lee YS et al. Pro-inflammatory macrophages increase in skeletal muscle of high fat-fed mice and correlate with metabolic risk markers in humans. *Obesity (Silver Spring)*. 2014;22(3):747-57.
77. Duguez S, Feasson L, Denis C, Freyssenet D. Mitochondrial biogenesis during skeletal muscle regeneration. *Am J Physiol Endocrinol Metab*. 2002;282(4):E802-9.
78. Theeuwes WF, Gosker HR, Langen RCJ, Pansters NAM, Schols A, Remels AHV. Inactivation of glycogen synthase kinase 3beta (GSK-3beta) enhances mitochondrial biogenesis during myogenesis. *Biochim Biophys Acta Mol Basis Dis*. 2018;1864(9 Pt B):2913-26.
79. Wagatsuma A, Kotake N, Yamada S. Muscle regeneration occurs to coincide with mitochondrial biogenesis. *Mol Cell Biochem*. 2011;349(1-2):139-47.
80. Vechetti IJ, Jr., Valentino T, Mobley CB, McCarthy JJ. The role of extracellular vesicles in skeletal muscle and systematic adaptation to exercise. *J Physiol*. 2021;599(3):845-61.
81. Théry C, Witwer KW, Aikawa E et al. Minimal information for studies of extracellular vesicles 2018 (MISEV2018): a position statement of the International Society for Extracellular Vesicles and update of the MISEV2014 guidelines. *Journal of Extracellular Vesicles*. 2018;7(1):1535750.
82. Li Y, Han C, Wang J et al. Exosomes Mediate the Beneficial Effects of Exercise. *Adv Exp Med Biol*. 2017;1000:333-53.
83. Thery C, Zitvogel L, Amigorena S. Exosomes: composition, biogenesis and function. *Nat Rev Immunol*. 2002;2(8):569-79.
84. van Dommelen SM, Vader P, Lakhal S et al. Microvesicles and exosomes: opportunities for cell-derived membrane vesicles in drug delivery. *J Control Release*. 2012;161(2):635-44.
85. Murchison EP, Hannon GJ. miRNAs on the move: miRNA biogenesis and the RNAi machinery. *Curr Opin Cell Biol*. 2004;16(3):223-9.
86. Lee Y, Kim M, Han J et al. MicroRNA genes are transcribed by RNA polymerase II. *EMBO J*. 2004;23(20):4051-60.

87. Kirby TJ, McCarthy JJ. MicroRNAs in skeletal muscle biology and exercise adaptation. *Free Radic Biol Med*. 2013;64:95-105.
88. Gregory RI, Yan KP, Amuthan G et al. The Microprocessor complex mediates the genesis of microRNAs. *Nature*. 2004;432(7014):235-40.
89. Yi R, Qin Y, Macara IG, Cullen BR. Exportin-5 mediates the nuclear export of pre-microRNAs and short hairpin RNAs. *Genes Dev*. 2003;17(24):3011-6.
90. Macrae IJ, Zhou K, Li F et al. Structural basis for double-stranded RNA processing by Dicer. *Science*. 2006;311(5758):195-8.
91. Pasquinelli AE. MicroRNAs and their targets: recognition, regulation and an emerging reciprocal relationship. *Nat Rev Genet*. 2012;13(4):271-82.
92. Friedman RC, Farh KK, Burge CB, Bartel DP. Most mammalian mRNAs are conserved targets of microRNAs. *Genome Res*. 2009;19(1):92-105.
93. van Rooij E, Quiat D, Johnson BA et al. A family of microRNAs encoded by myosin genes governs myosin expression and muscle performance. *Dev Cell*. 2009;17(5):662-73.
94. Chen JF, Tao Y, Li J et al. microRNA-1 and microRNA-206 regulate skeletal muscle satellite cell proliferation and differentiation by repressing Pax7. *J Cell Biol*. 2010;190(5):867-79.
95. Dey BK, Gagan J, Dutta A. miR-206 and -486 induce myoblast differentiation by downregulating Pax7. *Mol Cell Biol*. 2011;31(1):203-14.
96. Chen JF, Mandel EM, Thomson JM et al. The role of microRNA-1 and microRNA-133 in skeletal muscle proliferation and differentiation. *Nat Genet*. 2006;38(2):228-33.
97. Nie Y, Sato Y, Wang C, Yue F, Kuang S, Gavin TP. Impaired exercise tolerance, mitochondrial biogenesis, and muscle fiber maintenance in miR-133a-deficient mice. *FASEB J*. 2016;30(11):3745-58.
98. Kadoglou NP, Iliadis F, Angelopoulou N et al. The anti-inflammatory effects of exercise training in patients with type 2 diabetes mellitus. *Eur J Cardiovasc Prev Rehabil*. 2007;14(6):837-43.
99. Hayashino Y, Jackson JL, Hirata T et al. Effects of exercise on C-reactive protein, inflammatory cytokine and adipokine in patients with type 2 diabetes: a meta-analysis of randomized controlled trials. *Metabolism*. 2014;63(3):431-40.

100. Balducci S, Zanuso S, Nicolucci A et al. Anti-inflammatory effect of exercise training in subjects with type 2 diabetes and the metabolic syndrome is dependent on exercise modalities and independent of weight loss. *Nutr Metab Cardiovasc Dis*. 2010;20(8):608-17.
101. You T, Arsenis NC, Disanzo BL, Lamonte MJ. Effects of exercise training on chronic inflammation in obesity : current evidence and potential mechanisms. *Sports Med*. 2013;43(4):243-56.
102. Powers SK, Bomkamp M, Ozdemir M, Hyatt H. Mechanisms of exercise-induced preconditioning in skeletal muscles. *Redox Biol*. 2020;35:101462.
103. Dinulovic I, Furrer R, Di Fulvio S, Ferry A, Beer M, Handschin C. PGC-1alpha modulates necrosis, inflammatory response, and fibrotic tissue formation in injured skeletal muscle. *Skelet Muscle*. 2016;6:38.
104. Shefer G, Rauner G, Yablonka-Reuveni Z, Benayahu D. Reduced satellite cell numbers and myogenic capacity in aging can be alleviated by endurance exercise. *PLoS One*. 2010;5(10):e13307.
105. Dinulovic I, Furrer R, Beer M, Ferry A, Cardel B, Handschin C. Muscle PGC-1alpha modulates satellite cell number and proliferation by remodeling the stem cell niche. *Skelet Muscle*. 2016;6(1):39.
106. Lin Y, Zhao Y, Li R, Gong J, Zheng Y, Wang Y. PGC-1α is associated with C2C12 Myoblast differentiation. *Open Life Sciences*. 2014;9(11):1030-6.
107. Fruhbeis C, Helmig S, Tug S, Simon P, Kramer-Albers EM. Physical exercise induces rapid release of small extracellular vesicles into the circulation. *J Extracell Vesicles*. 2015;4:28239.
108. Aswad H, Forterre A, Wiklander OP et al. Exosomes participate in the alteration of muscle homeostasis during lipid-induced insulin resistance in mice. *Diabetologia*. 2014;57(10):2155-64.
109. Safdar A, Saleem A, Tarnopolsky MA. The potential of endurance exercise-derived exosomes to treat metabolic diseases. *Nat Rev Endocrinol*. 2016;12(9):504-17.
110. Nie Y, Sato Y, Garner RT et al. Skeletal muscle-derived exosomes regulate endothelial cell functions via reactive oxygen species-activated nuclear factor-kappaB signalling. *Exp Physiol*. 2019;104(8):1262-73.

CHAPTER 2. OBESITY AND EXERCISE TRAINING ALTER INFLAMMATORY PATHWAY SKELETAL MUSCLE EXTRACELLULAR VESICLE miRNAs

Authors: Brian P. Sullivan[1], Yaohui Nie[1], Sheelagh Evans[1], Chris K. Kargl[1], Zach R. Hettinger[1], Ron T. Garner[2], Monica J. Hubal[3], Shihuan Kuang[1], Julianne Stout[4], Timothy P. Gavin[1] FACSM

Affiliations:
[1]Purdue University, West Lafayette, IN
[2]Husson University, Bangor, ME
[3]Indiana University- Purdue University Indianapolis, Indianapolis, IN
[4]Indiana University School of Medicine-West Lafayette, West Lafayette, IN

Corresponding Author: Timothy P. Gavin PhD, Department of Health and Kinesiology, Purdue University, 800 W. Stadium Ave., West Lafayette, IN 47907. Phone: (765) 494-3179, Fax: (765) 496-1239, Email: gavin1@purdue.edu

Abstract

Obesity is associated with chronic inflammation characterized by increased levels of inflammatory cytokines. Extracellular vesicles (EVs) contain a variety of molecules including microRNAs (miR), mRNAs, and proteins. Typically, miRs act through post-transcriptional regulation of mRNA targets via mRNA degradation and/or translational repression. Exercise training can reduce chronic inflammation. **Purpose:** The current study examined if obesity and concurrent exercise training alter skeletal muscle: (1) EV miR content, and (2) inflammatory signaling. **Methods:** Vastus lateralis biopsies were obtained from sedentary lean (LN) and sedentary individuals with obesity (OB) for analyses of targeted whole skeletal muscle mRNA and skeletal muscle derived EV miR (via small RNA-seq) before and after seven days of concurrent aerobic and resistance training. **Results:** Pathway analysis of skeletal muscle derived EV miRs indicates that: 1) obesity alters EV miR targeting anabolic pathways, indicative of increased Wnt/β-catenin, and reduced IGF-1 signaling; 2) exercise training alters EV miR targeting IL-10, IL-8, toll-like receptor signaling (TLR), and NF-κB pathways in which RELA, an NF-κB subunit, is common. In whole skeletal muscle, IL-8 mRNA was reduced 50% (LN: Pre=1.0 ± 0.26, Post=0.57 ± 0.07; OB: Pre=0.89 ± 0.15, Post=0.37 ± 0.04) and Jun mRNA was reduced 25% after exercise training (LN: Pre=1.0 ± 0.12, Post=0.75 ± 0.06; OB: Pre=0.98 ± 0.07, Post=0.76 ± 0.08) consistent with the anti-inflammatory effects of exercise on skeletal muscle. **Conclusion:** Obesity and seven days of concurrent exercise training differentially alter

skeletal muscle derived EV miR contents targeting inflammatory and anabolic pathways. The target cells for skeletal muscle derived EVs and the physiological relevance of altered miR contents requires further investigation.

Introduction

Obesity is associated with chronic inflammation (1), which is characterized by increased levels of several proinflammatory cytokines including interleukin 6 (IL-6), tumor necrosis factor α (TNF-α) and C-reactive protein (CRP). Chronic inflammation contributes to the development of skeletal muscle insulin resistance, type 2 diabetes mellitus (T2D), cardiovascular disease (CVD), and numerous cancers (1-4). Skeletal muscle is the largest secretory organ in lean humans (1) and is responsible for 80% of insulin stimulated glucose disposal (3). Obesity causes biochemical and morphological alterations within skeletal muscle including insulin resistance (4), immune cell infiltration (5), and ectopic fat accumulation (6). These adverse changes result in reduced muscle quality, insulin insensitivity, and an increased inflammatory secretome (1, 7).

Many proteins have been identified that are expressed and released by skeletal muscle, termed myokines (8). Myokines are often regulated by skeletal muscle contraction, act in an anti-inflammatory manner, and tend to have positive effects on glucose and lipid metabolism (9). Obesity alters the expression of myokines released from skeletal muscle at rest and following exercise (10), consistent with increased inflammation and impaired substrate metabolism.

Exercise is a highly effective method for reducing both local and systemic inflammation in obese and T2D patients, with the greatest reductions appearing to come from concurrent aerobic and resistance exercise training (11-13). Exercise training can improve myokine expression in obesity resulting in expression closer to that of lean controls (14). While myokines appear to play a key role in the benefits of exercise training, other factors secreted from skeletal muscle appear important as well.

Extracellular Vesicles are nano particles that are secreted by all cells and contain functional mRNAs, microRNAs (miR), lipids, and proteins (15). miRs alter gene expression by binding to target mRNA and act through the RNA Silencing complex to reduce target mRNA translation via translational repression or degradation of the target mRNA (16). The impact of EV miRs on cell-to-cell signaling is of increasing interest. EVs from adipose tissue are a possible regulator of obesity associated dysfunction and EV signaling may act as an important link between obesity

and peripheral tissue insulin sensitivity (17). The miR content of EVs derived from human adipocytes is altered in obese individuals consistent with observed impairments in peripheral tissue insulin sensitivity (18). Weight loss reduces peripheral insulin resistance and alters the miR content of adipocyte derived EVs consistent with lean controls and reduced insulin resistance (17). While the impact of skeletal muscle EVs during obesity is less clear, we have previously demonstrated that skeletal muscle EVs are capable of regulating endothelial cell function (19). Together these studies indicate the potential of EVs to drive systemic metabolic improvements.

Currently little work has been performed investigating the relationship between obesity and skeletal muscle derived EV miRs or between exercise training and skeletal muscle EV miRs. Muscle contraction increases the release of EVs from skeletal muscle (20, 21). However, it has yet to be examined if exercise training alters the miR content of skeletal muscle derived EVs in humans. Therefore, the aims of the present study were to examine if 1) obesity or 2) short-term concurrent exercise training alter skeletal muscle EV miR content or inflammation. We hypothesized: 1) obesity would alter the EV miR profile consistent with increased inflammatory signaling; and 2) one week of concurrent exercise training would alter the skeletal muscle EV miR profile consistent with reduced inflammation.

Methods

This study conforms to the standards set out by the latest revision of the Declaration of Helsinki and was approved by the Purdue University Institutional Review Board. Eight healthy, sedentary, lean (LN) individuals (3 women, 5 men; Body Mass Index (BMI) < 25 kg/m^2) and eight healthy, sedentary, individuals with obesity (OB) (3 women, 5 men; BMI ≥ 30 kg/m^2) between the ages of 18-35 were recruited to participate in this study. Subjects were nonsmoking with no known chronic disease. Sedentary participants were defined as participating in less than 1 h of strenuous physical activity per week and no subject reported any form of regular physical activity. Qualified individuals were administered both verbal and written descriptions of the study. Subjects provided voluntary written consent prior to the beginning of the study.

Day 1. Subjects reported to the Max E. Wastl Human Performance Laboratory where height and weight were recorded. Fasting blood was drawn from a catheter inserted into an antecubital vein for the measurement of insulin, glucose, total cholesterol (TC), high density lipoprotein

(HDL), low density lipoprotein (LDL), and triglycerides (TG). Additional blood was taken for the measurement of plasma IL-6, CRP, and TNF-α. The homeostasis model assessment for insulin resistance (HOMA-IR) and β cell function (HOMA-β) was subsequently calculated (22). Following the blood draw, subjects underwent a *vastus lateralis* biopsy from a predetermined, randomized leg. Biopsy samples were stored at −80°C until analysis. A section of the biopsy sample (~100 mg) was placed on ice in EV free/serum free DMEM for the isolation of skeletal muscle EVs. Excess muscle was flash frozen and stored at -80ºC for further analysis.

Day 2. Subjects reported to the A. H. Ismail Center for Health, Exercise and Nutrition for the determination of maximal oxygen consumption ($\dot{V}O_2MAX$) and one repetition maximum (1-RM). $\dot{V}O_2MAX$ was measured on an electronically braked cycle ergometer (Lode, Excaliber Sport, Groningen, Netherlands) as previously described (23). A 5-minute warm up was performed at 50 W immediately followed by a 25 W increase every 2 minutes until volitional fatigue. Minute ventilation ($\dot{V}E$), oxygen uptake ($\dot{V}O_2$), and carbon dioxide production ($\dot{V}CO_2$) were continuously monitored via open circuit spirometry (True Max 2400, Parvo Medics, Salt Lake City, UT). Heart rate (model T31, Polar Electro Inc., Woodbury, NY) and rating of perceived exertion were measured at each workload. Subjects were verbally encouraged to continue for as long as possible. The criterion used to assess $\dot{V}O_2MAX$ included: 1) a heart rate in excess of 90% of age predicted max (220 - age); 2) a respiratory exchange ratio greater than or equal to 1.10; and 3) identification of a plateau ($\leq$ 150 ml increase) in $\dot{V}O_2$ despite a further increase in workload. In all tests, at least two of three criteria were met.

After a 15 min rest period following the $\dot{V}O_2MAX$ test, Leg Press (Technogym- Element, Fairfield, NJ) 1-repetion maximum (1-RM) was determined. Subjects performed the leg press with their feet shoulder width apart on the platform with their knees bent at 90° at approximately 80% of the subjects body weight. Subjects were given a 30 second to 1-minute rest period before attempting the subsequent weight. The weight was increased by 9.1 kg for each consecutive attempt until the subject was unable to fully extend the knees. The highest successfully lifted weight was designated as the 1-RM. The 1-RM of two lean and six obese subjects exceeded the maximum weight of the equipment (136.4 kg). In these cases, 1-RM was estimated based on the maximal number of repetitions the subject was able to complete at 136.4 kg (24).

Exercise Training Protocol. At least 2 days following the initial visit, subjects began a 7-consecutive day, concurrent exercise training protocol. On each day (1-7) subjects performed 45 minutes of cycle ergometer exercise at 70% $\dot{V}O_{2MAX}$. In addition, subjects performed a bout of resistance exercise consisting of 3 sets of 8-12 repetitions on the leg press at 80% of 1-RM with 2-minute rest between sets on days 2, 4, and 6.

Final Visit. Subjects reported to the Max E. Wastl Human Performance Laboratory 12-14 hours following the completion of the exercise training protocol. At this visit subjects repeated the blood draw and muscle biopsy procedures.

Blood Analysis. Plasma IL-6, CRP and TNF-α were measured by Quantikine enzyme-linked immunosorbent assay (25) according to the manufacturer's instructions (R&D Systems Inc, Minneapolis, MN, USA) (IL-6 – HS600B; CRP – DCRP00; TNF-α - HSTA00E). Prior to analysis, samples were placed on ice and allowed to thaw. All samples were analyzed in duplicate, with the mean of both values being reported.

Quantitative real-time PCR. Total muscle RNA was extracted by using a Trizol reagent (Thermo Fisher Scientific) as previously described (26). For mRNA reverse transcription, first strand cDNA was generated by random hexamer primers with MMLV Reverse Transcriptase (Thermo Fisher Scientific). For mature miRNA reverse transcription, multiple adenosine nucleotides were first added to the 3' end of total RNA with *Escherichia coli* Poly (A) polymerase (New England BioLabs, Ipswich, MA, USA), and cDNA was then synthesized with a Poly T primer including an adaptor sequence using MMLV Reverse Transcriptase. Real-time PCR detection was performed using SYBR green based chemistry on a CFX Connect (BioRad, Hercules, CA, USA). Primers for mRNA and miR are listed in Table 2.1. Gene expression was determined with the $2^{-\Delta\Delta Ct}$ relative quantification method and normalized to 18s for mRNA. Housekeeping genes were validated to ensure their expression was not influenced by the experimental procedure.

Extracellular Vesicle Isolation. Following *vastus lateralis* biopsies, approximately 100 mg of muscle was washed with PBS and gently minced in a 5 cm cell culture dish. Minced muscle was incubated in EV free DMEM at standard culture conditions (37°C, 5% CO_2) for 24 hr to facilitate EV secretion. EV containing media was collected and EVs were isolated via differential ultracentrifugation as previously described (19). Breifly, Medium was centrifuged at 2,000g for

10 min, pelleted cells and debris were discarded. The medium was then centrifuged at 4ºC at 10,000g for 30 min, followed by filtration through a 0.22μm syringe filter. Filtered medium was ultra-centrifuged 4ºC at 100,000g for 70 min. Pelleted EVs were washed with PBS and ultra-centrifuged 4ºC at 100,000g for 70 min for a second time. EVs were resuspended in PBS from electron microscopy or Trizol reagent (Thermo Fisher Scientific) for the isolation of total EV RNA as previously described (26).

Transmission Electron Microscopy. Following isolation, the characterization of EVs was performed on a Tecnai T20 transmission electron microscope (FEI, 200 kV) as previously described (27). Briefly, EVs in PBS were pipetted onto carbon coated, copper electron microscopy grids and incubated for approximately 2 minutes. Excess liquid was blotted away, and grids were washed with water to remove salts. Excess liquid was blotted away, and grids were negative stained with 2% phosphotungstic acid for 1 minute.

Western Blot. Western blotting analysis was performed using standard SDS-Page procedures. Briefly, protein was isolated from cell lysates in RIPA Buffer (50mm Tris HCL 7.4 pH, 150mm NaCl, 2mm EDTA, 0.1% SDS, 0.1% Triton x-100, 0.5% Sodium Deoxycholate) with phosphatase inhibitors (0.2 mM NA_3VO_4, 50 mM NaF) and a protease inhibitor cocktail (P8340, Sigma-Aldrich, St. Louis, MO, USA). 20 μg of total protein from EVs was fractionated on SDS-polyacrylamide gels; transferred to PVDF membrane; and incubated with CD63 (Santa Cruz Biotechnology) and Alix (Cell Signaling Technologies) primary antibodies. Horseradish peroxide–conjugated secondary antibodies (Cell Signaling Technology, Danvers, MA) were incubated with the membrane and images were obtained by chemiluminescence using a ChemiDoc Touch Imaging System and densitometric analysis performed by ImageLab software (BioRad, Hercules, CA, USA).

microRNA Seq. Isolated EV RNA from a subset of samples (4/group/time) were analyzed by the Purdue University Genomics Core and raw miR sequence reads were analyzed by the Purdue University Bioinformatics Core. Adapter trimming followed by clipping of 4 bases from either ends of the reads and quality trimming was performed through cutadapt software (version 1.13) (28) (The Bioo Scientific kit "*NEXTflex Illumina Small RNA Sequencing Kit v3*"). After adaptor trimming, reads were trimmed based on quality such that bases above Phred Score 30 and reads with a minimum length of 5 were retained.

Adaptor and quality trimmed reads were used by DeconSeq tool (Version 0.4.3) (29) to detect bacterial contamination. DeconSeq tool generates clean and contaminated reads for each sample. Clean reads were extracted using in house scripts for downstream analysis. Select samples (1 LN Pre, 2 LN Post, and 1 OB Post) were eliminated from further analysis due to high levels of bacterial contamination.

Adaptor, quality trimmed, and clean reads were processed through miRDeep2 software (version 2.0.0.8) (30) for miRNA analysis. The preprocessing of reads was achieved through the mapper.pl script from miRDeep2 which performs steps such as discarding the reads shorter than 15 base pairs and reads collapsing. Preprocessed reads were mapped against the Human reference genome.

Quantification and expression profiling of known miRNAs was performed by the quantifier.pl script from miRDeep2 using the collapsed reads and Human miRNAs (downloaded from miRBase). The quantifier script from miRDeep2 generated the read counts for the known miRNAs from each uncontaminated sample. Combined count matrices for all miRNAs and samples were generated using the custom scripts. The DESeq2 package (version 1.16.1) (31) was used to calculate differential expression of known miRNAs between LN and OB at rest (BMI; 3 LN Pre; 4 OB Pre) and before and after concurrent exercise training (ExTr; n=5/time point; 2 LN; 3 OB).

Biological Pathway Analysis. Differentially expressed miRs between LN and OB ($p<0.05$; n=22) and before and after exercise training ($p<0.05$; n=28) were uploaded into Ingenuity Pathway Analysis (IPA) suite (Qiagen Inc., Redwood City, CA) for biological pathway analysis. Non-adjusted p-value was utilized as the pathway analysis lowers the likelihood of a false positive/negative. IPA utilizes miR seed sequence binding with cognate mRNA targets to identify miR: mRNA target interactions across multiple available bioinformatic data sources. We utilized a conservative approach within the miR target filter for mRNA target filter where only experimentally verified interactions, determined via miRTarBase (32), and/or highly predicted targets containing binding sites with 8-mer seed binding, determined via TargetScan (33), were selected as miRNA/mRNA pairs. This approach yielded a BMI related gene target list of mRNAs and an ExTr related gene target list of mRNAs. Each gene list was used by IPA to determine enriched canonical pathways targeted by exercise training and obesity miRNAs.

Representation of each canonical pathway was tested using Fisher Exact Test of ratios of miRNA targeted genes in our dataset as compared to the total number of genes in each IPA pathway.

Statistical analysis. Student's t-test was used to analyze group differences in age, BMI, 1-RM and $\dot{V}O_2MAX$. All other data was analyzed using a two-way (2 groups × 2 time points) mixed-factorial analysis of variance. Following a significant F ratio, Fisher's LSD post-hoc analysis was performed. Relationships between variables were analyzed using linear regression. Significance was established at $P \leq 0.05$ level and data reported as Mean ± SE. All data were analyzed in GraphPad Prism (Version 7.02).

Results

Subject Characteristics. Subject Characteristics for all participants are located in Table 2.2, for the LN vs. OB miRSEQ subset are located in Table 2.3, and for the exercise training subset are located in Table 2.4. Both the LN vs. OB and ExTr miRSEQ subset cohorts were representative of the full cohorts; both subset cohorts displayed similar trends to those observed in the full cohort and no significant differences were observed between either subset or the full cohort.

As designed, OB had a significantly greater BMI than LN and there was no observed weight loss in either group as a result of the exercise training. OB demonstrated lower relative $\dot{V}O_2MAX$ before and higher fasting insulin, HOMA-IR, HOMA-β, TG, plasma TNF-α and CRP before and after training. Concurrent exercise training reduced HOMA-β and TG in both LN and OB and reduced TC only in LN.

miRSEQ and IPA Analysis by BMI. Differential analysis revealed that 22 miRs were differentially expressed between LN and OB (Table 2.5). Using a conservative filter (only miRs with experimentally confirmed or highly conserved predicted targets), we identified the 22 differentially expressed BMI miRs target 3,419 mRNAs (Supplemental Digital Content Table 2.1). Starting with the 3,419 BMI mRNA targets, IPA was used to identify enriched biological pathways. Using a p value filter of $p < 0.01$, 133 canonical pathways were identified as enriched in the BMI data set (Supplemental Digital Content Table 2.2). Table 2.6 represents the top 10 (determined by p-value) canonical pathways identified by IPA in the BMI data set. Of the top 10 canonical pathways identified by IPA, the Wnt/β-catenin (Figure 2.2) and IGF-1 signaling

pathways (Figure 2.3) were of particular interest because: 1) IGF-1 and Wnt ligand expression are reduced in muscle from individuals with obesity (34); and 2) increased inflammation causes dysregulation in both of these pathways (35, 36).

miRSEQ and IPA Analysis by ExTr. Differential analysis revealed that 28 miRs were differentially expressed following ExTr (Table 2.7). Again, using a conservative filter, we identified the 28 differentially expressed ExTr miRs target 3,070 mRNAs (Supplemental Digital Content Table 2.3). Starting with the 3,070 ExTr mRNA targets, IPA was used to identify enriched biological pathways. Using a p-value filter for pathway significance of $p < 0.01$, 113 canonical pathways were identified as enriched in the ExTr data set (Supplemental Digital Content Table 2.4). Table 2.8 represents the top 10 canonical pathways identified by IPA in the ExTr dataset. The top canonical pathways in the ExTr dataset were primarily inflammation related pathways and the top 2 were IL-6 and IL-10 signaling (Figure 2.4).

Muscle mRNA. Whole skeletal muscle mRNA for components of the Wnt/β-catenin and IGF-1 signaling pathways were measured to further investigate results from pathway analysis (Figure 2.5). A significant interaction effect was observed for *IGF-1* mRNA, where *IGF-1* mRNA was increased in LN following ExTr compared to LN pre and OB at pre and post. The expression of *β-catenin* mRNA was increased 50% following exercise training, but no differences were observed between LN and OB. The expression of key Wnt ligands, *Wnt3a, Wnt5a,* and *Wnt7a* were all reduced in OB at rest and following concurrent exercise training by approximately 45%, 20% and 35% respectively. A trend was observed for an increase in Wnt5a expression following concurrent exercise training ($p = 0.07$).

Whole skeletal muscle mRNA for components of the IL-6 and IL-10 pathways are in Figure 2.6. One week of concurrent exercise training reduced *IL-8, Jun* and *FOS* mRNA expression in both LN and OB by approximately 50%, 25% and 65% respectively. A trend for a reduction in *IL-10* was observed following exercise training ($p = 0.10$). No differences were observed in muscle expression of *IL-6, IL-8, IL-10, Jun* or *FOS* mRNA between LN and OB either before or following exercise training.

Discussion

The present study demonstrates that obesity alters skeletal muscle derived EV miR targeting many inflammatory and anabolic pathways including the Wnt/ β-catenin and IGF-1 signaling

pathways. In addition, one week of concurrent exercise training alters skeletal muscle derived EV miR targeting several pathways including the IL-6 and IL-10 pathways. To our knowledge this is the first report demonstrating that obesity and exercise training independently alter the miR content of skeletal muscle derived EVs.

Obesity alters EV miRs targeting anabolic pathways. Obesity is a disease of chronic inflammation characterized by an increase in circulating inflammatory cytokines (1, 2). Confirming this, circulating TNF-α and CRP were greater in individuals with than without obesity (Table 1). We had hypothesized that EVs isolated from muscle of individuals with obesity would contain pro-inflammatory signals. In contrast to our hypothesis, common pro-inflammatory pathways were not among the Top 10 pathways identified.

Biological pathway analysis found that obesity alters the expression of EV miRs targeting components of the IGF-1 and Wnt/β-Catenin signaling pathways. The Wnt/β-catenin signaling pathway regulates the release of pro- and anti-inflammatory cytokines in different cell types and is implicated in the progression of metabolic syndrome (35). Alterations in Wnt/β-catenin signaling could contribute to an increase in the production of proinflammatory cytokines such as IL-6, IL-8 and TNF-α (35).

Individuals with obesity appear to be resistant to anabolic stimuli, likely the result of insulin resistance, lipid accumulation, and/or inflammation (37). Anabolic resistance in obese individuals can lead to a reduction in the regenerative capacity of skeletal muscle following injury (38). Impairments in IGF-1/AKT/mTOR and Wnt/β-Catenin signaling have been observed in obese animals during muscle regeneration, suggesting that impaired signaling in these pathways has negative consequences for skeletal muscle mass maintenance (39, 40). Previously, we reported that skeletal muscle IGF-1 mRNA and protein and the mRNA expression of key Wnt ligands are reduced at rest and following acute resistance exercise in humans with obesity (34). In the present study, skeletal muscle *IGF-1, Wnt3a, Wnt5a* and *Wnt7a* mRNA are all reduced in subjects with obesity. Skeletal muscle EVs regulate Wnt signaling during myogenesis (18, 41), indicating that altered EV content could contribute to impaired regenerative capacity in obesity (38).

Exercise training alters extracellular vesicle miRs targeting inflammation. Concurrent exercise training has potent anti-inflammatory effects and reduces both local and systemic inflammation in individuals with or without obesity (11-13). Contrary to our hypothesis, one

week of concurrent exercise training did not reduce circulating markers of inflammation IL-6, TNF-α, or CRP in either LN or OB. This is likely due to the short duration of exercise training employed in the current study, suggesting a greater duration of exercise training is necessary to observe changes in these circulating inflammatory markers.

Biological pathway analysis indicates that one week of concurrent exercise training alters skeletal muscle derived EV miR targeting components of the IL-6 and IL-10 pathways, consistent with a reduction in inflammation. Additionally, we identified that EV miR are altered following training in a manner that indicates increased PPAR signaling. Upregulation of PPAR signaling leads to improvements in exercise tolerance, lipid metabolism and mitochondrial biogenesis via peroxisome proliferator-activated receptor gamma coactivator 1-alpha (PGC1-α) (42). These findings seem to agree with previous research that suggests that skeletal muscle EVs regulate the beneficial effects of exercise (21), as improvements in these pathways typically occur following exercise training. However, the extent to which skeletal muscle EVs exert systemic effects is unclear. In the present study, one week of exercise training was not sufficient to reduce systemic inflammation but does appear to reduce skeletal muscle inflammation. To confirm this, we examined the mRNA expression of key components of the IL-6 and IL-10 pathways via qRT-PCR. The expression of *IL-8, Jun* and *FOS* were reduced following exercise training and a trend was observed for a reduction in *IL-10* suggesting that skeletal muscle inflammation improves earlier in response to exercise training than systemic inflammation.

Previously, we have demonstrated that skeletal muscle EVs are capable of exerting potent paracrine effects on inflammatory signaling in non-muscle cells; endothelial cells treated with skeletal muscle derived EVs exhibit improvements in proliferation, migration and tube formation via activation of the nuclear factor-κB pathway (19). Recent evidence indicates that EVs exert endocrine effects in addition to their potent paracrine effects (41). Following intraperitoneal injection, skeletal muscle-derived EVs can be found within cells of at least 8 different organs in addition to skeletal muscle including brain, liver, heart, lungs, gastrointestinal tract, spleen, kidney and pancreas in mice (43). Additionally, it appears that skeletal muscle EVs contribute to the crossover effects of unilateral exercise (44). Twenty-four hours following injection of GFP labelled skeletal muscle EVs into the right *tibialis anterior* of mice, fluorescence was detected in the right quadriceps and the left *tibialis anterior* (43). These results indicate that when skeletal muscle EVs reach the circulation they exert endocrine effects (41), however it is unclear if a

physiologically relevant quantity of *in vivo* produced skeletal muscle EVs are able to reach the circulation. Recent work indicates that skeletal muscle EVs are capable of reaching the circulation, but the majority of *in vivo* produced skeletal muscle EVs remain in the extracellular environment (45). These findings highlight skeletal muscle EVs important role in paracrine signaling and indicate a potential role in endocrine signaling. It has been widely speculated, but as yet unproven, that the post exercise increase in skeletal muscle EV secretion, contributes to the increased number of EVs in the circulation following acute exercise (20, 21, 45). Therefore, the improvements in systemic inflammation which occur with longer duration exercise training may be attributable to endocrine effects of skeletal muscle EVs. Further research is needed to verify this hypothesis.

Limitations. In the present study, we did not control for EV origin. Skeletal muscle contains a variety of cell types including endothelial cells, satellite cells, neural cells, macrophages, and pericytes. However, the contribution of EVs of non-skeletal muscle origin is likely minimal as approximately 80% of total mapped reads were for skeletal muscle specific miR (miR-1, -133, -206, -486 and -499).

In conclusion, obesity alters the miR content of skeletal muscle EVs targeting the anabolic pathways IGF-1 and Wnt/β-Catenin. Skeletal muscle expression of *IGF-1* and *Wnt* ligands mRNA were lower in individuals with obesity compared to lean. Also, one week of concurrent exercise training alters the miR content of skeletal muscle EVs targeting inflammatory pathways IL-6 and IL-10; and skeletal muscle expression of *IL-8, IL-10, FOS,* and *Jun* mRNA were lower following exercise training. Thus, differences in skeletal muscle EV content are observed in individuals with obesity compared to lean and in response to exercise training consistent with skeletal muscle being an important paracrine/endocrine organ. Future work should investigate the importance of skeletal muscle EVs on tissue crosstalk in health and disease.

References

1. Pedersen BK, Febbraio MA. Muscles, exercise and obesity: skeletal muscle as a secretory organ. *Nat Rev Endocrinol*. 2012;8(8):457-65.
2. Haddad F, Zaldivar F, Cooper DM, Adams GR. IL-6-induced skeletal muscle atrophy. *J Appl Physiol (1985)*. 2005;98(3):911-7.
3. Thiebaud D, Jacot E, DeFronzo RA, Maeder E, Jequier E, Felber JP. The effect of graded doses of insulin on total glucose uptake, glucose oxidation, and glucose storage in man. *Diabetes*. 1982;31(11):957-63.
4. Lackey DE, Olefsky JM. Regulation of metabolism by the innate immune system. *Nat Rev Endocrinol*. 2016;12(1):15-28.
5. Patsouris D, Cao JJ, Vial G et al. Insulin resistance is associated with MCP1-mediated macrophage accumulation in skeletal muscle in mice and humans. *PLoS One*. 2014;9(10):e110653.
6. Shulman GI. Ectopic fat in insulin resistance, dyslipidemia, and cardiometabolic disease. *N Engl J Med*. 2014;371(12):1131-41.
7. Collins KH, Paul HA, Hart DA et al. A High-Fat High-Sucrose Diet Rapidly Alters Muscle Integrity, Inflammation and Gut Microbiota in Male Rats. *Sci Rep*. 2016;6:37278.
8. Febbraio MA, Pedersen BK. Contraction-induced myokine production and release: is skeletal muscle an endocrine organ? *Exerc Sport Sci Rev*. 2005;33(3):114-9.
9. Eckardt K, Gorgens SW, Raschke S, Eckel J. Myokines in insulin resistance and type 2 diabetes. *Diabetologia*. 2014;57(6):1087-99.
10. Wu H, Ballantyne CM. Skeletal muscle inflammation and insulin resistance in obesity. *J Clin Invest*. 2017;127(1):43-54.
11. Balducci S, Zanuso S, Nicolucci A et al. Anti-inflammatory effect of exercise training in subjects with type 2 diabetes and the metabolic syndrome is dependent on exercise modalities and independent of weight loss. *Nutr Metab Cardiovasc Dis*. 2010;20(8):608-17.
12. Petersen AM, Pedersen BK. The anti-inflammatory effect of exercise. *J Appl Physiol (1985)*. 2005;98(4):1154-62.

13. You T, Arsenis NC, Disanzo BL, Lamonte MJ. Effects of exercise training on chronic inflammation in obesity : current evidence and potential mechanisms. *Sports Med*. 2013;43(4):243-56.
14. Shin KO, Bae JY, Woo J et al. The effect of exercise on expression of myokine and angiogenesis mRNA in skeletal muscle of high fat diet induced obese rat. *J Exerc Nutrition Biochem*. 2015;19(2):91-8.
15. Thery C, Zitvogel L, Amigorena S. Exosomes: composition, biogenesis and function. *Nat Rev Immunol*. 2002;2(8):569-79.
16. Rottiers V, Naar AM. MicroRNAs in metabolism and metabolic disorders. *Nat Rev Mol Cell Biol*. 2012;13(4):239-50.
17. Hubal MJ, Nadler EP, Ferrante SC et al. Circulating adipocyte-derived exosomal MicroRNAs associated with decreased insulin resistance after gastric bypass. *Obesity (Silver Spring)*. 2017;25(1):102-10.
18. Forterre A, Jalabert A, Berger E et al. Proteomic analysis of C2C12 myoblast and myotube exosome-like vesicles: a new paradigm for myoblast-myotube cross talk? *PLoS One*. 2014;9(1):e84153.
19. Nie Y, Sato Y, Garner RT et al. Skeletal muscle-derived exosomes regulate endothelial cell functions via reactive oxygen species-activated nuclear factor-kappaB signalling. *Exp Physiol*. 2019;104(8):1262-73.
20. Fruhbeis C, Helmig S, Tug S, Simon P, Kramer-Albers EM. Physical exercise induces rapid release of small extracellular vesicles into the circulation. *J Extracell Vesicles*. 2015;4:28239.
21. Whitham M, Parker BL, Friedrichsen M et al. Extracellular Vesicles Provide a Means for Tissue Crosstalk during Exercise. *Cell Metab*. 2018;27(1):237-51 e4.
22. Matthews DR, Hosker JP, Rudenski AS, Naylor BA, Treacher DF, Turner RC. Homeostasis model assessment: insulin resistance and beta-cell function from fasting plasma glucose and insulin concentrations in man. *Diabetologia*. 1985;28(7):412-9.
23. Gavin TP, Stallings HW, 3rd, Zwetsloot KA et al. Lower capillary density but no difference in VEGF expression in obese vs. lean young skeletal muscle in humans. *J Appl Physiol (1985)*. 2005;98(1):315-21.

24. Brzycki M. Strength Testing—Predicting a One-Rep Max from Reps-to-Fatigue. *Journal of Physical Education, Recreation & Dance*. 1993;64(1):88-90.
25. Théry C, Witwer KW, Aikawa E et al. Minimal information for studies of extracellular vesicles 2018 (MISEV2018): a position statement of the International Society for Extracellular Vesicles and update of the MISEV2014 guidelines. *Journal of Extracellular Vesicles*. 2018;7(1):1535750.
26. Nie Y, Sato Y, Wang C, Yue F, Kuang S, Gavin TP. Impaired exercise tolerance, mitochondrial biogenesis, and muscle fiber maintenance in miR-133a-deficient mice. *FASEB J*. 2016;30(11):3745-58.
27. Keerthikumar S, Gangoda L, Liem M et al. Proteogenomic analysis reveals exosomes are more oncogenic than ectosomes. *Oncotarget*. 2015;6(17):15375-96.
28. Martin M. Cutadapt removes adapter sequences from high-throughput sequencing reads. *EMBnet.journal*. 2011;17(1):3.
29. Schmieder R, Edwards R. Fast identification and removal of sequence contamination from genomic and metagenomic datasets. *PLoS One*. 2011;6(3):e17288.
30. Friedlander MR, Mackowiak SD, Li N, Chen W, Rajewsky N. miRDeep2 accurately identifies known and hundreds of novel microRNA genes in seven animal clades. *Nucleic Acids Res*. 2012;40(1):37-52.
31. Love MI, Huber W, Anders S. Moderated estimation of fold change and dispersion for RNA-seq data with DESeq2. *Genome Biol*. 2014;15(12):550.
32. Hsu SD, Lin FM, Wu WY et al. miRTarBase: a database curates experimentally validated microRNA-target interactions. *Nucleic Acids Res*. 2011;39(Database issue):D163-9.
33. Bartel DP. MicroRNAs: target recognition and regulatory functions. *Cell*. 2009;136(2):215-33.
34. Sullivan BP, Weiss JA, Nie Y et al. Skeletal muscle IGF-1 is lower at rest and after resistance exercise in humans with obesity. *European Journal of Applied Physiology*. 2020.
35. Ma B, Hottiger MO. Crosstalk between Wnt/beta-Catenin and NF-kappaB Signaling Pathway during Inflammation. *Front Immunol*. 2016;7:378.
36. Costamagna D, Costelli P, Sampaolesi M, Penna F. Role of Inflammation in Muscle Homeostasis and Myogenesis. *Mediators Inflamm*. 2015;2015:805172.

37. Beals JW, Burd NA, Moore DR, van Vliet S. Obesity Alters the Muscle Protein Synthetic Response to Nutrition and Exercise. *Front Nutr*. 2019;6:87.
38. Fu X, Zhu M, Zhang S, Foretz M, Viollet B, Du M. Obesity Impairs Skeletal Muscle Regeneration Through Inhibition of AMPK. *Diabetes*. 2016;65(1):188-200.
39. Brown LA, Lee DE, Patton JF et al. Diet-induced obesity alters anabolic signalling in mice at the onset of skeletal muscle regeneration. *Acta Physiol (Oxf)*. 2015;215(1):46-57.
40. Zhou D, Strakovsky RS, Zhang X, Pan YX. The skeletal muscle Wnt pathway may modulate insulin resistance and muscle development in a diet-induced obese rat model. *Obesity (Silver Spring)*. 2012;20(8):1577-84.
41. Rome S, Forterre A, Mizgier ML, Bouzakri K. Skeletal Muscle-Released Extracellular Vesicles: State of the Art. *Front Physiol*. 2019;10:929.
42. Calvo JA, Daniels TG, Wang X et al. Muscle-specific expression of PPARgamma coactivator-1alpha improves exercise performance and increases peak oxygen uptake. *J Appl Physiol (1985)*. 2008;104(5):1304-12.
43. Jalabert A, Vial G, Guay C et al. Exosome-like vesicles released from lipid-induced insulin-resistant muscles modulate gene expression and proliferation of beta recipient cells in mice. *Diabetologia*. 2016;59(5):1049-58.
44. Pietrangelo T, Bondi D, Kinel E, Verratti V. The Bottom-Up Rise Strength Transfer in Elderly After Endurance and Resistance Training: The BURST. *Front Physiol*. 2018;9:1944.
45. Estrada AL, Valenti Z, Hehn G, Allen CP, Kruh-Garcia NA, Lark DS. Skeletal muscle tissue secretes more extracellular vesicles than white adipose tissue and myofibers are a major source ex vivo but not in vivo. *bioRxiv*. 2020:2020.09.27.313932.

Table 2.1. Primer sequences for qRT-PCR.

Gene Name	Gene ID	Forward (5'-3')	Reverse (5'-3')
18s	106632259	GGCCCTGTAATTGGAATGAGTC	CCAAGATCCAACTACGAGCTT
IGF-1	3479	GCTCTTCAGTTCGTGTGTGGA	GCCTCCTTAGATCACAGCTCC
β–Catenin	1499	AGCTTCCAGACACGCTATCAT	CGGTACAACGAGCTGTTTCTAC
Wnt3a	89780	AGGAAATTCAGCCCACCAGC	AGGAAATTCAGCCCACCAGC
Wnt5a	7474	TCGACTATGGCTACCGCTTTG	CACTCTCGTAGGAGCCCTTG
Wnt7a	7576	CAAGGAGCCGTGTAGAAGTGT	GCAAGGTGGGTACCTGCAA
IL-8	3576	TTTTGCCAAGGAGTGCTAAAGA	AACCCTCTGCACCCAGTTTTC
IL-10	3586	GACTTTAAGGGTTACCTGGGTTG	TCACATGCGCCTTGATGTCTG
Jun	3725	TCCAAGTGCCGAAAAAGGAAG	CGAGTTCTGAGCTTTCAAGGT
FOS	2353	GGGGCAAGGTGGAACAGTTAT	CCGCTTGGAGTGTATCAGTCA

Table 2.2. Subject Characteristics. INT – interaction; OB – obesity; Ex. Tr. – Exercise training; V̇O2MAX - maximal oxygen consumption; 1 RM- one repetition maximum; BMI - body mass index; HOMA-IR - homeostasis model assessment – insulin resistance; HOMA-β - homeostasis model assessment – β-cell function; TC – Total Cholesterol; HDL - high density lipoprotein; LDL - low density lipoprotein; TG – Triglycerides; TNF-α - Tumor Necrosis Factor α; CRP - C-reactive Protein; IL-6 - Interleukin-6. * Significantly different than all other groups. Mean ± SE.

	Pre		**Post**		**INT**	**OB**	**Ex. Tr.**
	LN (n=8)	**OB (n=8)**	**LN (n=8)**	**OB (n=8)**			
Age	27.0 ± 1.6	26.6 ± 1.2	-	-	-	0.85	-
Height (m)	1.78 ± 0.04	1.74 ± 0.04	-	-	-	0.51	-
Weight (kg)	74.4 ± 4.8	107.6 ± 7.7	74.3 ± 4.8	106.8 ± 7.7	0.14	<0.01	0.07
BMI (kg/m^2)	22.9 ± 1.0	35.2 ± 2.0	22.8 ± 1.0	35.0 ± 1.2	0.14	<0.01	0.07
VO_2max (L/min)	2.50 ± 0.27	2.79 ± 0.26	-	-	-	0.46	-
VO_2max (ml/kg/min)	33.6 ± 1.9	25.6 ± 2.1	-	-	-	0.01	-
1 RM (kg)	136.6 ± 17.6	182.6 ± 23.8	-	-	-	0.14	-
1 RM (kg/kg)	1.84 ± 0.18	1.68 ± 0.19	-	-	-	0.55	-
Glucose (mg/dl)	90.6 ± 3.7	86.3 ± 3.9	89.8 ± 2.0	90.6 ± 3.4	0.35	0.66	0.53
Insulin (uIU/ml)	8.8 ± 0.8	29.0 ± 6.9	7.9 ± 0.9	26.4 ± 7.4	0.84	<0.01	0.68
HOMA-IR	1.9 ± 0.2	6.2 ± 1.6	1.7 ± 0.2	5.8 ± 1.6	0.93	<0.01	0.76
HOMA-β	138.9 ± 34.3	653.6 ± 193.2	110.4 ± 14.7	395.1 ± 126.8	0.07	0.02	0.03
TC (mg/dl)	180.3 ± 11.7	190.6 ± 14.8	*163.9 ± 11.0	201.9 ± 12.8	<0.01	-	-
HDL (mg/dl)	47.1 ± 3.3	42.4 ± 3.9	47.5 ± 3.3	44.8 ± 5.3	0.48	0.51	0.34
LDL (mg/dl)	113.0 ± 10.4	120.9 ± 15.7	101.3 ± 9.4	135.0 ± 14.2	0.32	0.11	0.93
TG (mg/dl)	110.3 ± 10.3	136.9 ± 14.6	76.4 ± 7.8	110.8 ± 12.3	0.91	0.02	0.02
TNF-α (pg/ml)	0.7 ± 0.1	2.6 ± 1.8	0.6 ± 0.1	2.5 ± 1.6	0.12	0.04	0.67
CRP (pg/ml)	1175 ± 401	5283 ± 876	906 ± 131	5331 ± 721	0.61	<0.01	0.72
Il-6 (pg/ml)	1.4 ± 0.2	3.8 ± 1.6	1.8 ± 0.8	2.0 ± 0.4	0.27	0.17	0.51

Table 2.3. Subject characteristics for lean (LN) vs obese (OB) miRNA SEQ samples. V̇O2MAX - maximal oxygen consumption; 1 RM- one repetition maximum; BMI - body mass index; HOMA-IR - homeostasis model assessment – insulin resistance; HOMA-β - homeostasis model assessment – β-cell function; TC – Total Cholesterol; HDL - high density lipoprotein; LDL - low density lipoprotein; TG – Triglycerides; TNF-α - Tumor Necrosis Factor α; CRP - C-reactive Protein; IL-6 - Interleukin-6. Mean ± SE.

	LN (n=3)	**OB (n=4)**	**p-value**
Age	28.7 ± 2.4	26.8 ± 2.3	0.59
Height (m)	1.74 ± 0.07	1.72 ± 0.06	0.80
Weight (kg)	68.3 ± 5.3	95.7 ± 8.7	0.06
BMI (kg/m^2)	22.4 ± 0.5	32.2 ± 1.0	<0.01
VO_2max (L/min)	2.21 ± 0.49	2.34 ± 0.34	0.82
VO_2max (ml/kg/min)	31.6 ± 4.4	23.8 ± 3.4	0.21
1 RM (kg)	113.6 ± 22.7	164.4 ± 42.5	0.39
1 RM (kg/kg)	1.63 ± 0.20	1.66 ± 0.34	0.96
Glucose (mg/dl)	82.7 ± 5.0	84.0 ± 6.9	0.89
Insulin (uIU/ml)	10.0 ± 1.0	26.0 ± 9.3	0.21
HOMA-IR	2.02 ± 0.1	5.37 ± 1.9	0.20
HOMA-β	218.4 ± 74.6	770.0 ± 330.0	0.22
TC (mg/dL)	204.3 ± 13.9	201.8 ± 24.6	0.94
HDL (mg/dL)	55.0 ± 2.1	42.0 ± 4.7	0.08
LDL (mg/dL)	125.0 ± 14.0	129.8 ± 23.8	0.88
TG (mg/dL)	121.3 ± 16.0	149.5 ± 21.6	0.37
TNF-α (pg/µL)	0.73 ± 0.17	0.87 ± 0.05	0.38
CRP (pg/µL)	1440.4 ± 1075.7	3604.8 ± 932.7	0.19
Il-6 (pg/µL)	1.85 ± 0.54	2.94 ± 0.48	0.19

Table 2.4. Subject characteristics for exercise training miRNA SEQ samples. V̇O2MAX - maximal oxygen consumption; 1 RM- one repetition maximum; BMI - body mass index; HOMA-IR - homeostasis model assessment – insulin resistance; HOMA-β - homeostasis model assessment – β-cell function; TC – Total Cholesterol; HDL - high density lipoprotein; LDL - low density lipoprotein; TG – Triglycerides; TNF-α - Tumor Necrosis Factor α; CRP - C-reactive Protein; IL-6 - Interleukin-6. Mean ± SE.

	Pre (n=5)	**Post (n=5)**	**p-value**
Age	28.4 ± 1.6	-	-
Height (m)	1.73 ± 0.06	-	-
Weight (kg)	86.1 ± 9.1	85.2 ± 8.4	0.27
BMI (kg/m^2)	28.7 ± 2.5	28.4 ± 2.4	0.25
VO_2max (L/min)	2.21 ± 0.27	-	-
VO_2max (ml/kg/min)	25.8 ± 3.9	-	-
1 RM (kg)	134.8 ± 29.9	-	-
1 RM (kg/kg)	1.53 ± 0.21	-	-
Glucose (mg/dl)	78.6 ± 3.85	86.6 ± 1.5	0.10
Insulin (uIU/ml)	22.6 ± 8.0	22.6 ± 9.6	1.00
HOMA-IR	4.5 ± 1.7	4.8 ± 2.0	0.92
HOMA-β	700.6 ± 262.1	349.1 ± 151.3	0.11
TC (mg/dL)	215.6 ± 15.8	208.0 ± 21.1	0.52
HDL (mg/dL)	48.6 ± 4.8	50.4 ± 6.7	0.66
LDL (mg/dL)	137.2 ± 17.4	137.0 ± 20.7	0.98
TG (mg/dL)	148.8 ± 16.6	104.0 ± 13.9	0.07
TNF-α (pg/μL)	0.78 ± 0.1	0.93 ± 0.1	0.05
CRP (pg/μL)	3480.3 ± 825.7	3108.1 ± 806.0	0.56
Il-6 (pg/μL)	2.9 ± 0.4	1.91 ± 0.5	0.04

Table 2.5. Skeletal muscle extracellular vesicle microRNAs differentially expressed in individuals with obesity compared to lean controls.

Mature miRNA	Raw Counts		log2 Fold Change	p-value
	Lean	Obese		
hsa-let-7f-5p	82557.65	68740.5	-0.63	0.03
hsa-miR-1-3p	4564095	3056018	-0.98	0.01
hsa-miR-1275	3	15.75	2.04	0.01
hsa-miR-143-5p	17	63.5	1.71	0
hsa-miR-144-3p	281.33	169.25	-1.22	0.04
hsa-miR-155-5p	26.67	73.5	1.07	0.01
hsa-miR-302b-3p	0.67	8.5	2.66	0.03
hsa-miR-30c-1-3p	48.33	33.5	-0.85	0.03
hsa-miR-30e-5p	39744	27021.75	-0.97	0.03
hsa-miR-3168	13.67	6.75	-1.35	0.03
hsa-miR-337-3p	51	114.25	0.81	0.04
hsa-miR-3613-5p	918.67	580.75	-1.08	0.05
hsa-miR-376b-5p	1.33	9.25	2.48	0.01
hsa-miR-376c-5p	1.33	9.25	2.48	0.01
hsa-miR-409-5p	20.67	55.5	1.07	0.02
hsa-miR-432-5p	18	52.75	1.17	0.02
hsa-miR-4485-3p	0.33	6.75	1.63	0.03
hsa-miR-548a-3p	11.33	4.5	-1.94	0.02
hsa-miR-548ay-5p	16.67	6.75	-1.61	0.01
hsa-miR-654-5p	2.67	13.5	1.82	0.02
hsa-miR-7641	10.67	36	1.48	0.05
hsa-miR-7977	48.67	166.75	1.53	0.02

Table 2.6. Top 10 significant canonical pathways by p-value from Biological Pathway Analysis for differentially expressed skeletal muscle extracellular vesicle microRNAs in individuals with obesity compared to lean controls. Ratio = number of molecules in dataset/ total number of molecules in the pathway. Z-Score – indicates predicted upregulation or downregulation of pathway compared to lean controls.

Ingenuity Canonical Pathways	-log(p-value)	Ratio	Z-score	Molecules
Cardiac Hypertrophy Signaling (Enhanced)	7.4	0.24	-2.01	ACE, ACVR1, ACVR1C, ADRA2A, ADRB2, AGTR1, APEX1, ATF2, ATP2A2, BORCS8-MEF2B, CAMK2A, CD40LG, CHP1, CTNNB1, DIAPH2, EDN1, EDNRA, EDNRB, EIF2B3, EIF4E, ELK1, ENPP6, FASLG, FGF1, FGF10, FGF16, FGF17, FGF18, FGF20, FGF7, FZD3, FZD6, FZD7, GDPD1, GNA13, GNAI2, GNG2, GNG5, GSK3A, HAND1, HAND2, HDAC4, HDAC7, HSPB2, HSPB7, IGF1, IGF1R, IKBKE, IL13, IL13RA1, IL17C, IL17RD, IL2RB, IL3, IL36G, IL4R, INPP5F, ITGA2, JUN, KRAS, LIF, MAP3K1, MAP3K13, MAP3K2, MAP3K8, MAPK13, MEF2A, MEF2B, MKNK2, MRAS, MYC, NFATC2, NRAS, PDE12, PDE3A, PDE4A, PDE6B, PDE6D, PDE6G, PDE7A, PIK3CB, PIK3R6, PLCD3, PLCH2, PPP3CA, PPP3R1, PPP3R2, PRKACA, PRKACB, PRKAR2A, PRKCA, PRKCG, PRKCI, PTGS2, RALA, RALB, RAP1A, RAP1B, RASD2, RELA, RHOA, ROCK1, RPS6KB1, TGFBR1, TGFBR2, TGFBR3, TNFSF10, TNFSF11, TNFSF13B, TNFSF15, TNFSF9, WNT1, WNT11, WNT4, WNT5A, WNT7B, WNT8A, WNT9A
Molecular Mechanisms of Cancer	7.24	0.25		APAF1, ARHGEF18, ARHGEF3, ATR, BAK1, BCL2, BCL2L1, BMP1, CAMK2A, CASP3, CCND1, CCND2, CCNE2, CDC25A, CDK11B, CDK14, CDK15, CDK18, CDK19, CDK6, CDK8, CDK9, CDKN1A, CDKN1B, CDKN2B, CRK, CTNNB1, CTNND1, CYCS, E2F5, E2F6, E2F7, ELK1, FADD, FANCD2, FAS, FASLG, FOS, FZD3, FZD6, FZD7, GNA13, GNAI2, GNAT1, GRB2, GSK3A, HIF1A, ITGA2, JUN, KRAS, LRP1, MAPK13, MRAS, MYC, NAIP, NFKBIA, NRAS, PAK1, PIK3CB, PIK3R6, PMAIP1, PRKACA, PRKACB, PRKAR2A, PRKCA, PRKCG, PRKCI, PSENEN, RALA, RALB, RAP1A, RAP1B, RASA1, RASD2, RASGRF1, RELA, RHOA, RHOB, RHOG, RHOJ, RND2, SMAD1, SMAD2, SMAD9, SUV39H1, TAB1, TAB2, TCF4, TGFBR1, TGFBR2, TP53, TYK2, WNT1, WNT11, WNT4, WNT5A, WNT7B, WNT8A, WNT9A
Ovarian Cancer Signaling	5.35	0.30	-0.89	BCL2, CCND1, CD44, CTNNB1, EDN1, EDNRA, EGFR, FSHB, FZD3, FZD6, FZD7, GJA1, KRAS, MLH1, MRAS, NRAS, PIK3CB, PIK3R6, PRKACA, PRKACB, PRKAR2A, PTGS2, RALA, RALB, RAP1A, RAP1B, RASD2, RPS6KB1, SUV39H1, TCF4, TCF7, TCF7L2, TP53, VEGFA, VEGFB, WNT1, WNT11, WNT4, WNT5A, WNT7B, WNT8A, WNT9A
PEDF Signaling	5.3	0.35	-0.19	BCL2, BCL2L1, BDNF, ELK1, FAS, FASLG, GDNF, HNF1B, IKBKE, KRAS, MAPK13, MRAS, NFKBIA, NGF, NRAS, PIK3CB, PIK3R6, RALA, RALB, RAP1A, RAP1B, RASD2, RELA, RHOA, ROCK1, TCF4, TCF7, TCF7L2, TP53
Gαi Signaling	5.06	0.30	0.69	ADRA2A, AGTR1, APLNR, CHRM2, CNR1, CNR2, DRD3, GNAI2, GNG10, GNG12, GNG13, GNG2, GNG5, GPR17, GRB2, HRH3, HTR1A, HTR1E, HTR1F, KRAS, MRAS, NPR3, NPY1R, NRAS, PRKACA, PRKACB, PRKAR2A, RALA, RALB, RAP1A, RAP1B, RASD2, RGS14, RGS4, RGS7, S1PR1, TBXA2R, XCR1
Wnt/β-catenin Signaling	4.98	0.28	0.60	ACVR1, ACVR1C, CCND1, CD44, CSNK1A1, CSNK1D, CSNK1G2, CSNK2A1, CSNK2A2, CTNNB1, DKK1, DKK4, FZD3, FZD6, FZD7, GJA1, GSK3A, JUN, KREMEN1, LRP1, MAP4K1, MYC, PIN1, PPP2CA, PPP2R1A, PPP2R5A, PTPA, RARB, RARG, SFRP1, SOX12, SOX13, SOX21, TAB1, TCF4, TCF7, TCF7L2, TGFBR1, TGFBR2, TGFBR3, TP53, WNT1, WNT11, WNT4, WNT5A, WNT7B, WNT8A, WNT9A
Death Receptor Signaling	4.88	0.33	0.37	ACTA1, ACTB, ACTC1, APAF1, BCL2, CASP2, CASP3, CYCS, DFFB, FADD, FAS, FASLG, HSPB2, HSPB7, IKBKE, LIMK1, MAP4K4, NAIP, NFKBIA, PARP11, PARP16, PARP3, RELA, RIPK1, ROCK1, TNFRSF10A, TNFRSF10B, TNFSF10, TNFSF15, TNKS2
PI3K/AKT Signaling	4.85	0.30	0.65	BCL2, BCL2L1, CCND1, CDKN1A, CDKN1B, CTNNB1, EIF4E, GRB2, GSK3A, GYS1, IKBKE, INPP5B, INPP5D, INPP5F, INPP5J, ITGA2, KRAS, MAP3K8, MRAS, NFKBIA, NRAS, PIK3CB, PPP2CA, PPP2R1A, PPP2R5A, PTGS2, PTPA, RALA, RALB, RAP1A, RAP1B, RASD2, RELA, RHEB, RPS6KB1, THEM4, TP53, TYK2, YWHAQ
IGF-1 Signaling	4.81	0.31	-1.96	CCN1, CCN2, CCN3, CSNK2A1, CSNK2A2, ELK1, FOS, GRB2, IGF1, IGF1R, IGFBP5, JUN, KRAS, MRAS, NEDD4, NRAS, PIK3CB, PIK3R6, PRKACA, PRKACB, PRKAR2A, PRKCI, RALA, RALB, RAP1A, RAP1B, RASA1, RASD2, RPS6KB1, SOCS1, SOCS3, SOCS4, YWHAQ
PTEN Signaling	4.57	0.29	0.17	BCL2, BCL2L1, CASP3, CCND1, CDKN1A, CDKN1B, CSNK2A1, CSNK2A2, EGFR, FASLG, FLT4, FOXG1, FOXO4, GRB2, GSK3A, IGF1R, IKBKE, INPP5B, INPP5D, INPP5F, INPP5J, ITGA2, KRAS, MRAS, NRAS, PIK3CB, RALA, RALB, RAP1A, RAP1B, RASD2, RELA, RPS6KB1, SIRT6, TGFBR1, TGFBR2, TGFBR3

Table 2.7. Skeletal muscle extracellular vesicle miRNAs differentially expressed following concurrent exercise training compared to baseline.

Mature miRNA	Raw Counts		log2 Fold Change	p-value
	Pre	Post		
hsa-let-7f-2-3p	87.4	57	-0.68	0.04
hsa-miR-101-5p	20.4	9.6	-1.08	0.01
hsa-miR-1301-3p	74.8	132.8	0.93	0.03
hsa-miR-1307-3p	179.8	317	0.86	0.04
hsa-miR-146b-5p	181.6	312.6	0.91	0.01
hsa-miR-190a-5p	126.8	71.2	-0.92	0.03
hsa-miR-199a-5p	1881.2	1072.2	-0.71	0.05
hsa-miR-199b-5p	2681.4	1524.8	-0.72	0.01
hsa-miR-208b-5p	79.2	40	-0.99	0.02
hsa-miR-23a-5p	9.4	19.2	1.08	0.03
hsa-miR-296-3p	3.4	8	1.31	0.03
hsa-miR-3605-3p	4.2	10	1.25	0.04
hsa-miR-3609	16.6	8.2	-1.03	0.02
hsa-miR-3615	10.6	25	1.26	0.03
hsa-miR-370-3p	33.4	56.8	0.95	0.01
hsa-miR-3960	20.2	43	1.25	0.03
hsa-miR-409-3p	140.6	272	0.94	0.00
hsa-miR-4326	2.8	8.4	1.49	0.03
hsa-miR-4485-3p	18.6	87.2	2.59	0.00
hsa-miR-4485-5p	3.6	18.4	2.57	0.00
hsa-miR-4488	6	31.6	2.67	0.00
hsa-miR-4497	16.8	35.2	1.23	0.01
hsa-miR-483-3p	43.6	86.8	1.00	0.04
hsa-miR-483-5p	22.2	52.6	1.20	0.02
hsa-miR-485-5p	20	37.2	0.92	0.03
hsa-miR-486-5p	19897.6	35386.8	0.86	0.04
hsa-miR-629-5p	28	46.2	0.76	0.04
hsa-miR-7-5p	141	209.6	0.67	0.04

Table 2.8. Top 10 significant canonical pathways by p-value from Biological Pathway Analysis for differentially expressed extracellular vesicle microRNA following exercise training. Ratio = number of molecules in dataset/ total number of molecules in the pathway. Z-Score – indicates predicted upregulation or downregulation of pathway compared to baseline.

Ingenuity Canonical Pathways	-log(p-value)	Ratio	Z-score	Molecules
IL-10 Signaling	9.21	0.44		CCR5, CHUK, FCGR2A, FOS, HMOX1, IL10, IL10RB, IL1F10, IL1R1, IL1RAP, IL1RAPL2, IL1RL2, IL1RN, IL33, IL36A, IL36B, IL36G, IL36RN, IL37, JUN, LBP, MAP4K4, MAPK13, MAPK14, RELA, SOCS3, SP1, TNF, TRAF6, TYK2
IL-6 Signaling	8.81	0.34	-4.1	AKT2, CHUK, CRP, CSNK2B, CXCL8, FOS, GRB2, HRAS, HSPB7, IL1F10, IL1R1, IL1RAP, IL1RAPL2, IL1RL2, IL1RN, IL33, IL36A, IL36B, IL36G, IL36RN, IL37, IL6ST, JUN, LBP, MAP2K7, MAP4K4, MAPK13, MAPK14, MAPK3, MAPKAPK2, MRAS, NGFR, PIK3R2, RAF1, RAP1A, RASD1, RASD2, RELA, SOCS3, SOS2, TNF, TRAF6, VEGFA
Role of Macrophages, Fibroblasts and Endothelial Cells in Rheumatoid Arthritis	7.83	0.25		AKT2, APC2, CAMK2D, CCL5, CEBPA, CHP1, CHUK, CREB1, CREB3L3, CSF1, CXCL8, FOS, FRZB, FZD3, FZD4, FZD6, HRAS, IL10, IL17A, IL1F10, IL1R1, IL1RAP, IL1RAPL2, IL1RL2, IL1RN, IL33, IL36A, IL36B, IL36G, IL36RN, IL37, IL6ST, IRAK1, IRAK2, IRAK4, JUN, LRP1, LRP6, LTB, MAP2K7, MAPK14, MAPK3, MAPKAPK2, MIF, MRAS, NGFR, NOS2, OSM, PDGFC, PIK3R2, PLCH2, PLCZ1, PPP3R2, PRKCQ, PRKCZ, PROK1, RAF1, RAP1A, RASD1, RASD2, RELA, RHOA, ROR2, RYK, SOCS3, TCF7L2, TLR1, TLR10, TLR4, TLR9, TNF, TRAF1, TRAF6, VEGFA, VEGFD, WNT1, WNT2, WNT3A
PPAR Signaling	7.68	0.35	4.12	CHUK, CITED2, FOS, GRB2, HRAS, IL1F10, IL1R1, IL1RAP, IL1RAPL2, IL1RL2, IL1RN, IL33, IL36A, IL36B, IL36G, IL36RN, IL37, INS, JUN, MAP4K4, MAPK3, MRAS, NCOR2, NGFR, PDGFC, PDGFRA, PPARA, PPARGC1A, RAF1, RAP1A, RASD1, RASD2, RELA, SOS2, TNF, TRAF6
Toll-like Receptor Signaling	7.37	0.38	-3.9	CHUK, FOS, IL12A, IL1F10, IL1RN, IL33, IL36A, IL36B, IL36G, IL36RN, IL37, IRAK1, IRAK2, IRAK4, JUN, LBP, MAP4K4, MAPK13, MAPK14, PPARA, RELA, TLR1, TLR10, TLR4, TLR9, TNF, TOLLIP, TRAF1, TRAF6
Hepatic Cholestasis	6.46	0.27		ADCY1, CD40LG, CHUK, CXCL8, CYP7B1, IL12A, IL17A, IL17C, IL1F10, IL1R1, IL1RAP, IL1RAPL2, IL1RL2, IL1RN, IL2, IL33, IL36A, IL36B, IL36G, IL36RN, IL37, INS, IRAK1, IRAK2, IRAK4, JUN, LBP, LEP, LTB, NGFR, OSM, PPARA, PRKACA, PRKAG1, PRKAG2, PRKAR1B, PRKCQ, PRKCZ, RARA, RELA, SLC10A1, SLCO1C1, TGFB2, TLR4, TNF, TNFSF10, TNFSF13, TNFSF14, TNFSF4, TRAF6
HMGB1 Signaling	6.26	0.28	-3.02	AKT2, CD40LG, CXCL8, FOS, HRAS, IL12A, IL17A, IL17C, IL1F10, IL1R1, IL2, IL33, IL36A, IL36B, IL36G, IL37, JUN, KAT6B, LEP, LTB, MAP2K7, MAPK13, MAPK14, MAPK3, MRAS, NGFR, OSM, PIK3R2, RAC2, RAP1A, RASD1, RASD2, RELA, RHOA, RHOB, RHOG, RHOV, RND1, SP1, TGFB2, TLR4, TNF, TNFSF10, TNFSF13, TNFSF14, TNFSF4
Cardiac Hypertrophy Signaling (Enhanced)	5.66	0.21	-4.75	ADCY1, AKT2, ATP2A3, CAMK2D, CD40LG, CHP1, CHUK, CTF1, CXCL8, EDN1, EDNRA, EIF2B5, EIF4E, FGF1, FGF10, FGF11, FGF14, FGF17, FGF23, FGF7, FICD, FZD3, FZD4, FZD6, GDE1, GDPD1, GNA11, GNAI2, GNG5, GSK3A, H2BFM, HDAC4, HDAC8, HRAS, HSPB7, IFNAR1, IGF1, IL10RB, IL12A, IL12RB2, IL17A, IL17C, IL1F10, IL1R1, IL1RL2, IL2, IL2RB, IL33, IL36A, IL36B, IL36G, IL37, IL6ST, ITGA5, JUN, LEP, LTB, MAP2K7, MAP3K11, MAP3K8, MAP3K9, MAPK13, MAPK14, MAPK3, MAPKAPK2, MKNK1, MKNK2, MRAS, NGFR, NKX2-5, NPPA, OSM, PDE2A, PDE4A, PIK3R2, PLCH2, PLCZ1, PLN, PPP3R2, PRKACA, PRKAG1, PRKAG2, PRKAR1B, PRKCQ, PRKCZ, PTEN, RAF1, RAP1A, RASD1, RASD2, RELA, RHOA, TGFB2, TNF, TNFSF10, TNFSF13, TNFSF14, TNFSF4, WNT1, WNT2, WNT3A
G Beta Gamma Signaling	5.29	0.29	-4.35	ADCY1, AKT2, BTK, CACNA1B, CACNA2D4, CACNB1, CACNB2, CACNB4, CACNG2, CACNG4, CACNG7, CACNG8, CAV3, EGFR, GNA11, GNAI2, GNAT1, GNG5, GRB2, HRAS, KCNJ5, MAPK3, MRAS, PAK1, PRKACA, PRKAG1, PRKAG2, PRKAR1B, PRKCQ, PRKCZ, RAF1, RAP1A, RASD1, RASD2, SOS2
NF-κB Signaling	5.21	0.26	-5.73	AKT2, BCL10, CD40, CD40LG, CHUK, CSNK2B, EGFR, FADD, HRAS, IL1F10, IL1R1, IL1RN, IL33, IL36A, IL36B, IL36G, IL36RN, IL37, INS, IRAK1, IRAK4, MAP2K7, MAP3K8, MAP4K4, MRAS, NGFR, PDGFRA, PIK3R2, PRKACA, PRKCQ, PRKCZ, RAF1, RAP1A, RASD1, RASD2, RELA, TGFA, TLR1, TLR10, TLR4, TLR9, TNF, TNFRSF11A, TNIP1, TRAF6, ZAP70

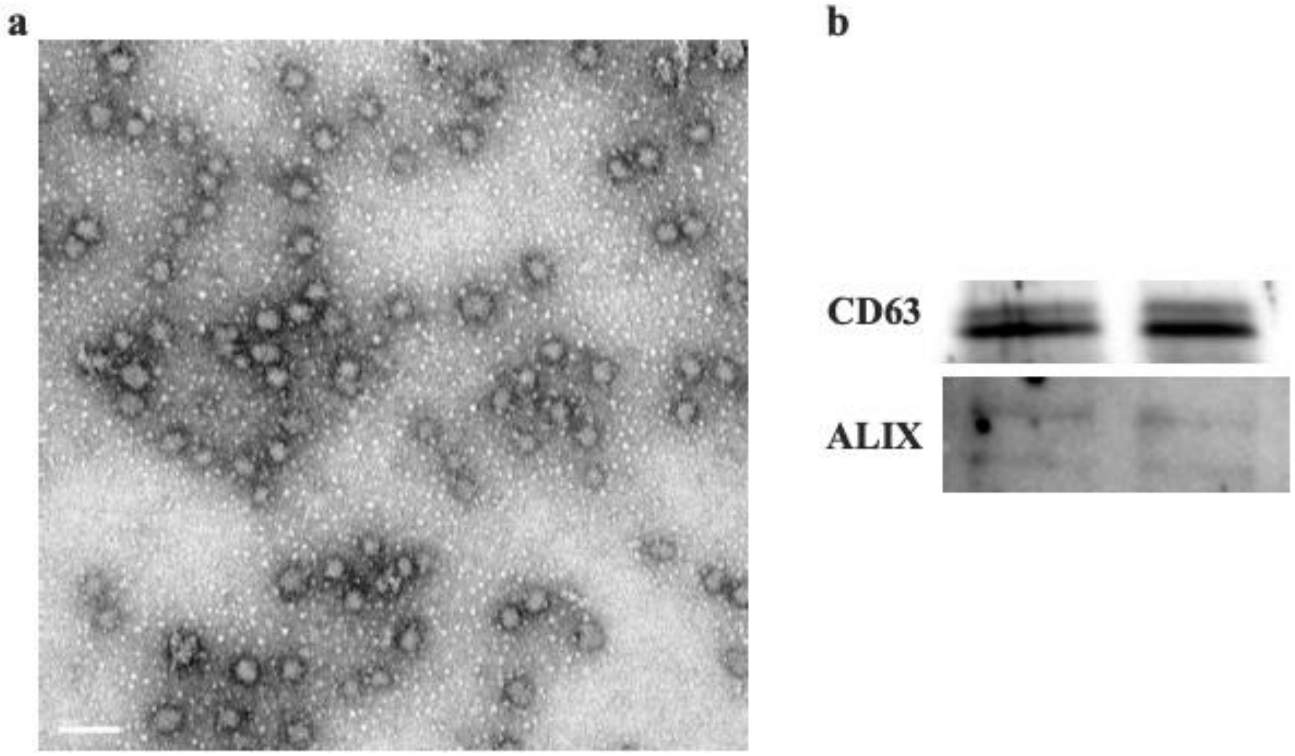

Figure 2.1. Characterization of skeletal muscle derived extracellular vesicles (EVs). (a) Representative transmission electron microscopy (TEM) image of EVs isolated from whole human skeletal muscle by ultracentrifugation. Scale bar = 100 nm. (b) Representative immunoblot images confirming the presence of the EV markers CD63 and Alix in EVs isolated from whole human muscle.

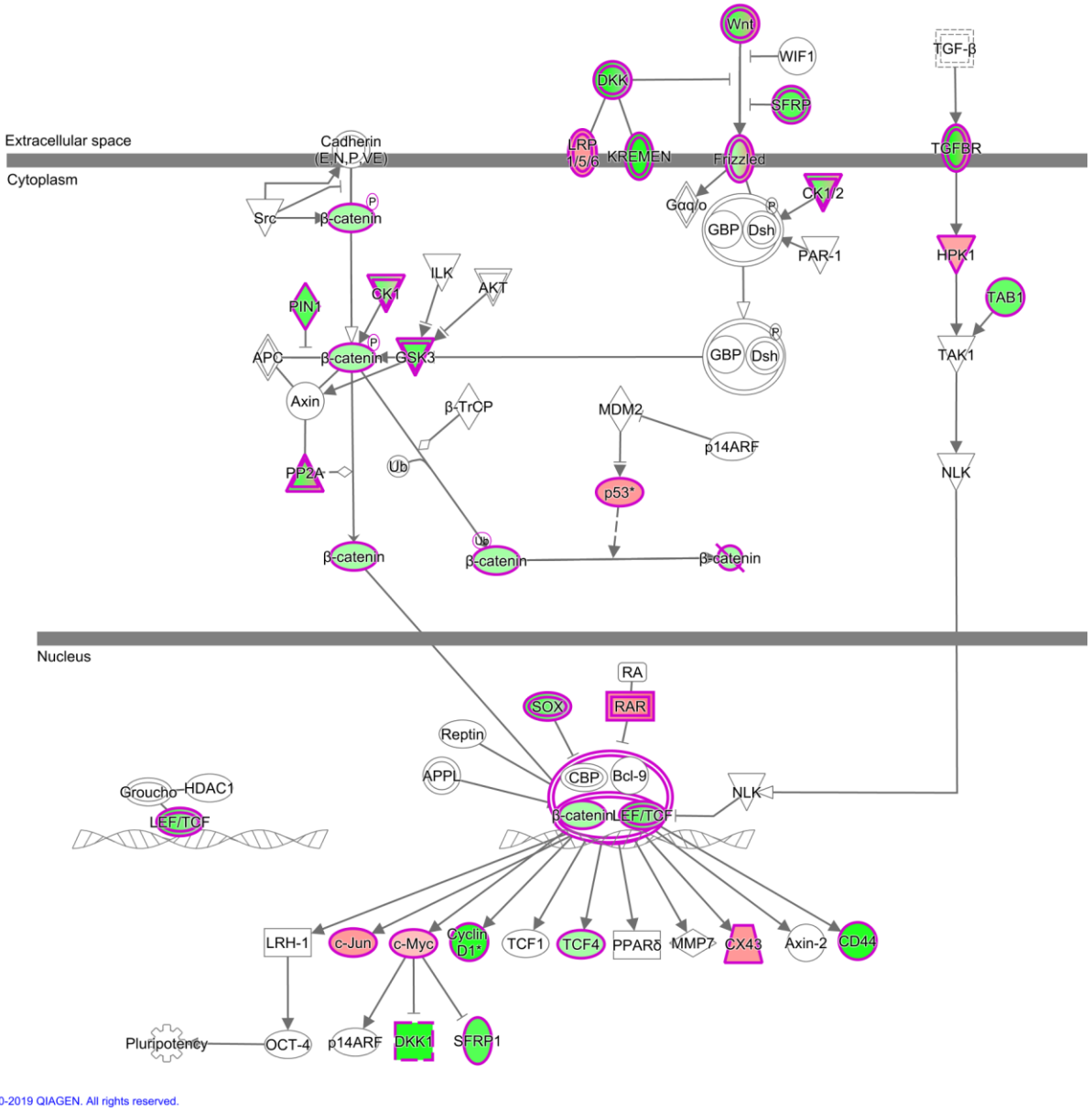

Figure 2.2. The Wnt/ b-Catenin Signaling pathway is targeted by differentially expressed microRNAs in obese skeletal muscle extracellular vesicles. The canonical pathway for Wnt/ β-Catenin was highly ranked as a target for the differentially expressed extracellular vesicles microRNAs isolated from obese skeletal muscle. Green color indicates predicted downregulation of target transcripts by differentially expressed microRNAs (i.e. upregulated microRNA that inhibit mRNA target production) and red color indicates predicted upregulation of mRNA Targets. The pathway was generated using QIAGEN's Ingenuity Pathway Analysis (IPA, QIAGEN Redwood City, www.qiagen.com/ingenuity).

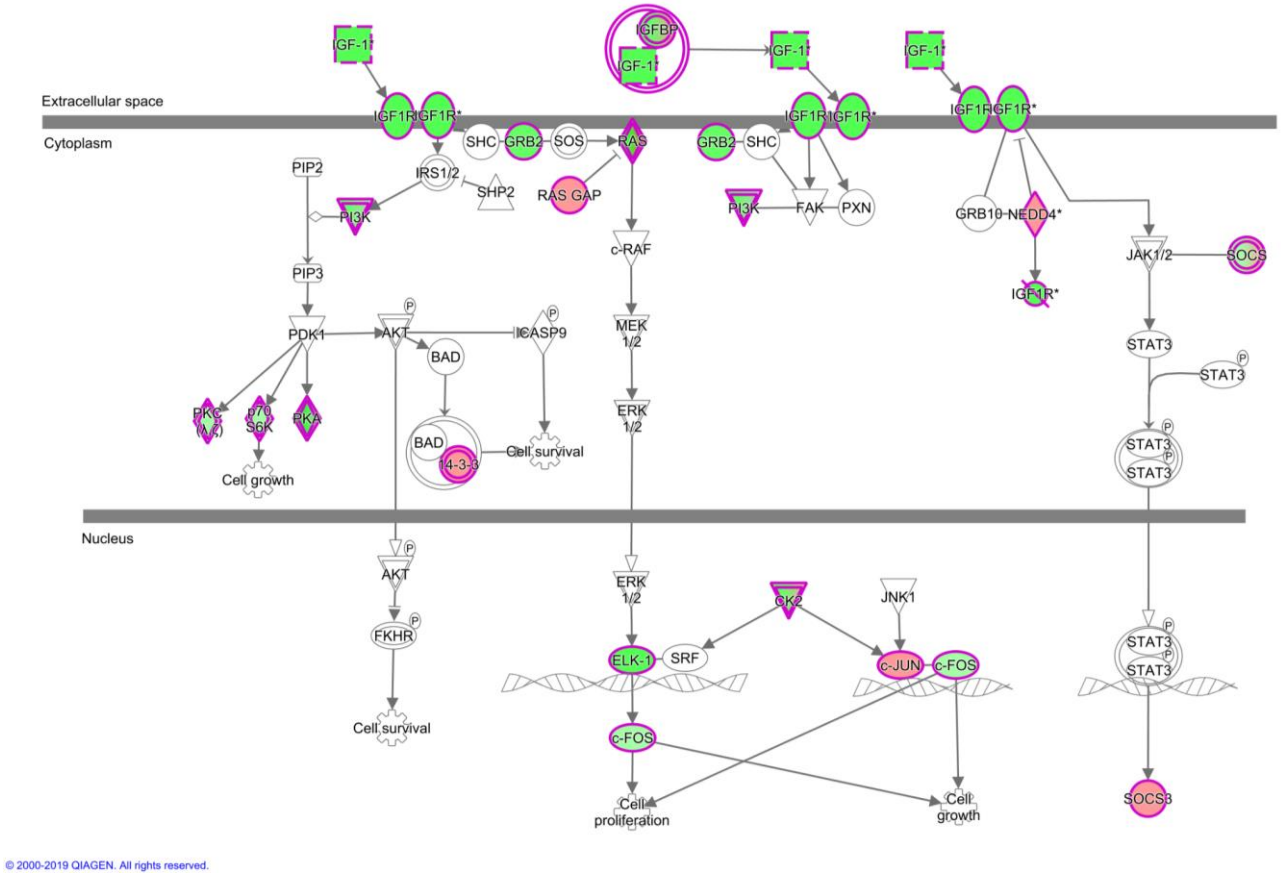

Figure 2.3. The IGF-1 Signaling pathway is targeted by differentially expressed microRNAs in obese skeletal muscle extracellular vesicles. The canonical pathway for IGF-1 was highly ranked as a target for the differentially expressed extracellular vesicles microRNAs isolated from obese skeletal muscle. Green color indicates predicted downregulation of target transcripts by differentially expressed microRNAs (i.e. upregulated microRNA that inhibit mRNA target production) and red color indicates predicted upregulation of mRNA Targets. The pathway was generated using QIAGEN's Ingenuity Pathway Analysis (IPA, QIAGEN Redwood City, www.qiagen.com/ingenuity).

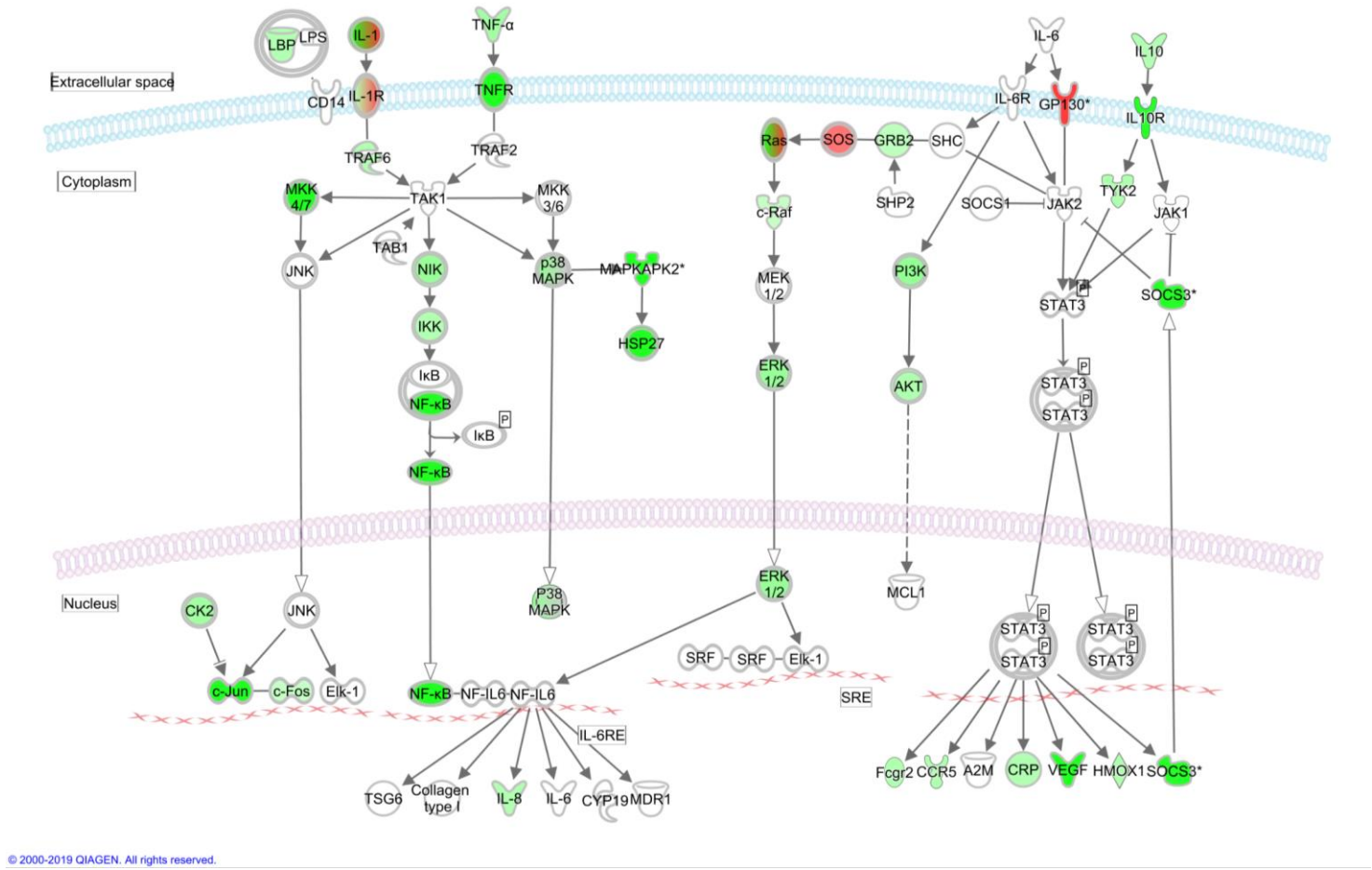

Figure 2.4. The IL-6 and IL-10 Signaling pathways are targeted by differentially expressed skeletal muscle extracellular vesicles microRNAs following concurrent exercise training in lean and obese humans. The canonical pathways for IL-6 and IL-10 were highly ranked as a target for the differentially expressed extracellular vesicles microRNAs isolated from skeletal muscle following exercise training. Green color indicates predicted downregulation of target transcripts by differentially expressed microRNAs (i.e. upregulated microRNA that inhibit mRNA target production) and red color indicates predicted upregulation of mRNA Targets. The pathway was generated using QIAGEN's Ingenuity Pathway Analysis (IPA, QIAGEN Redwood City, www.qiagen.com/ingenuity).

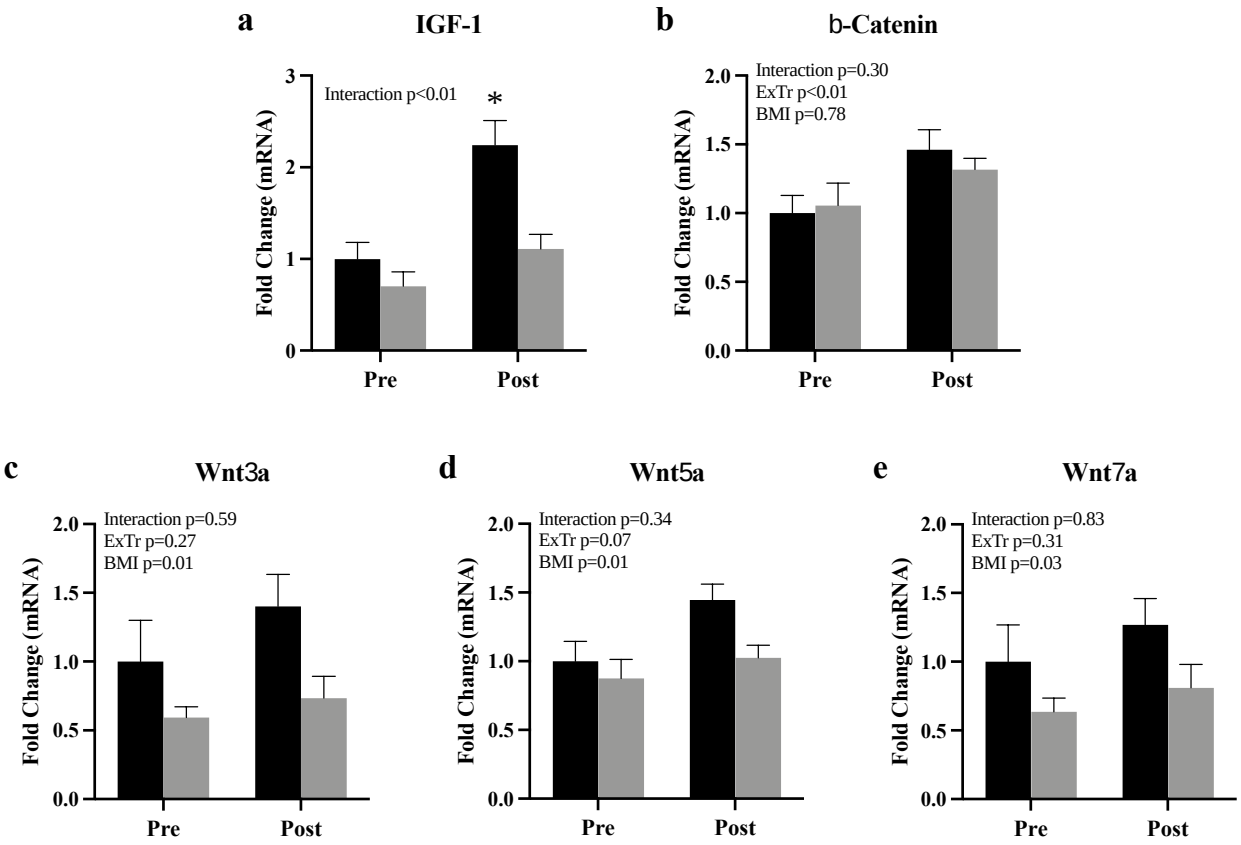

Figure 2.5. Whole skeletal muscle mRNA expression for (a) IGF-1, (b) b-Catenin, (c) Wnt3a, (d) Wnt5a and (e) Wnt7a before and after exercise training in LN and OB humans. * - Significantly different from all other groups ($P \leq 0.05$). LN Pre was set to 1. Black bars – LN; grey bars – OB. Mean ± SE. n=8/group.

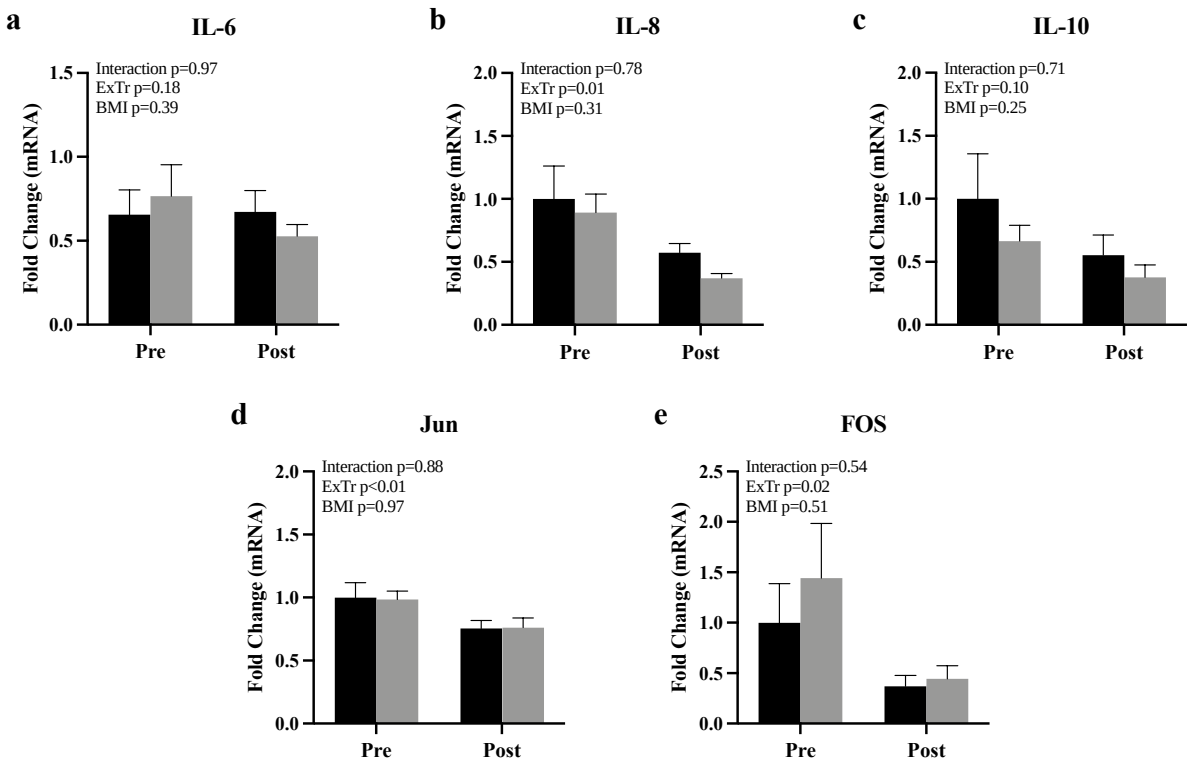

Figure 2.6. Whole skeletal muscle mRNA expression for (a) IL-6, (b) IL-8, (c) IL-10, (d) Jun and (e) Fos before and after exercise training in LN and OB humans. LN Pre was set to 1. Black bars – LN; grey bars – OB. Mean ± SE. n=8/group.

CHAPTER 3. EFFECTS OF PGC-1α OVEREXPRESSION ON CARDIOTOXIN-INDUCED DAMAGE AND REPAIR OF HUMAN MYOTUBES

Authors: Brian P. Sullivan[1], Allison Ellis[1], Chris K. Kargl[1], Shihuan Kuang[1], Timothy P. Gavin[1]

Affiliations:
[1]Purdue University, West Lafayette, IN

Corresponding Author: Timothy P. Gavin PhD, Department of Health and Kinesiology, Purdue University, 800 W. Stadium Ave., West Lafayette, IN 47907. Phone: (765) 494-3179, Fax: (765) 496-1239, Email: gavin1@purdue.edu

Abstract

Peroxisome proliferator-activated receptor-gamma coactivator-1 alpha (PGC1-α) is vital for the regulation of skeletal muscle energy metabolism and mitochondrial biogenesis but has also been implicated in the regulation of muscle plasticity, membrane integrity and muscle regeneration. The impact of PGC1-α on muscle fiber integrity and muscle regeneration in humans is critically understudied. The purpose of the present study was to examine if PGC1-α overexpression reduces cardiotoxin (CTX)-induced damage and improves regeneration after CTX treatment in human myotubes. **Methods**: Differentiated primary, human myotubes were transfected with adenovirus containing PGC1-α (Ad-PGC) or green fluorescent protein (Ad-GFP) for 24 hr. At 48 hr following transfection, myotubes were treated with 1.0 μM CTX or vehicle control (Veh) for 1 h. Cells were allowed to recover in skeletal muscle growth media for 3 days. Cells were isolated for analysis immediately (IP) and 3 days (3D) following CTX or Veh administration. Significance was established at $P \leq 0.05$. **Results**: Under normal conditions, Ad-PGC increased *PGC-1α* mRNA 50-fold, mitochondrial content 1.75-fold, and associated mitochondrial genes, SOD1, SOD2 and TFAM by 2, 6 and 3-fold respectively. Ad-PGC increased myotube fusion and attenuated the loss in myotube fusion index following CTX at IP (Ad-GFP = 58% of Veh; Ad-PGC= 80% of Veh). The percentage of EdU+ nuclei and total nuclei at 3D was reduced by ~50% in Ad-PGC. At 3D, Ad-PGC limited the increase in total nuclei during extended culture (Δ Nuclei: Ad-GFP= 180% of IP; Ad-PGC = 111% of IP) and limited the increase in myotube fusion in CTX treated cells from IP to 3D (Δ Myotube Fusion

Index: Ad-GFP= 151% of IP CTX; Ad-PGC= 109% of IP CTX). At 3D, PGC-AV treatment lowered mRNA expression of the myogenic regulatory factors, *MyoD*, *MRF4*, *Myf5* and *Myogenin*, indicating a reduction in proliferation and an increase in quiescent myoblasts. **Conclusion**: Overexpression of PGC-1α limits CTX induced decrease in the myotube fusion index but appears to limit the ability of undifferentiated cells to reenter the cell cycle, limiting the increase in total nuclei and myotube fusion index seen with Ad-GFP cells during extended culture.

Introduction

Exercise training mediated improvements in skeletal muscle quality and structural integrity protect against future damaging insults, known as exercise preconditioning (1). The protective effects of exercise training can be attributed in part to the exercise dependent increase in peroxisome proliferator-activated receptor γ coactivator 1α (PGC-1α), the master regulator of mitochondrial biogenesis, resulting in increased mitochondrial density and associated mitochondrial antioxidant capacity (2-4). PGC-1α exerts potent effects on muscle plasticity; protecting skeletal muscle from atrophy in unloading and denervation (5, 6), sarcopenia (7) and Duchenne muscular dystrophy (8, 9). There are a variety of mechanisms through which PGC-1α can improve muscle quality however, its role in improving muscle quality across a myriad of divergent disease states is still being elucidated.

Skeletal muscle regeneration is accompanied by an increase in PGC-1α and oxidative capacity; signifying the crucial regulatory role that mitochondrial biogenesis has during skeletal muscle regeneration (10-12). Aerobic exercise training increases the number and function of SCs (13); in contrast to exercise, PGC-1α overexpression in mice reduces SC number, however the proliferative potential of SCs is markedly increased, likely due to a remodeling of the SC niche (14). Correspondingly, blocking muscle PGC-1α expression in mice results in incomplete regeneration, characterized by smaller muscle FCSA and an increase in fibrotic tissue formation (15). Together these studies provide strong evidence that PGC-1α expression is vital for proper muscle regeneration due to its role regulating the extracellular matrix. However, PGC-1α may play an integral role in the regulation of SC activity during myogenesis and muscle regeneration through more direct means. Overexpression of PGC-1α in C2C12 myoblasts induces

differentiation, conversely the knockdown of PGC-1α ablates myotube formation (16). Additionally, PGC-1α overexpression accelerates the differentiation of primary human myoblasts and enhances myotube formation but doesn't alter proliferation rates (17). These findings provide evidence that PGC-1α enhances myoblast differentiation, however there are numerous gaps in our understanding of how PGC-1α effects SCs during muscle regeneration that need to be addressed.

Currently, our understanding of how PGC-1α alters SC function and muscle regeneration in humans is limited. The majority of previous *in vitro* work has often employed immortalized cell lines and the limited experiments that employ primary human cells often overexpresses PGC-1α in myoblasts (16-18). Myoblasts do not share many characteristics with quiescent SCs, limiting the translatability of these studies. During myoblast differentiation, myoblasts pause during the G1 phase and permanently exit the cell cycle before differentiating and fusing with existing myotubes or other differentiating myoblasts to form multinucleated myotubes (19). However, not all myoblasts differentiate leaving a distinct sub-population of undifferentiated, non-cycling myoblasts that are arrested in G0, commonly referred to as myogenic reserve cells (20). Myogenic reserve cells share numerous characteristics with quiescent SCs including their ability to self-renew, are Pax7+/MyoD- and are capable of reentering the cell cycle to generate progeny that contribute to the formation of multinucleated myotubes and the maintenance of the reserve cell population (20, 21). The present study will employ an extended culture model that will allow us to examine how PGC-1α adenovirus induced overexpression alters the ability of undifferentiated myoblasts and these myogenic reserve cells to contribute to the reformation of primary human myotubes following cardiotoxin (CTX) induced damage. The aim of the present study is to determine if overexpression of PGC-1α alters CTX induced damage and repair of primary human myotubes. We hypothesized that PGC-1α overexpression would protect against CTX induced damage and enhance repair of primary human myotubes.

Methods

This study was approved by the Purdue University Institutional Review Board in accordance with the Declaration of Helsinki. Written informed consent was obtained from all subjects prior to their participation in the study.

Isolation of Primary Human Myoblasts. Primary myoblasts were isolated as previously described (22). Briefly, muscle biopsies were performed on the vastus lateralis of eight, sedentary, lean individuals. Sedentary was defined as engaging in no more than 1 hour of physical activity per week. Muscle tissue was minced and digested in dispase II (Sigma-Aldrich) and Collagenase type 2 (Worthington Biochemical Corp.) for 20-30 min at 37°C. Filtered cells were pelleted and resuspended in Skeletal Muscle Growth Media (SkGM) (Cell Applications Inc.) containing 100 U/ml of penicillin and 100 μg/ml streptomycin, and plated on an uncoated dish for 90 minutes. Unattached cells were transferred to a collagen coated plate and grown to a minimum of 60% confluence in SkGM. Myoblasts were purified by magnetic activated cell sorting (MACS) with CD56+ microbeads (Miltenyi Biotec). The purified myoblasts were cultured in SkGM for use in the below experiments or frozen in liquid nitrogen for future use. All cells used in the below experiments were early passage and matched between groups.

Differentiation and Treatment of Myoblasts. In all experiments, passage 4 myoblasts were seeded on 6 and 48 well plates and grown in SkGM until 80% confluent. Myoblasts were terminally differentiated in differentiation media (SkDM) (Dulbecco's modified Eagle medium supplemented with 2% horse serum) for a total of 8 Days. On day 6 of differentiation, cells were incubated in SkDM for 24 hr containing adenovirus encoding for PGC-1α co-expressing GFP (Ad-PGC) or adenovirus expressing GFP alone (Ad-GFP) at a concentration of 7.5×10^6 pfu/ml. The adenoviruses overexpressing GFP and PGC-1α have been previously described (3, 5, 6). Following the 24 hr transfection, cells were washed with PBS and cultured in SkDM for an additional 24 hr before being treated with 1μM CTX or an equivalent volume of vehicle (PBS) for 1 hr. Previous *in vitro* studies have used 1μM of CTX for one hour resulting in a robust drop in myotube number and fusion index (23). Our own pilot experiments confirmed this while demonstrating that a significant portion of cultured cells maintain their viability. Cells were then washed with PBS and collected for respective assays. To assess how myotubes reform and regrow after injury, injured and uninjured myotubes were cultured for an additional 3 days in SkGM.

LDH Assay. The damage induced by CTX administration was quantified via LDH assay (CyQUANT, ThermoFisher Scientific) according to manufacturer's instructions as previously described (23). The LDH assay quantifies cytotoxicity by measuring the amount of red formazan produced as a part of a coupled enzymatic reaction in which LDH catalyzes the conversion of

lactate to pyruvate via NAD+ reduction and the oxidation of NADH by diaphorase. Immediately following CTX treatment, 50 µl of media was transferred to a 96 well plate and mixed with 50 µl of the LDH reaction mixture and incubated at room temperature for 30 min. Absorbance was measured at 680 and 490 nm. The 680 nm absorbance was subtracted from the 490 nm absorbance for each well. A fold change was calculated setting the GFP, vehicle treated myotubes to 1.

Cell Viability. The viability of human myotubes following CTX administration was assessed via a 3-(4,5-dimethylthiazol-2-yl)-2,5-diphenyltetrazolium bromide (MTT) assay as previously described (22, 24). The MTT assay measures cell metabolic activity by measuring the amount of formazan formed from MTT reduction by NADPH oxidoreductases. Following CTX treatment, the cells were washed with PBS and fresh media added to each well along with 50µl of 5 mg/ml MTT reagent to each well and incubated at standard culture conditions (37°C, 5% CO_2) for 2 hr. The media will then be drained, and the purple formazan dye will be dissolved in 100 µl of DMSO per well. Absorbance will be measured at 550 nm (accuscan; ThermoFisher Scientific).

Myoblast Proliferation and Differentiation following CTX treatment. Following CTX treatment of myotubes, the proliferation of undifferentiated, reserve cells was quantified by visualizing the incorporation of 5-ethynyl-2'-deoxyuridine (EdU) into actively dividing DNA. EdU staining was performed as previously described (25). Briefly, 2 mM EdU was added to the media 12 h prior to completion of treatment. Following completion of treatment, cells were fixed with ice-cold, 4% paraformaldehyde (PFA), washed and incubated in 100 mm Tris-HCl, pH 8.5 (Boston Biosciences, Royal Oak, MI, USA), 1 mm CuSO4 (Acros; ThermoFisher Scientific), 2.5 mm TAMRA Azide 568 (Invitrogen, Carlsbad, CA, USA) and 100 mm ascorbic acid (ThermoFisher Scientific) for 30 min. Prior to imaging, nuclei were co-stained with 4',6-diamidino-2-phenylindole (DAPI) (Invitrogen). Myoblasts were imaged immediately via fluorescence microscopy for co-localization of EdU to DAPI. The percentage of proliferating cells was determined using ImageJ (National Institutes of Health, Bethesda, MD, USA). Proliferation of undifferentiated, reserve cells was also quantified by calculating the change in total nuclei at 3 days compared to the total number of nuclei IP vehicle or CTX and expressed as a percent.

To quantify myotube formation, staining for myosin heavy chain (MHC) and DAPI was performed. Briefly, cells were fixed in 4% PFA for 15 min and then permeabilized with 100 mM glycine for 5 min at room temperature. Cells were then incubated in blocking buffer (PBS containing 5% goat serum, 2% bovine serum albumin, 0.2% triton X-100 and 0.1% sodium azide; Cell signaling Technologies) for 1 hr. Myotubes were subsequently incubated with MF20 antibody (DSHB), diluted 1:30 in blocking buffer overnight at 4°C. Cells were washed with PBS and incubated with secondary antibody (AlexaFlour 568, goat anti-mouse, IgG2B, ThermoFisher Scientific) and DAPI at a 1:500 and 1:1000 dilution respectively. Myotubes were visualized by fluorescence microscopy and analyzed in image J. The fusion index is the total number of nuclei incorporated into multinucleated, MHC^+ myotubes divided by the total number of nuclei in the field of view, expressed as a percentage. Myotube damage was quantified by calculating the change in the myotube fusion index immediately following CTX compared to each subjects Vehicle and expressed as a percent. Myotube reformation was quantified by calculating the change in myotube fusion index from immediately post CTX administration to 3 days following CTX and expressed as a percent.

RNA Isolation, Reverse Transcription and qRT-PCR. Total RNA was extracted using a Trizol reagent (Thermo Fisher Scientific) as previously described (26). For mRNA reverse transcription, first strand cDNA was generated by random hexamer primers with MMLV Reverse Transcriptase (Thermo Fisher Scientific). Real-time PCR detection was performed using SYBR green based chemistry on a CFX Connect (BioRad, Hercules, CA, USA). Primers are listed in Table 3.1. Gene expression was determined with the $2^{-\Delta\Delta Ct}$ relative quantification method and normalized to 18s. Housekeeping genes were validated to ensure expression was not influenced by the experimental procedure.

Western Blot. Western blotting analysis was performed using standard SDS-Page procedures. Briefly, protein was isolated from cell lysates in RIPA Buffer (50mm Tris HCL 7.4 pH, 150mm NaCl, 2mm EDTA, 0.1% SDS, 0.1% Triton x-100, 0.5% Sodium Deoxycholate) with phosphatase inhibitors (0.2 mM NA_3VO_4, 50 mM NaF) and a protease inhibitor cocktail (P8340, Sigma-Aldrich, St. Louis, MO, USA). 30 µg of total protein from muscle homogenates was fractionated on SDS-polyacrylamide gels; transferred to PVDF membrane; and incubated with PGC-1α primary antibody (Cell Signaling Technologies). Horseradish peroxide–conjugated secondary antibodies (Cell Signaling Technology, Danvers, MA) were incubated with the

membrane and images were obtained by chemiluminescence using a ChemiDoc Touch Imaging System and densitometric analysis performed by ImageLab software (BioRad, Hercules, CA, USA). Results were normalized to total protein.

Statistical Analysis. A two-way repeated measure analysis of variance (ANOVA) (PGC-1α × CTX) was used to analyze differences in gene expression, myotube fusion index, total nuclei, EdU and LDH. CTX serial dilution preliminary data were analyzed via a one-way non-repeated measures ANOVA. Following a significant F ratio, Fisher's LSD post-hoc analysis was performed. All other data were analyzed using Student's t-test. Significance was established at $P \leq 0.05$ level and data reported as Mean ± SE. All data was analyzed in GraphPad Prism (Version 9.10).

Results

Subject characteristics. Demographic characteristics for the six, sedentary lean subjects are located in Table 3.2. The average age of participants was 23.7 ± 2.4 years old. The average BMI for all subjects was 22.4 ± 0.9 kg/m^2. The HOMA-IR for all subjects was 2.1 ± 0.1, indicative of insulin sensitivity (27).

Dose and time-course of PGC-1α overexpression. In order to establish infection strategies, we exposed differentiated primary human myotubes (n=3) to different doses of adenovirus for 24 and 48 hr. PGC-1α protein and myotube fusion index was assessed. As predicted PGC-1α protein increased in a dose and time dependent manner (Figure 3.1A). Increased dose or time had a negligible effect on the myotube fusion index (Figure 3.1B). We chose to use the adenoviral dose of 7.5 x 10^6 pfu/ml for a transfection time of 24 hours as it increased PGC-1α protein expression approximately 50-fold over the non-viral control (0 pfu/ml). We chose to perform the adenoviral infection on day 6 of differentiation and perform all assays and harvest all cells 24 hr following transfection on day 8. The rationale for this approach was based upon data we obtained via MitoTracker Fluorometric assay which indicates that earlier transfection had minimal impact on mitochondrial content (Figure 3.1C).

Dosing of Cardiotoxin. The dose of CTX administered to differentiated myotubes was selected by assessing metabolic activity via MTT and myotube damage via fusion index following treatment with various doses of cardiotoxin (Figure 3.2). As expected, metabolic activity and the myotube fusion index were reduced in a dose dependent manner with the

greatest reduction occurring at the dose of 1.0 μM. Myotube fusion index returned to baseline in all but the 1.0 μM dose, however the greatest increase in myotube fusion occurred in the 1.0 μM group. Similarly, myotube metabolic activity increased after being cultured for 3 further days in SkGM, with the largest increase occurring at the 1.0 μM dose. We aimed to select a dose of CTX that would elicit the most amount of damage while maintaining the greatest cell viability. As shown by our pilot data this approach allowed for the greatest myogenic response. Consequently, we chose to perform all subsequent experiments at a dose of 1 μM.

PGC-1α overexpression increases mitochondrial density and the expression of mitochondrial genes. The effects of Ad-PGC on the gene expression of *PGC-1α* and related mitochondrial genes are located in Figure 3.3. As expected, Ad-PGC increased mitochondrial content by 60%, the expression of *PGC-1α* mRNA 50-fold and associated mitochondrial genes *SOD1, SOD2* and *TFAM* by approximately 2, 7.5 and 3-fold. Importantly, there were no differences between nonviral control treated cells and Ad-GFP in the expression of PGC-1α mRNA. Additionally, Ad-PGC reduced the expression of the E3 ubiquitin ligases, MuRF1 and Atrogin-1.

PGC-1a overexpression increases and preserves the myotube fusion index immediately following CTX-induced damage. We assessed myotube damage by fusion index and by measuring the activity of LDH released into the cell culture media. Results for myotube fusion index and media LDH following CTX or Veh administration are located in Figure 3.4. PGC-1α overexpression increased the myotube fusion index following CTX or Veh administration compared to GFP controls. CTX administration reduced the fusion index in both PGC and GFP treated cells. However, the reduction in fusion index was attenuated in PGC vs. GFP controls. CTX increased LDH activity in the media by approximately 5-fold in both GFP and PGC treated conditions. No differences were evident in media LDH activity between PGC and GFP. Immediately following CTX or Veh administration no differences were observed between GFP or PGC treated cells in the total number of nuclei.

Overexpression of PGC-1α reduces myoblast proliferation and myotube formation during recovery from CTX-induced damage. Following CTX administration, myotubes were allowed to recover for 3 days in SkGM. Proliferation of undifferentiated, reserve myoblasts was measured by EdU and by the counting of total nuclei; myotube reformation was measured by

fusion index (Figure 3.5). Ad-PGC reduced the percent of EdU+ nuclei 3 days following CTX or Veh administration in Ad-PGC treated cells. 3 days following CTX or Veh administration, an increase in total nuclei was noted in GFP treated cells only. No change in total nuclei was observed in PGC treated cells at 3 days compared to IP. Myotube fusion index was increased in all PGC treated cells 3 days post CTX or Veh administration compared to GFP treated cells. However, the fusion index increased significantly in GFP treated myotubes compared to PGC treated myotubes during the recovery period (150% vs 110% of IP CTX).

PGC-1α overexpression reduces expression of myogenic genes. Gene expression data 3 days following CTX or Veh administration is located in Figure 3.6. PGC-1α overexpression reduced *Pax3, MyoD, MRF4, Myf5, Myogenin, PCNA, p16, p53* and *CDK4* mRNA 3 days following CTX or Veh administration. A trend was observed for CTX to increase the expression of *MyoD* mRNA. No other differences in the expression of *Pax7, Pax3, MRF4, Myf5, Myogenin* or *PCNA* mRNA were noted.

Discussion

The principal findings of the present study are that PGC-1α overexpression in primary human myotubes, (1) is mildly protective against CTX-induced damage and (2) reduces the activation of undifferentiated, reserve myoblasts during extended culture. To our knowledge this is the first report that demonstrates the protective effects of PGC-1α overexpression in human myotubes against cardiotoxin induced damage.

PGC-1α mediates muscle fiber membrane integrity in a variety of disease states in mice including dystrophy, unloading and sarcopenia (5-9), however, the role of PGC-1α in the regulation of human muscle fiber integrity is critically understudied. In the present study we observed that overexpressing PGC-1α in primary human myotubes attenuates the CTX induced reduction in myotube fusion index. In contrast to this finding, Ad-PGC did not attenuate the CTX induced increase in LDH release. This discrepancy can likely be attributed to shifts in LDH isozyme composition. Transgenic mice overexpressing PGC-1α and adenoviral treated C2C12 myotubes increase transcription of *LDH B* and reduce transcription of *LDH A*, which code for the LDH H and LDH M subunits respectively (28). This shift in subunit composition and subsequent isozyme expression, increases the enzymatic activity of LDH to convert lactate to pyruvate by approximately 60% (28).

CTX generates significant necrosis *in vitro* by increasing cytosolic calcium, leading to an increase in the production of reactive oxygen species (ROS) and cytoskeleton degradation (29, 30). Mitochondria and the sarcoplasmic reticulum tightly regulate cellular calcium flux (31); subsequently, increases in PGC-1α can improve calcium handling by improving mitochondrial content, mitochondrial dynamics and by attenuating SR stress (32). In the present study, PGC-1α overexpression increased mitochondrial content, which may have attenuated myotube disruption by reducing sarcoplasmic Ca^{2+} levels after CTX (33). Additionally, Ad-PGC increased the expression of antioxidant enzymes, SOD1 and SOD2, and reduced the expression of the E3 ubiquitin ligases, MuRF1 and Atrogin-1; together, these PGC-1α induced alterations in gene expression could limit secondary damage by improving ROS scavenging (34, 35), and limiting the degradation of cytoskeletal proteins (6). While our findings are not able to provide unequivocal support for the mechanism(s) responsible for increased myotube integrity; our findings are in agreement with previous reports demonstrating the importance of PGC-1α for muscle integrity and extends these findings to humans.

In addition to the vital role that PGC-1α plays in the regulation of muscle fiber integrity, PGC-1α appears to be critical for the differentiation of myoblasts. As the master regulator of mitochondrial biogenesis, PGC-1α likely plays an important role in muscle regeneration; blocking mitochondrial biogenesis impairs muscle regeneration, resulting in smaller fibers and increased fibrosis (15). In the present study, PGC-1α overexpression increased the fusion index at all time points, in agreement with previous findings demonstrating that overexpressing PGC-1α accelerates and enhances myoblast differentiation in primary human and C2C12 myotubes (16, 17). However, we also observed that PGC-1α overexpression limits the restoration of myotube fusion after CTX induced myotube disruption.

The present study employed an extended culture model that allowed for undifferentiated myoblasts and myogenic reserve cells to function in a manner more akin to SCs than myoblasts, re-entering the cell cycle and producing progeny that maintain the reserve cell population or differentiate and aid in the reformation of myotubes. In the present study, PGC-1α overexpression appears to reduce the propensity for undifferentiated myoblasts and/or myogenic reserve cells to re-enter the cell cycle and proliferate. This appears to be in contrast to previously reported *in vivo* findings indicating that PGC-1α overexpression decreases the number of SCs,

but drastically increases the propensity for activation and proliferation (14). However, the authors attributed the increased propensity for SC activation to remodeling of the SC niche and not any direct effects of PGC-1α on SC's. Our gene expression data indicates that the dampened activation of myogenic reserve cells in Ad-PGC cultures is likely due to increased quiescence and not an increase in senescence. PGC-1α overexpression reduced the expression of the myogenic regulatory factors, *MyoD, MRF4, Myf5* and *Myogenin*, markers associated with senescence *p16*, *p53* and *CDK4*, and maintained the expression of *Pax7*. Our findings indicate that PGC-1α overexpression enhances myoblast differentiation but reduces the propensity for myogenic reserve cells and undifferentiated myoblasts to reenter the cell cycle.

Limitations. In the present study we did not measure β-galactosidase, however our results and those of previous reports make it unlikely that the lack of cellular expansion or increases in fusion index are due to increased senescence. We did not measure calcium influx induced by incubation with CTX, limiting the mechanistic conclusions that can be drawn. Additionally, we did not confirm that our pool of undifferentiated myoblasts were a true Pax7+/MyoD-, myogenic reserve cells population.

In conclusion, PGC-1α overexpression reduces CTX induced damage to myotubes but limits the reformation of myotubes by limiting the ability of myogenic reserve cells to reenter the cell cycle. Our findings indicate that PGC-1α promotes the maintenance of quiescence in myogenic reserve cells. Future work should investigate the mechanisms through which PGC-1α maintains the quiescence of myogenic reserve cells.

References

1. Powers SK, Bomkamp M, Ozdemir M, Hyatt H. Mechanisms of exercise-induced preconditioning in skeletal muscles. *Redox Biol*. 2020;35:101462.
2. Lin J, Wu H, Tarr PT et al. Transcriptional co-activator PGC-1 alpha drives the formation of slow-twitch muscle fibres. *Nature*. 2002;418(6899):797-801.
3. Huang TY, Zheng D, Houmard JA, Brault JJ, Hickner RC, Cortright RN. Overexpression of PGC-1alpha increases peroxisomal activity and mitochondrial fatty acid oxidation in human primary myotubes. *Am J Physiol Endocrinol Metab*. 2017;312(4):E253-E63.
4. Lira VA, Benton CR, Yan Z, Bonen A. PGC-1alpha regulation by exercise training and its influences on muscle function and insulin sensitivity. *Am J Physiol Endocrinol Metab*. 2010;299(2):E145-61.
5. Sandri M, Lin J, Handschin C et al. PGC-1alpha protects skeletal muscle from atrophy by suppressing FoxO3 action and atrophy-specific gene transcription. *Proc Natl Acad Sci U S A*. 2006;103(44):16260-5.
6. Brault JJ, Jespersen JG, Goldberg AL. Peroxisome proliferator-activated receptor gamma coactivator 1alpha or 1beta overexpression inhibits muscle protein degradation, induction of ubiquitin ligases, and disuse atrophy. *J Biol Chem*. 2010;285(25):19460-71.
7. Ji LL, Kang C. Role of PGC-1alpha in sarcopenia: etiology and potential intervention - a mini-review. *Gerontology*. 2015;61(2):139-48.
8. Handschin C, Chin S, Li P et al. Skeletal muscle fiber-type switching, exercise intolerance, and myopathy in PGC-1alpha muscle-specific knock-out animals. *J Biol Chem*. 2007;282(41):30014-21.
9. Selsby JT, Morine KJ, Pendrak K, Barton ER, Sweeney HL. Rescue of dystrophic skeletal muscle by PGC-1alpha involves a fast to slow fiber type shift in the mdx mouse. *PLoS One*. 2012;7(1):e30063.
10. Duguez S, Feasson L, Denis C, Freyssenet D. Mitochondrial biogenesis during skeletal muscle regeneration. *Am J Physiol Endocrinol Metab*. 2002;282(4):E802-9.
11. Charge SB, Rudnicki MA. Cellular and molecular regulation of muscle regeneration. *Physiol Rev*. 2004;84(1):209-38.

12. Theeuwes WF, Gosker HR, Langen RCJ, Pansters NAM, Schols A, Remels AHV. Inactivation of glycogen synthase kinase 3beta (GSK-3beta) enhances mitochondrial biogenesis during myogenesis. *Biochim Biophys Acta Mol Basis Dis*. 2018;1864(9 Pt B):2913-26.
13. Shefer G, Rauner G, Yablonka-Reuveni Z, Benayahu D. Reduced satellite cell numbers and myogenic capacity in aging can be alleviated by endurance exercise. *PLoS One*. 2010;5(10):e13307.
14. Dinulovic I, Furrer R, Beer M, Ferry A, Cardel B, Handschin C. Muscle PGC-1alpha modulates satellite cell number and proliferation by remodeling the stem cell niche. *Skelet Muscle*. 2016;6(1):39.
15. Wagatsuma A, Kotake N, Yamada S. Muscle regeneration occurs to coincide with mitochondrial biogenesis. *Mol Cell Biochem*. 2011;349(1-2):139-47.
16. Lin Y, Zhao Y, Li R, Gong J, Zheng Y, Wang Y. PGC-1α is associated with C2C12 Myoblast differentiation. *Open Life Sciences*. 2014;9(11):1030-6.
17. Haralampieva D, Salemi S, Dinulovic I et al. Human Muscle Precursor Cells Overexpressing PGC-1alpha Enhance Early Skeletal Muscle Tissue Formation. *Cell Transplant*. 2017;26(6):1103-14.
18. Brown EL, Foletta VC, Wright CR et al. PGC-1alpha and PGC-1beta Increase Protein Synthesis via ERRalpha in C2C12 Myotubes. *Front Physiol*. 2018;9:1336.
19. Asfour HA, Allouh MZ, Said RS. Myogenic regulatory factors: The orchestrators of myogenesis after 30 years of discovery. *Exp Biol Med (Maywood)*. 2018;243(2):118-28.
20. Yoshida N, Yoshida S, Koishi K, Masuda K, Nabeshima Y. Cell heterogeneity upon myogenic differentiation: down-regulation of MyoD and Myf-5 generates 'reserve cells'. *J Cell Sci*. 1998;111 (Pt 6):769-79.
21. Baroffio A, Hamann M, Bernheim L, Bochaton-Piallat M-L, Gabbiani G, Bader CR. Identification of self-renewing myoblasts in the progeny of single human muscle satellite cells. *Differentiation*. 1996;60(1):47-57.
22. Kargl CK, Nie Y, Evans S et al. Factors secreted from high glucose treated endothelial cells impair expansion and differentiation of human skeletal muscle satellite cells. *J Physiol*. 2019;597(20):5109-24.

23. Langone F, Cannata S, Fuoco C et al. Metformin protects skeletal muscle from cardiotoxin induced degeneration. *PLoS One*. 2014;9(12):e114018.
24. Nie Y, Sato Y, Garner RT et al. Skeletal muscle-derived exosomes regulate endothelial cell functions via reactive oxygen species-activated nuclear factor-kappaB signalling. *Exp Physiol*. 2019;104(8):1262-73.
25. Salic A, Mitchison TJ. A chemical method for fast and sensitive detection of DNA synthesis in vivo. *Proc Natl Acad Sci U S A*. 2008;105(7):2415-20.
26. Nie Y, Sato Y, Wang C, Yue F, Kuang S, Gavin TP. Impaired exercise tolerance, mitochondrial biogenesis, and muscle fiber maintenance in miR-133a-deficient mice. *FASEB J*. 2016;30(11):3745-58.
27. Stern SE, Williams K, Ferrannini E, DeFronzo RA, Bogardus C, Stern MP. Identification of individuals with insulin resistance using routine clinical measurements. *Diabetes*. 2005;54(2):333-9.
28. Summermatter S, Santos G, Perez-Schindler J, Handschin C. Skeletal muscle PGC-1alpha controls whole-body lactate homeostasis through estrogen-related receptor alpha-dependent activation of LDH B and repression of LDH A. *Proc Natl Acad Sci U S A*. 2013;110(21):8738-43.
29. Wang HX, Lau SY, Huang SJ, Kwan CY, Wong TM. Cobra venom cardiotoxin induces perturbations of cytosolic calcium homeostasis and hypercontracture in adult rat ventricular myocytes. *J Mol Cell Cardiol*. 1997;29(10):2759-70.
30. Mendez I, Gutierrez JM, Angulo Y, Calvete JJ, Lomonte B. Comparative study of the cytolytic activity of snake venoms from African spitting cobras (Naja spp., Elapidae) and its neutralization by a polyspecific antivenom. *Toxicon*. 2011;58(6-7):558-64.
31. Rizzuto R, De Stefani D, Raffaello A, Mammucari C. Mitochondria as sensors and regulators of calcium signalling. *Nat Rev Mol Cell Biol*. 2012;13(9):566-78.
32. Gill JF, Delezie J, Santos G et al. Peroxisome proliferator-activated receptor gamma coactivator 1alpha regulates mitochondrial calcium homeostasis, sarcoplasmic reticulum stress, and cell death to mitigate skeletal muscle aging. *Aging Cell*. 2019;18(5):e12993.
33. Romero-Garcia S, Prado-Garcia H. Mitochondrial calcium: Transport and modulation of cellular processes in homeostasis and cancer (Review). *Int J Oncol*. 2019;54(4):1155-67.

34. Ebbeling CB, Clarkson PM. Exercise-induced muscle damage and adaptation. *Sports Med*. 1989;7(4):207-34.
35. Gissel H. The role of Ca2+ in muscle cell damage. *Ann N Y Acad Sci*. 2005;1066:166-80.

Table 3.1. Summary of Primers used for qRT-PCR.

Gene Name	Gene ID	Forward (5'-3')	Reverse (5'-3')
18s	106632259	GGCCCTGTAATTGGAATGAGTC	CCAAGATCCAACTACGAGCTT
PGC-1α	10891	TCTGAGTCTGTATGGAGTGACAT	CCAAGTCGTTCACATCTAGTTCA
SOD1	6647	GGTGGGCCAAAGGATGAAGAG	CCACAAGCCAAACGACTTCC
SOD2	6648	GCTCCGGTTTTGGGGTATCTG	GCGTTGATGTGAGGTTCCAG
TFAM	7019	ATGGCGTTTCTCCGAAGCAT	TCCGCCCTATAAGCATCTTGA
MuRF1	84676	CTTCCAGGCTGCAAATCCCTA	ACACTCCGTGACGATCCATGA
Atrogin-1	114907	GCCTTTGTGCCTACAACTGAA	CTGCCCTTTGTCTGACAGAAT
Pax7	5081	ACCCCTGCCTAACCACATC	GCGGCAAAGAATCTTGGAGAC
Pax3	5077	AGCTCGGCGGTGTTTTTATCA	CTGCACAGGATCTTGGAGACG
MyoD	4654	CGCCATCCGCTATATCGAGG	CTGTAGTCCATCATGCCGTCG
MRF4	4618	GGAGCGCCATCAGCTATATTG	ATCCGCACCCTCAAGATTTTC
Myf5	4617	CTGCCAGTTCTCACCTTCTGA	AACTCGTCCCCAAATTCACCC
Myogenin	4656	GGGGAAAACTACCTGCCTGTC	AGGCGCTCGATGTACTGGAT
PCNA	5111	CCTGCTGGGATATTAGCTCCA	CAGCGGTAGGTGTCGAAGC
p16	1029	ATGGAGCCTTCGGCTGACT	GTAACTATTCGGTGCGTTGGG
p53	7157	CAGCACATGACGGAGGTTGT	TCATCCAAATACTCCACACGC
CDK4	1019	CCATCAGCACAGTTCGTGAGGT	TCAGTTCGGGATGTGGCACAGA

Table 3.2. Subject Characteristics. Values are Mean ± SE (n=6). BMI- body mass index. HOMA-IR- homeostasis model assessment for insulin resistance. HDL- high density lipoprotein. LDL- low density lipoprotein.

Characteristics	**Value**
Age (yr)	23.7 ± 2.4
BMI (kg/m^2)	22.4 ± 0.9
Glucose (mg/dl)	91.5 ± 1.9
Insulin (μU/ml)	9.3 ± 0.1
HOMA-IR	2.1 ± 0.6
Total Cholesterol (mg/dl)	171.5 ± 12.4
HDL (mg/dl)	48.8 ± 4.7
LDL (mg/dl)	102.7 ± 13.3
Triglycerides (mg/dl)	100.8 ± 16.5

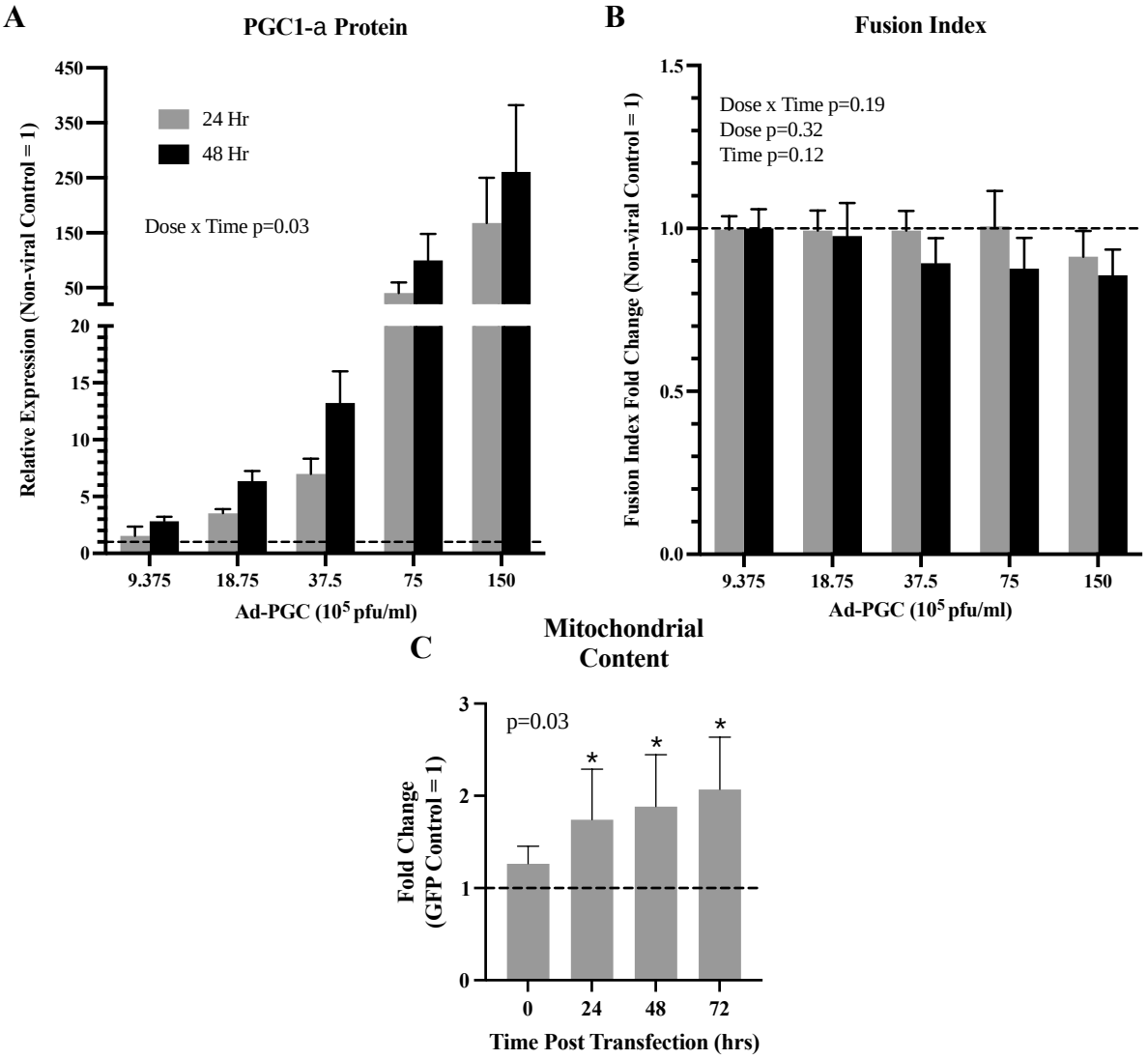

Figure 3.1. Overexpression of PGC-1α increases the expression of PGC-1α protein in a dose and time dependent manner in primary human myotubes. Human skeletal muscle cells were isolated from vastus lateralis needle biopsies and exposed to varying doses (plaque-forming units (pfu)/ml media) of PGC-1α adenovirus on Day 6 of differentiation for either 24 or 48 hr and collected on Day 8. (A) Expression of PGC-1α protein following 24 or 48 hr transfection with PGC-1α adenovirus. (B) Fusion index following 24 or 48 hr transfection with PGC-1α adenovirus. (C) Mitochondrial content assessed fluorometrically via MitoTracker Green FM at various times after 24 hr transfection with 75 x 10^5 pfu/ml of PGC-1α adenovirus. Light grey bars – 24 hr; dark grey bars – 48 hr. *-Significantly different than GFP Control ($P \leq 0.05$). n=3/group. Mean ± SE.

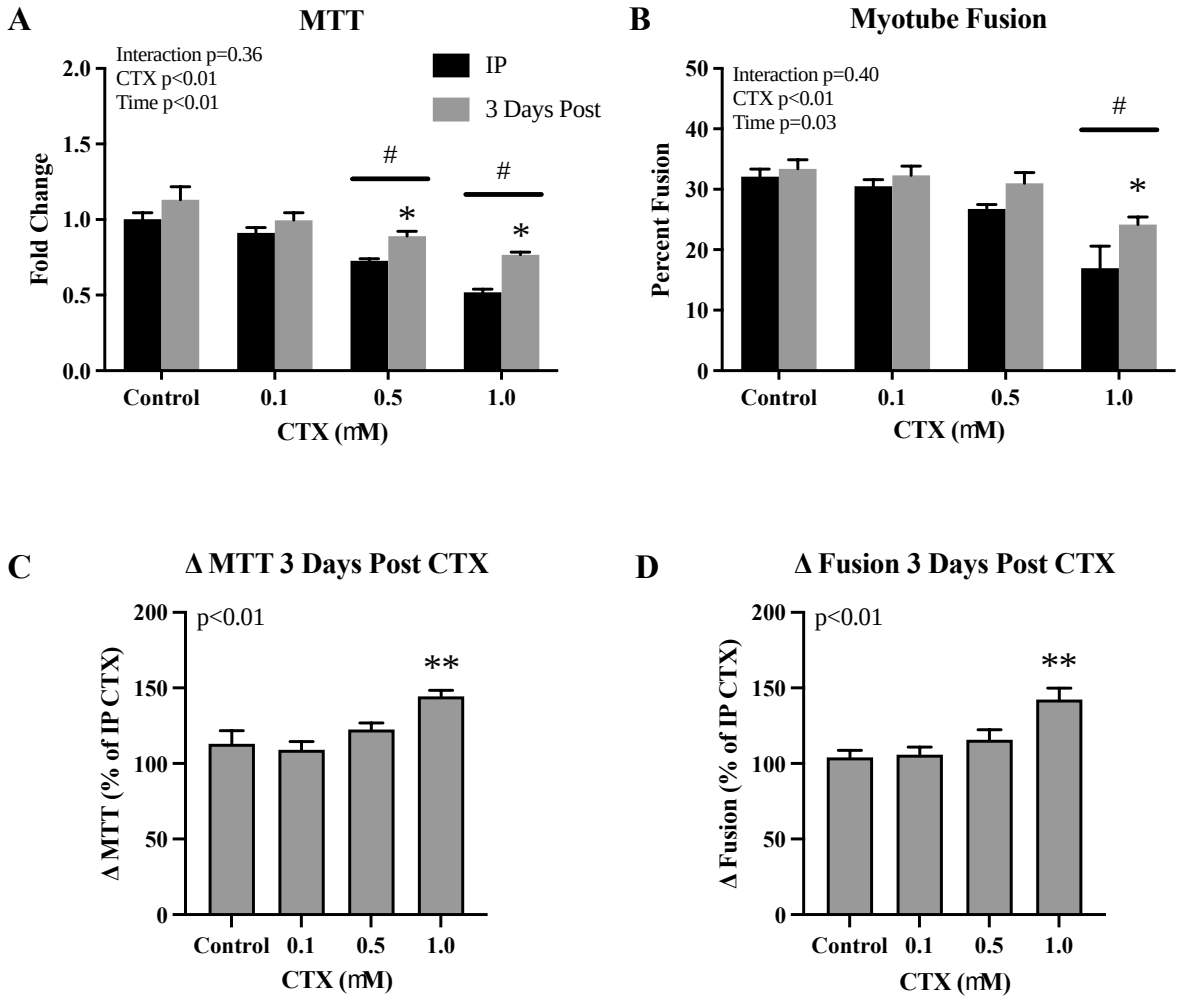

Figure 3.2. Cardiotoxin (CTX) reduces cell viability and myotube fusion in a dose dependent manner. Differentiated primary human myotubes from lean donors were exposed to cardiotoxin at various doses for 1 hr and either harvested immediately or placed in skeletal muscle growth media for 3 days to facilitate myotube recovery. (A) Cell viability measured via MTT assay and (B) myotube fusion immediately and 3 days after exposure to various doses of CTX for 1 hr. The change in (C) cell viability and (D) myotube fusion after 3 days of recovery in skeletal muscle growth media compared to immediately following CTX administration. Graphs A and B: Black bars – Immediately post (IP); grey bars – 3 Days Post. * - Significantly different than own IP ($P \leq 0.05$). # - Significantly different than control ($P \leq 0.05$). ** - Significantly different than all other groups ($P \leq 0.05$). Mean ± SE. n=4 - 7/group.

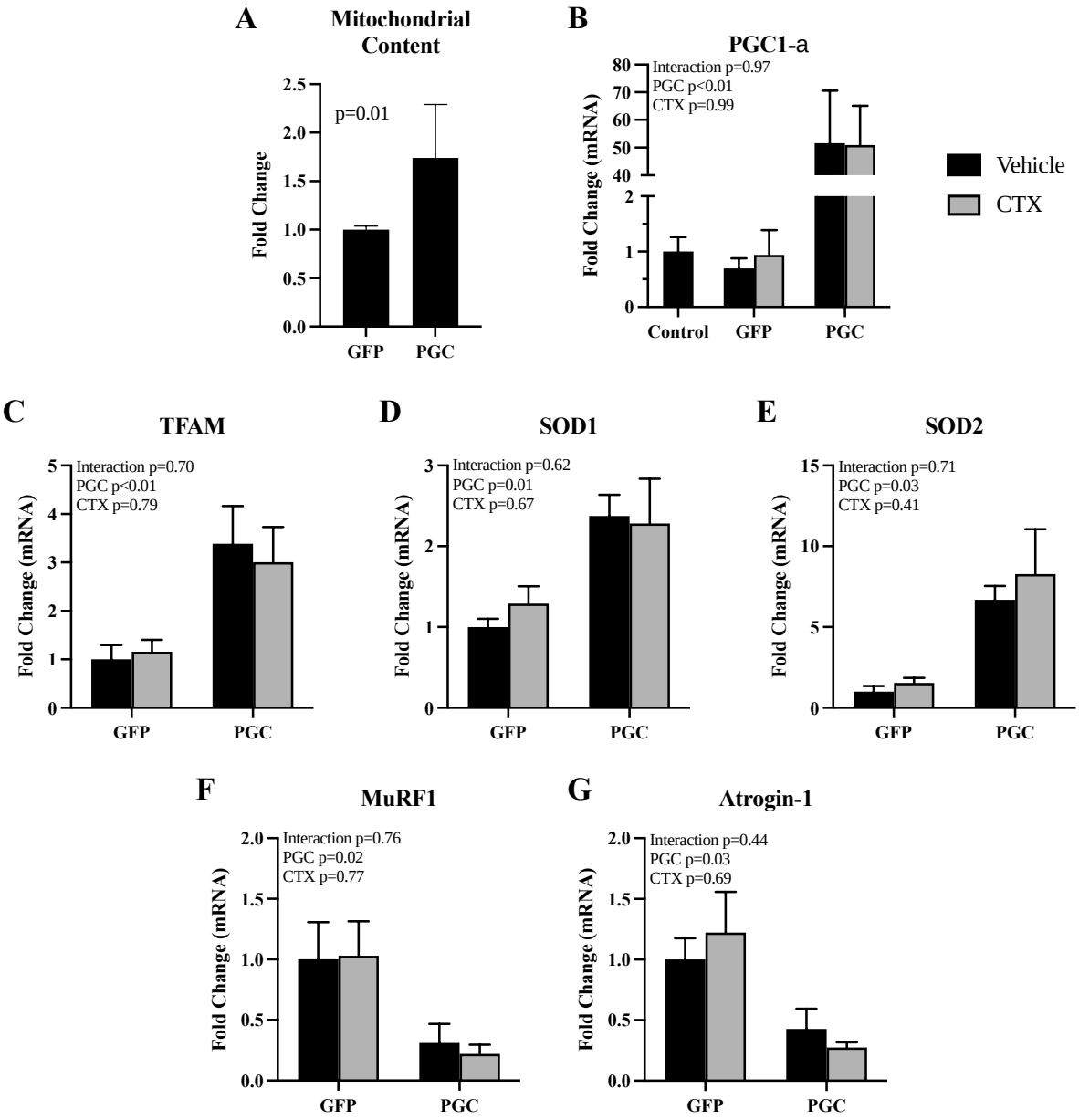

Figure 3.3. PGC-1α increases mitochondrial content and associated mitochondrial genes and reduces the expression of the E3 ubiquitin ligases. (A) Mitochondrial content assessed fluorometrically via MitoTracker Green FM in primary human myotubes overexpressing PGC-1α or GFP controls. mRNA expression of (B) *PGC-1α*, (C) *TFAM*, (D) *SOD1*, (E) *SOD2*, (F) *MuRF1* and (G) *Atrogin-1* immediately after 1 hr treatment with vehicle (control) or CTX in myotubes overexpressing PGC-1α or GFP controls. Black bars – vehicle; grey bars – CTX. Mean ± SE. n=5/group.

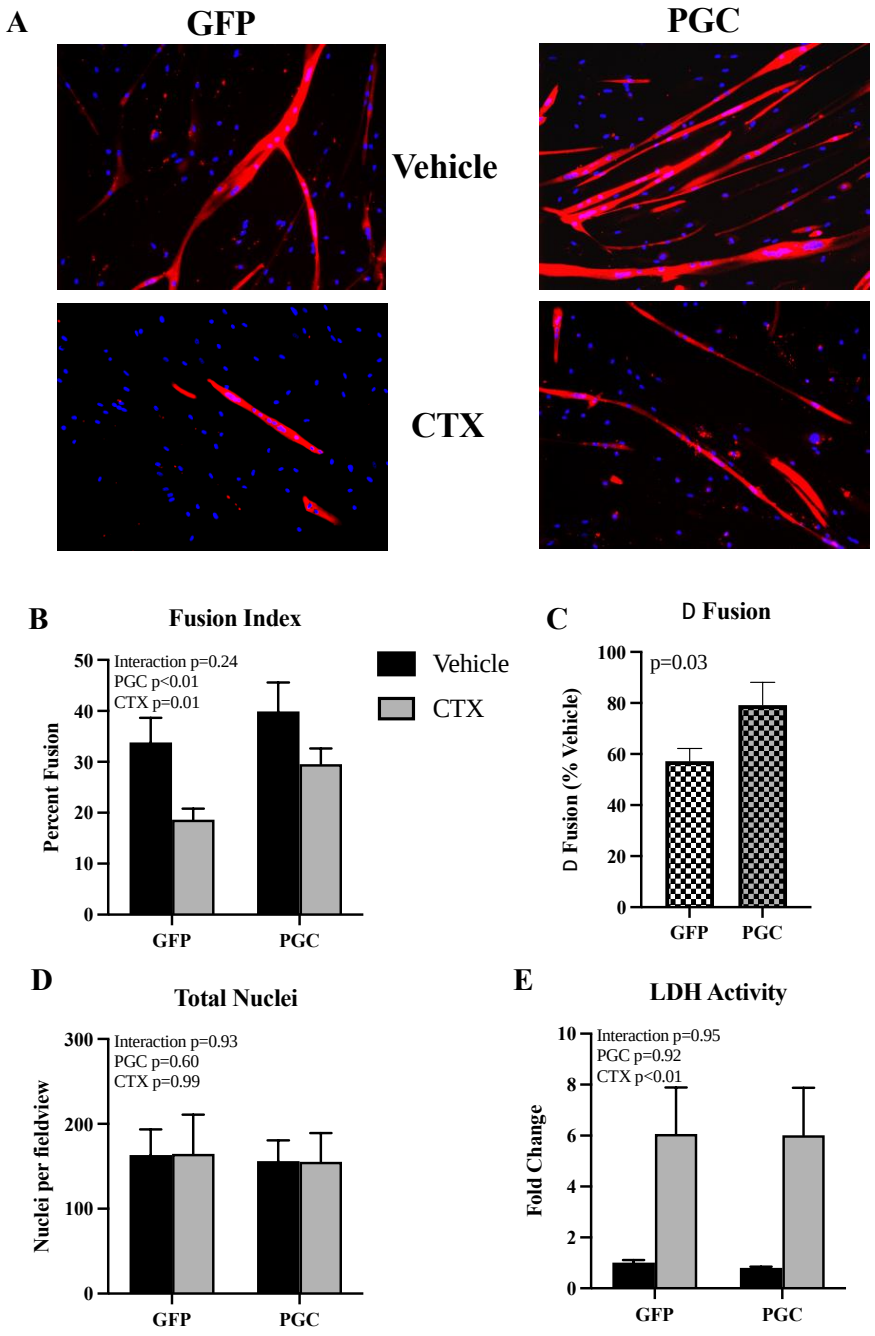

Figure 3.4. PGC-1α overexpression increases and prevents CTX associated reduction in the myotube fusion index. (A) Representative images of primary human myotubes overexpressing GFP or PGC-1α after vehicle or CTX treatment stained for Myosin Heavy Chain (MF20) and nuclei (DAPI). (B) Quantification of myotube fusion, (D) total nuclei/ field view and (E) LDH activity in the cell culture media following CTX or vehicle in myotubes overexpressing PGC-1α or GFP. (C) Quantification of the change in myotube fusion index following CTX in primary human myotubes overexpressing GFP or PGC-1α. Black bars – vehicle; grey bars – CTX. Mean ± SE. n=6/group.

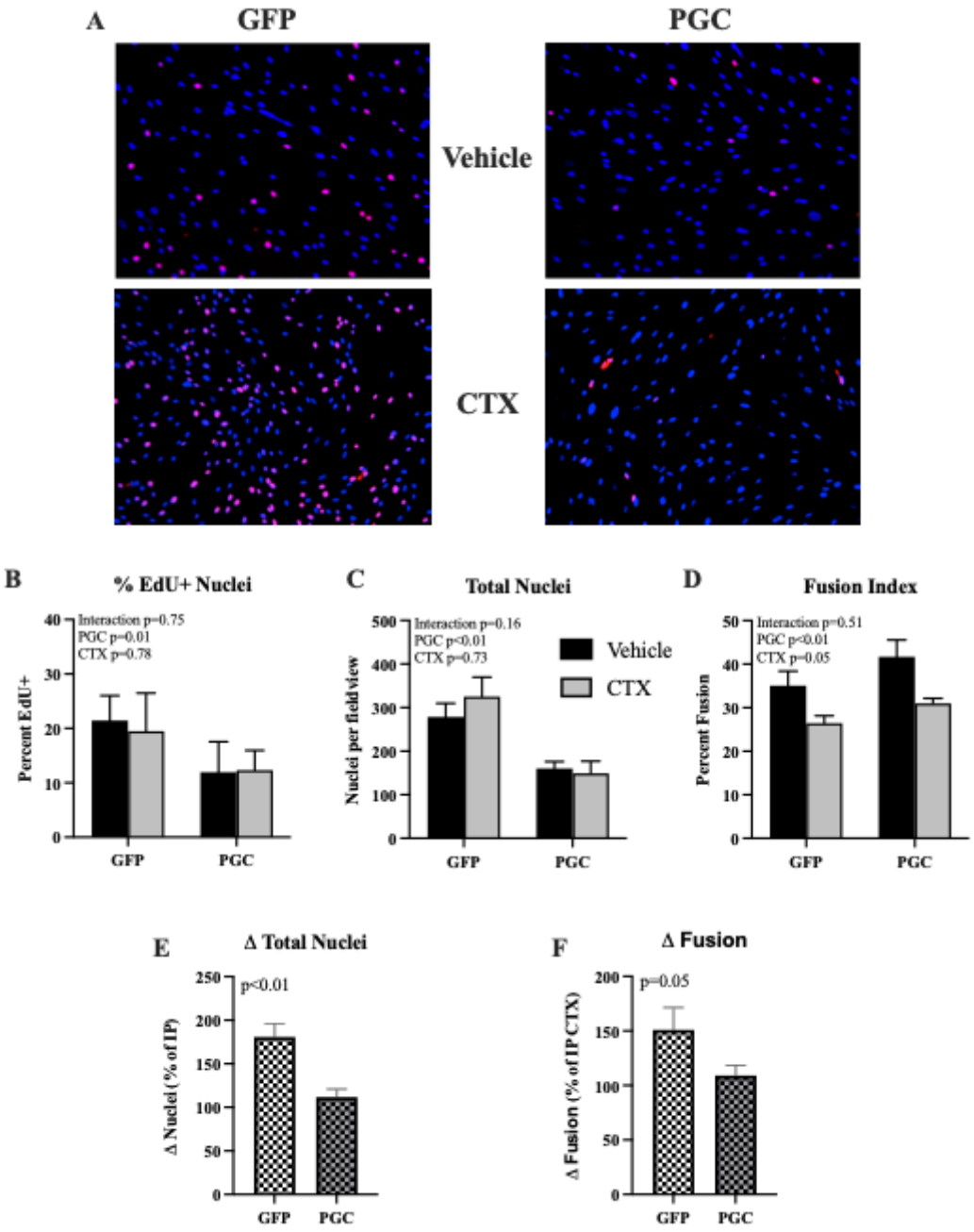

Figure 3.5. PGC-1α overexpression limits the expansion of undifferentiated, reserve myoblasts and myotube fusion during extended culture of primary human myotubes treated with either vehicle or CTX. (A) Representative images of primary human myotubes overexpressing GFP or PGC-1α, grown in skeletal muscle growth media for 3 days after treatment with vehicle or CTX and stained with EdU (red) and DAPI (blue). Quantification of (B) the percent EdU+ nuclei, (C) total nuclei/ filed view and (D) fusion index 3 days following CTX or vehicle treatment of myotubes overexpressing PGC-1α or GFP. Quantification of (E) the change in nuclei from immediately post to 3 days post vehicle or CTX (vehicle and CTX are pooled), and (F) the change in myotube fusion from immediately post to 3 days post CTX. Black bars – vehicle; grey bars – CTX. Mean ± SE. n=6/group.

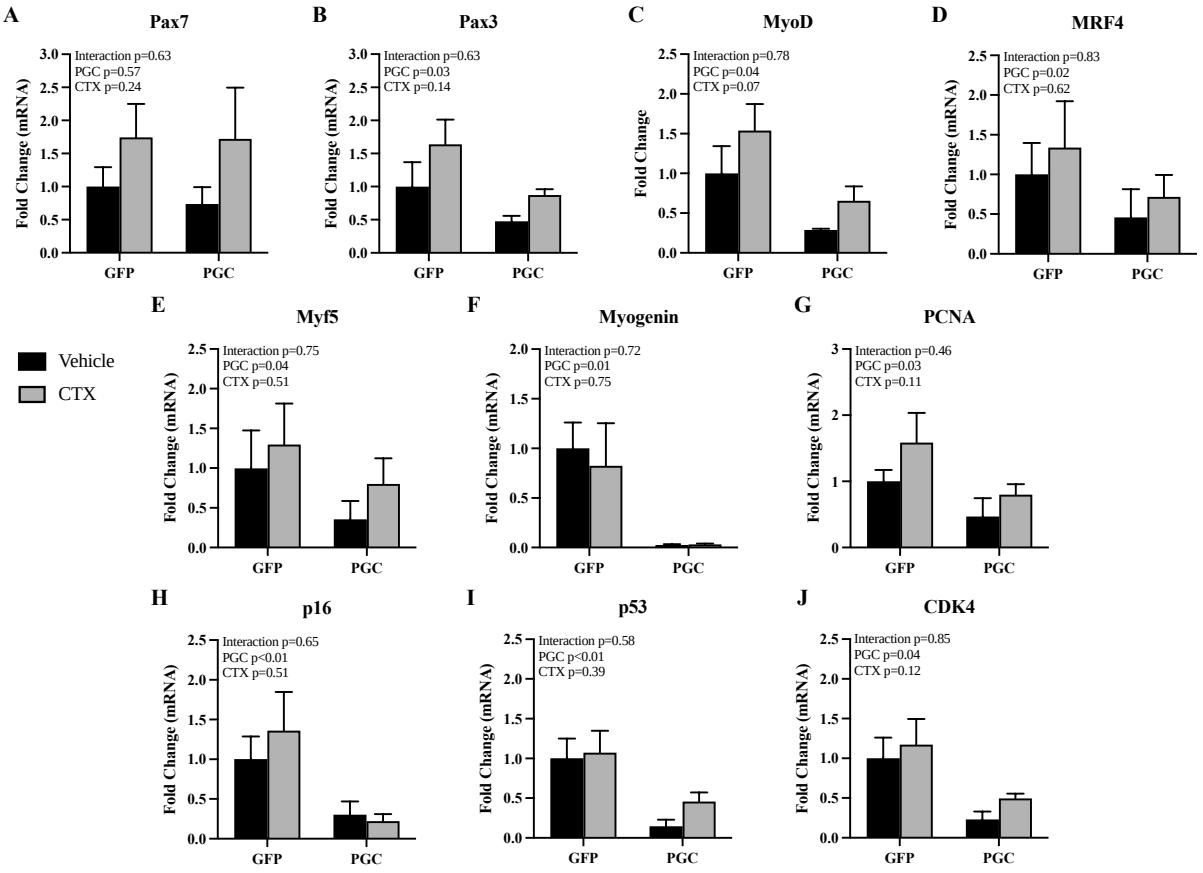

Figure 3.6. PGC-1α overexpression reduces the expression of myogenic regulatory factors and senescent markers 3 days following CTX or vehicle administration. mRNA expression of (A) *Pax7*, (B) *Pax3*, (C) *MyoD*, (D) *MRF4*, (E) *Myf5*, (F) *Myogenin*, (G) *PCNA*, (H) *p16*, (I) *p53* and (J) *CDK4* 3 days following treatment with vehicle (control) or CTX in myotubes overexpressing PGC-1α or GFP controls. Black bars – vehicle; grey bars – CTX. Mean ± SE. n=4-5/group.

CHAPTER 4. IMPACT OF AN OBESOGENIC ENVIRONMENT ON CARDIOTOXIN INDUCED DAMAGE AND REPAIR OF LEAN AND OBESE HUMAN MYOTUBES

Authors: Brian P. Sullivan[1], Allison Ellis[1], Chris K. Kargl[1], Shihuan Kuang[1], Timothy P. Gavin[1]

Affiliations:
[1]Purdue University, West Lafayette, IN

Corresponding Author: Timothy P. Gavin PhD, Department of Health and Kinesiology, Purdue University, 800 W. Stadium Ave., West Lafayette, IN 47907. Phone: (765) 494-3179, Fax: (765) 496-1239, Email: gavin1@purdue.edu

Abstract

Obesity (BMI ≥ 30 kg/m^2) is associated with a reduction in skeletal muscle quality and an impaired myogenic response to muscle damage. Macrophages and adipose tissue infiltrate into skeletal muscle and secrete pro-inflammatory cytokines and lipids that negatively regulate muscle integrity and muscle regeneration. The purpose of the present study is to determine if exposure to an obesogenic environment alters cardiotoxin (CTX) induced damage and repair of primary human myotubes from lean and obese donors. **Methods:** Terminally differentiated, primary human myotubes from lean and obese donors were cultured in obesogenic differentiation media (Ob-DM) (250 μM Palmitate, 250 μM Oleate, 100 nM Insulin and 2.5 ng/ml TNF-α) or control media (BSA-DM) for 48 hr and treated with 1.0 μM CTX or vehicle control (Veh) for 1 h. Cells recovered in obesogenic (Ob-GM) or control growth media (BSA-GM) for 3 days. **Results:** Ob-DM reduced the expression of the glucose transporters *glut1* and *glut4* in both groups by 28% and 21% respectively. Control treated OB myotubes exhibited 22% lower mitochondrial content, a 30% reduction in *PPARα* and a 17% reduction in *Glut1* mRNA. Ob-DM reduced myotube fusion in LN and OB myotubes by about 6%. OB myotubes exposed to Ob-DM incurred greater CTX-induced increase in LDH than all other groups (BSA-DM: LN=4.4 au; OB=6.8 au | Ob-DM: LN=4.1 au; OB=7.5 au). At 3D, Ob-GM limited the increase in myotube fusion index (BSA-GM=135% of immediately post CTX (IP) | Ob-GM= 126% of IP) and total nuclei during recovery from CTX induced injury (BSA-GM=133% of IP | Ob-GM= 116% of IP). OB myotubes exhibit reduced expression of *MyoD,* and *IGF-1* and increased expression of *Myostatin* mRNA 3 days post CTX. Ob-GM reduced mRNA expression of *MyoD*

and *myf5* mRNA 3 days post CTX. **Conclusion:** Exposure to obesogenic media increases CTX-induced damage of primary human myotubes from OB donors and limits increases in nuclei and the reformation of primary human myotubes from LN and OB donors.

Introduction

Skeletal muscle of persons with obesity (BMI ≥ 30 kg/m^2) is associated with morphological and biochemical alterations that result in reduced skeletal muscle quality, dysregulated metabolism and impaired muscle mass maintenance (1-4). The maintenance of skeletal muscle mass in obesity is of vital importance to preserve muscle quality and reduce the risk of sarcopenic obesity. In individuals with obesity, lipids ectopically accumulate in non-adipose tissues, including skeletal muscle. High levels of intermuscular adipose tissue (IMAT) are correlated with macrophage accumulation in skeletal muscle of persons with obesity, promoting reduced insulin sensitivity and chronic inflammation in skeletal muscle (3, 5). IMAT contributes to reductions in skeletal muscle quality in persons with obesity by directly modulating skeletal muscle contractile function (6). Obesity is also associated with an increase in intramyocellular lipids, increasing membrane rigidity and reducing membrane integrity (7, 8).

Intercellular communication is a vital process that regulates the physiological function of neighboring cells. IMAT has a distinct pro-inflammatory secretome, more akin to visceral than subcutaneous adipose tissue, secreting elevated proinflammatory cytokines and lipids (3, 9). Inflammatory macrophages aggregate around IMAT and secrete a plethora of inflammatory molecules (7, 10). Together these secretomes bathe skeletal muscle in an excess of lipids and pro-inflammatory cytokines. Lipid overload and chronic inflammation are associated with the negative regulation of muscle metabolism and impairments in muscle regeneration (11). Following muscle damage the inflammatory response is dysregulated (11-13), and SC proliferation is markedly reduced in obese rodents (14-16). Reductions in SC activity and the dysregulated inflammatory response in individuals with obesity may be due to chronic exposure to elevated inflammatory cytokines and lipids from accumulated macrophages and IMAT.

Currently our understanding of how obesity reduces membrane integrity and alters SC function during muscle regeneration in humans is limited. Studying the mechanisms of skeletal muscle damage and repair in human subjects is challenging, consequently the majority of *in vivo* humans' subjects research induces only moderate amounts of muscle damage and relies on

indirect markers of muscle damage (17). Due to the difficulties associated with effective *in vivo* interventions in humans, the majority of research on muscle damage and regeneration in humans has to be performed *in vitro*. While it appears that many donor metabolic characteristics are retained in primary myotubes, such as impaired lipid oxidation in obesity and diabetes (18, 19), the magnitude of observed *in vivo* impairments are reduced *in vitro,* particularly for normoglycemic, obese individuals (20-22). However, many metabolic perturbations present *in vivo* can be observed *in vitro* by treatment with lipids, insulin or inflammatory cytokines (19, 23, 24). Consequently, we have designed a study that utilizes an obesogenic media, consisting of fatty acids, insulin and tumor necrosis factor alpha (TNF-α), to replicate the *in vivo,* obese environment, with the aim of elucidating how the cellular environment alters cardiotoxin (CTX) induced damage and repair of primary human myotubes from lean (LN) and obese (OB) donors. We hypothesized that myotubes from OB donors, cultured in an obesogenic environment would incur greater damage and display a diminished recovery compared to myotubes from LN donors.

Methods

This study was approved by the Purdue University Institutional Review Board in accordance with the Declaration of Helsinki. Written informed consent was obtained from all subjects prior to their participation in the study.

Isolation of Primary Human Myoblasts. Primary myoblasts were isolated as previously described (25). Briefly, muscle biopsies were performed on the vastus lateralis of seven individuals with (OB) and seven without obesity (LN) using the modified Bergstrom technique. Muscle tissue was minced and digested in dispase II (Sigma-Aldrich) and Collagenase type 2 (Worthington Biochemical Corp.) for 20-30 min at 37°C. Filtered cells were pelleted and resuspended in Skeletal Muscle Growth Media (SkGM) (Cell Applications Inc.) and plated on an uncoated dish for 90 minutes. Unattached cells were transferred to a collagen coated plate and grown to a minimum of 60% confluence in SkGM. Myoblasts were purified by magnetic activated cell sorting (MACS) with CD56+ microbeads (Miltenyi Biotec). The purified myoblasts were cultured in SkGM for use in the below experiments or frozen in liquid nitrogen for future use. All cells used in the below experiments were early passage and matched between groups.

Differentiation and Treatment of Myoblasts. For all experiments, passage 4 myoblasts were seeded on 6 and 24 well plates and grown in SkGM until 80 % confluent. Myoblasts were terminally differentiated in differentiation media (SkDM) (Dulbecco's modified Eagle medium supplemented with 2% horse serum) for 6 Days. On day 6 of differentiation, cells were incubated in obesogenic SkDM (Ob-DM) (250 μM Palmitate, 250 mM Oleate, 100 nM Insulin and 2.5 ng/ml TNF-α) or control SkDM, containing an equivalent amount of bovine serum albumin (BSA), and phosphate buffered saline (PBS) (BSA-DM) for 48 hr. At the conclusion of the 48 hr incubation period, cells were treated with 1μM CTX or an equivalent volume of vehicle (PBS) for 1 hr. Previous *in vitro* studies have used 1μM of CTX for one hour resulting in a robust drop in myotube number and myotube fusion index and an approximate 5-fold increase in lactate dehydrogenase (LDH) activity in the media (26). Our pilot experiments confirmed this while demonstrating that a significant portion of cultured cells maintain their viability. Cells were then washed with PBS 3 times and collected for respective assays. To assess how myotubes reform and regrow after injury, injured myotubes were cultured for an additional 3 days in obesogenic SkGM (Ob-GM) or control SkGM (BSA-DM).

Preparation of Obesogenic and Control Media. Obesogenic media consisted of 250 μM palmitate, 250 μM oleate, 100 nM Insulin and 2.5 ng/ml TNF-α in either SkDM or SkGM. We chose the dosage of 250 μM to replicate hyperlipidemia associated with obesity and included oleate and palmitate at equivalent concentrations to replicate the ratio of saturated fatty acids/unsaturated fatty acids and palmitate/oleate (1:1) typically observed in obesity and type 2 diabetes (23, 27, 28). Oleate and palmitate were conjugated to BSA as previously described (29). First, palmitate or oleate was dissolved in 150 mM NaCl and heated to 70°C or 55°C. Once dissolved, palmitate and oleate were added to a 37°C, BSA solution and stirred for 1 hr. The final solution was diluted to create a final stock solution of 2 mM and pH adjusted with NaOH to 7.4. The final molar ratio of oleate/palmitate to BSA was 3:1 which is close to what is commonly observed in human sera (30). Control conditions contained an equivalent amount of BSA. Insulin was added to the obesogenic media at 100nM to replicate elevated levels in obesity. Chronic exposure to elevated insulin leads to impairments in insulin sensitivity, a common trait of obesity (31). To replicate the chronic inflammation that accompanies obesity (32), we included TNF-α in the obesogenic media at a dose of 2.5 ng/ml. This low dose of TNF-α does not impair differentiation as severely as higher doses (33).

Lactate Dehydrogenase (LDH) Assay. The damage induced by CTX administration was quantified via LDH assay (CyQUANT, ThermoFisher Scientific) according to manufacturer's instructions as previously described (26). The LDH assay quantifies cytotoxicity by measuring the production of red formazan as part of a coupled enzymatic reaction in which LDH catalyzes the conversion of lactate to pyruvate via NAD+ reduction and the oxidation of NADH by diaphorase. Immediately following CTX treatment, 50 µl of media was transferred to a 96 well plate and mixed with 50 µl of the LDH reaction mixture and incubated at room temperature for 30 min. Absorbance was measured at 680 and 490 nm. The 680 nm absorbance was subtracted from the 490 nm absorbance for each well. A fold change was calculated setting the vehicle treated, control myotubes to 1.

Cell Viability. The viability of human myotubes following CTX administration was assessed via a 3-(4,5-dimethylthiazol-2-yl)-2,5-diphenyltetrazolium bromide (MTT) assay as previously described (25, 34). The MTT assay measures cell metabolic activity by measuring the amount of formazan formed from MTT reduction by NADPH oxidoreductases. Following CTX treatment, cells were washed with PBS and fresh media added to each well along with 50 µl of 5 mg/ml MTT reagent to each well and incubated at standard culture conditions (37°C, 5% CO_2) for 2 hr. The media will then be drained, and the purple formazan dye was dissolved in 100 µl of DMSO per well. Absorbance was measured at 550 nm (accuscan; ThermoFisher Scientific).

Myoblast Proliferation and Differentiation following CTX treatment. The proliferation of undifferentiated, reserve cells was quantified by visualizing the incorporation of 5-ethynyl-2'-deoxyuridine (EdU) into actively dividing DNA 3 days following CTX administraton. EdU staining was performed as previously described (35). Briefly, 2 mM EdU was added to the media 12 h prior to completion of treatment. Following completion of treatment, cells were fixed with ice-cold, 4% paraformaldehyde (PFA), washed and incubated in 100 mm Tris-HCl, pH 8.5 (Boston Biosciences, Royal Oak, MI, USA), 1 mm CuSO4 (Acros; ThermoFisher Scientific), 2.5 mm TAMRA Azide 568 (Invitrogen, Carlsbad, CA, USA) and 100 mm ascorbic acid (ThermoFisher Scientific) for 30 min. Prior to imaging, nuclei were co-stained with 4',6-diamidino-2-phenylindole (DAPI) (Invitrogen). Myoblasts were imaged immediately via fluorescence microscopy for co-localization of EdU to DAPI. The percentage of proliferating cells was determined using ImageJ (National Institutes of Health, Bethesda, MD, USA). Proliferation of undifferentiated, reserve cells was also quantified by calculating the change in

total nuclei at 3 days compared to the total number of nuclei immediately post (IP) CTX and expressed as a percent.

To quantify myotube formation, staining for myosin heavy chain (MHC) and DAPI was performed. Briefly, cells were fixed in 4% PFA for 15 min and then permeabilized with 100 mM glycine for 5 min at room temperature. Cells were then incubated in blocking buffer (PBS containing 5% goat serum, 2% bovine serum albumin, 0.2% triton X-100 and 0.1% sodium azide; Cell signaling Technologies) for 1 hr. Myotubes were subsequently incubated with MF20 antibody (DSHB), diluted 1:30 in blocking buffer overnight at 4°C. Cells were washed with PBS and incubated with secondary antibody (AlexaFlour 568, goat anti-mouse, IgG2B, ThermoFisher Scientific) and DAPI at a 1:500 and 1:1000 dilution respectively. Myotubes were visualized by fluorescence microscopy and analyzed in image J. The fusion index (FI) is the total number of nuclei incorporated into multinucleated, MHC^{+} myotubes divided by the total number of nuclei in the field of view and expressed as a percentage. Myotube damage was quantified by calculating the change in the myotube FI index immediately following CTX compared to each subjects Vehicle control for that condition and expressed as a percent. Myotube reformation was quantified by calculating the change in myotube FI index 3 days following CTX as a percent of each subjects IP CTX.

RNA Isolation, Reverse Transcription and qRT-PCR. Total RNA was extracted using a Trizol reagent (Thermo Fisher Scientific) as previously described (36). For mRNA reverse transcription, first strand cDNA was generated by random hexamer primers with MMLV Reverse Transcriptase (Thermo Fisher Scientific). For mature miRNA reverse transcription, multiple adenosine nucleotides were first added to the 3' end of total RNA with *Escherichia coli* Poly (A) polymerase (New England BioLabs, Ipswich, MA, USA), and cDNA will then be synthesized with a Poly T primer including an adaptor sequence using MMLV Reverse Transcriptase. Real-time PCR detection was performed using SYBR green based chemistry on a CFX Connect (BioRad, Hercules, CA, USA). Primers for mRNA and miR are listed in Table 4.1. Gene expression was determined with the $2^{-\Delta\Delta Ct}$ relative quantification method and normalized to 18s. Housekeeping genes were validated to ensure their expression was not be influenced by the experimental procedure.

Statistical Analysis. A two-way, mixed-factorail measures analysis of variance (ANOVA) (Donor BMI vs Obesogenic Media) was used to analyze differences between groups. Following

a significant F ratio, Fisher's LSD post-hoc analysis was performed. Subject characteristics were analyzed with a student's t-test. Significance was established at $P \leq 0.05$ level and data reported as Mean ± SE. All data were analyzed in GraphPad Prism (Version 9.10).

Results

Subjects Characteristics. Demographic characteristics are located in table 4.2. As designed, OB had a significantly greater BMI than LN. OB had higher fasting insulin and consequently presented with higher HOMA-IR. No differences between LN and OB were noted for blood glucose, total cholesterol, high density lipoprotein (HDL), low density lipoprotein (LDL) or triglycerides. All subjects were young (LN- 24.4 ± 2.0 years; OB- 27.1 ± 1.8 years) and age was not different between groups.

Dosing of Cardiotoxin. The dose of CTX administered to differentiated myotubes was selected by assessing metabolic activity via MTT and myotube damage via FI following treatment with various doses of cardiotoxin (Figure 4.1). As expected, metabolic activity and the myotube FI index were reduced in a dose dependent manner with the greatest reduction occurring at the dose of 1.0 μM. Myotube FI returned to baseline in all but the 1.0 μM dose, however the greatest increase in myotube FI occurred in the 1.0 μM group. Similarly, myotube metabolic activity increased after being cultured for 3 further days in SkGM, with the largest increase occurring at the 1.0 μM dose. We aimed to select a dose of CTX that would elicit the most amount of damage while maintaining the greatest cell viability. As shown by our pilot data this approach allowed for the greatest myogenic response. Consequently, we chose to perform all subsequent experiments at a dose of 1 μM.

Impact of obesity and obesogenic media on mitochondrial content and metabolic genes. The expression of select mitochondrial and metabolic genes in primary human myotubes from LN and OB donors following incubation in either control or obesogenic media for 48 hours are located in Figure 4.2. Ob-DM reduced the expression of *Glut1 and Glut* 4 by approximately 30 and 21% respectively compared to control media. Myotubes from OB donors exhibited ~22% reduced mitochondrial content and comparable reductions in the expression of *TFAM, PPARα* and *Glut1* mRNA. No differences in the expression of *SOD2* mRNA were observed.

Obesogenic media reduces myotube fusion and increases the susceptibility of OB myotubes to damage. We assessed myotube damage by measuring myotube FI, the activity of

LDH released into the cell culture media and cell metabolic activity via MTT, as an indicator of cell viability after treatment with either CTX or Veh. Results for myotube FI, LDH activity and MTT with CTX or without CTX (Veh) treatment are located in Figure 3.4. In Veh, Ob-DM reduced myotube FI. In CTX, neither group nor Ob-DM altered the CTX-induced drop in myotube FI. In Veh, there were no differences in LDH activity between groups or media conditions. In CTX, there was a significant interaction effect in LDH activity with a greater CTX-induced increase in LDH activity in OB myotubes cultured in Ob-DM compared to all other group+media conditions. A trend was observed for Ob-GM to reduce myotube metabolic activity in both LN and OB myotubes after treatment with Veh. Following CTX, a significant effect of BMI and obesogenic media were noted, indicating that the CTX induced reduction in MTT was independently exacerbated in OB myotubes and myotubes exposed to an obesogenic environment. No interaction effect was observed for MTT.

Obesogenic media reduces myotube formation during recovery from CTX-induced damage. Following CTX administration, myotubes were cultured in Ob-GM or BSA-GM for 3 days to facilitate myotube reformation. The proliferation of undifferentiated myoblasts was measured by EdU and by the change in total nuclei; cell viability/metabolic activity by MTT and myotube reformation by the change in FI index. Results for myoblast proliferation, cell viability and myotube reformation following CTX administration are located in Figure 3.4. No differences were observed in the percent of EdU+ nuclei 3 days following CTX administration between BSA-DM and Ob-DM or between LN and OB. The total number of nuclei per field view was reduced 3 days following CTX administration in LN and OB myotubes cultured in Ob-GM. Ob-GM lowered the change in nuclei per field view from immediately post to 3 days post CTX (BSA-GM vs Ob-GM: LN=133% vs 116%; OB= 134% vs 115%). LN and OB myotubes cultured in Ob-GM exhibited reduced myotube FI 3 days following CTX, as well as a blunted increase in myotube FI at 3 days compared to immediately post CTX (BSA-GM vs Ob-GM: LN= 135% vs 124%; OB= 137% vs 128%). No effects of BMI were noted at the end of the recovery period.

Obesity and obesogenic media alter anabolic and myogenic gene expression following CTX. Gene expression data 3 days following CTX administration is located in Figure 3.5. Ob-GM reduced the expression of *MRF4* equally in LN and OB myotubes. OB and Ob-GM independently reduced the expression of *MyoD* mRNA. Myotubes from OB donors had

significantly reduced expression of *IGF-1* mRNA expression, but no differences were noted with Ob-GM. *Myostatin* mRNA is increased in OB myotubes, no differences were noted with Ob-GM. No differences in the expression of *Myf5* or *PCNA* mRNA were observed.

Discussion

The principal findings of the present study are that incubation with obesogenic media, (1) increases CTX-induced damage of primary human myotubes from OB donors and (2) limits the reformation of primary human myotubes from LN and OB donors. To our knowledge this is the first report that demonstrates the interaction between genetic factors and the environment in the susceptibility of primary human myotubes from obese donors to damage.

Obesity is associated with reduced membrane integrity and an increased susceptibility to damage (8). In the present study, Ob-DM amplified the release and activity of LDH and reduced metabolic activity assessed by MTT in OB but not LN myotubes, indicative of increased necrosis following CTX. Contrary to this finding, the difference in myotube FI immediately following CTX was similar in LN and OB myotubes.

CTX generates damage in skeletal muscle cells by increasing cytosolic calcium, increasing the formation of reactive oxygen species, cytoskeleton degradation and eventually leading to necrosis (37, 38). Mitochondria regulate cellular oxidative stress (39) and along with the sarcoplasmic reticulum regulate cytosolic calcium levels (40). In the present study, increased CTX-induced damage of OB myotubes cultured in OB-DM may be partially attributed to reductions in mitochondrial content and an increase in the formation of diacylglycerol (DAG). The composition and subcellular localization of DAG and other lipotoxic lipid species such as ceramides in skeletal muscle have severe metabolic and structural consequences. Palmitate administration increases the formation of disaturated 18:0 DAG (41) and total DAG formation, which is increased further following insulin administration (21). Individuals with obesity have increased levels of total muscle DAG, but importantly increased levels of total membrane DAG and membrane disaturated 18:0 DAG are observed, both of which are positively correlated with insulin resistance (42). DAG activates protein kinase C (PKC), increasing the formation of reactive oxygen species (ROS) (43). In addition to DAG, palmitate increases the formation of ceramides, both of these lipid species increase endoplasmic reticulum Ca^{2+} loss (43, 44).

Together, these mechanisms can lead to the exacerbation of damage by reducing Ca2+ handling and increasing ROS.

Of note, our obesogenic media contained an equal concentration of oleate which may have ameliorated some of the deleterious effects of palmitate in LN myotubes (45). It is possible that the 'memory' of obese cells to an obesogenic environment leads to a maladaptive response (46). Further investigation is needed to elucidate this complex topic.

During differentiation, not all myoblasts will differentiate, the undifferentiated myoblasts, often called myogenic reserve cells, will pause during the G0 phase of the cell cycle (46). These reserve cells are Pax7+/MyoD-, and are able to reenter the cell cycle when reintroduced to growth conditions and produce progeny that contribute to the formation of myotubes and the maintenance of the reserve cell population (47, 48). We employed a model that was specifically designed to take advantage of these myogenic reserve cells ability to act in a manner more akin to SCs than myoblasts during differentiation. The presence of Ob-GM impaired reserve cell proliferation and differentiation as highlighted by the reductions in *MRF4* and *MyoD* mRNA and the attenuated increase in FI and nuclei per field view 3 days following CTX administration. Interestingly, the percentage of EdU positive nuclei was not different between BSA-GM and Ob-GM, despite the observed difference in total nuclei. This discrepancy could likely be attributed to the timing of EdU assessment in our study. We assessed EdU 3 days following CTX, therefore the 12 hr incubation with EdU began approximately 60 hr following removal of CTX; this window of time could explain the discrepancy in our findings (49). The proliferative potential of reserve cells in our model is less understood than newly plated myoblasts and this deserves further investigation.

Previously, we observed that the expression of IGF-1 mRNA and protein are reduced in skeletal muscle of individuals with obesity before and after a bout of resistance exercise (4). IGF-1 plays an important role in regulating myoblast proliferation and differentiation. Increases in IGF-1 in myoblasts promotes proliferation and induces the expression of the myogenic regulatory factors and reduces myostatin expression (50). Reduced *IGF-1* mRNA observed in OB myotubes in the present study could contribute to reductions in *MyoD* mRNA and increased *Myostatin* mRNA expression. However, IGF-1 is only lower in OB and not Ob-GM in the present study, thus reduced IGF-1 cannot account for reduction in *MyoD* and *MRF4* mRNA observed with Ob-GM. Increased fatty acids, DAGs and ceramides may reduce myoblast

proliferation and differentiation via PKC activation of myostatin or inhibition of MyoD (11). In the present study we did not measure DAG formation or PKC activity, future studies should address this possible mechanism impairing SC function in obesity. Additionally, we did not measure Ca^{2+} flux induced by incubation with CTX. In the present study we did not confirm that obesogenic media induces hallmarks of metabolic dysfunction associated with obesity, such as insulin resistance or impaired fatty acid oxidation.

In conclusion, obesogenic media increases CTX-induced damage of primary human myotubes from OB donors and limits increases in nuclei and the reformation of primary human myotubes from LN and OB donors. Our findings indicate that the interplay between genetics and the environment regulate the susceptibility to muscle damage. Future work is needed to elucidate the mechanisms that regulate membrane integrity and regeneration in obesity.

References

1. Gavin TP, Stallings HW, 3rd, Zwetsloot KA et al. Lower capillary density but no difference in VEGF expression in obese vs. lean young skeletal muscle in humans. *J Appl Physiol (1985)*. 2005;98(1):315-21.
2. Malenfant P, Joanisse DR, Theriault R, Goodpaster BH, Kelley DE, Simoneau JA. Fat content in individual muscle fibers of lean and obese subjects. *Int J Obes Relat Metab Disord*. 2001;25(9):1316-21.
3. Sachs S, Zarini S, Kahn DE et al. Intermuscular adipose tissue directly modulates skeletal muscle insulin sensitivity in humans. *Am J Physiol Endocrinol Metab*. 2019;316(5):E866-E79.
4. Sullivan BP, Weiss JA, Nie Y et al. Skeletal muscle IGF-1 is lower at rest and after resistance exercise in humans with obesity. *European Journal of Applied Physiology*. 2020.
5. Patsouris D, Cao JJ, Vial G et al. Insulin resistance is associated with MCP1-mediated macrophage accumulation in skeletal muscle in mice and humans. *PLoS One*. 2014;9(10):e110653.
6. Biltz NK, Collins KH, Shen KC, Schwartz K, Harris CA, Meyer GA. Infiltration of intramuscular adipose tissue impairs skeletal muscle contraction. *J Physiol*. 2020;598(13):2669-83.
7. Kahn D, Perreault L, Macias E et al. Subcellular localisation and composition of intramuscular triacylglycerol influence insulin sensitivity in humans. *Diabetologia*. 2021;64(1):168-80.
8. Knoblauch MA, O'Connor DP, Clarke MS. Obese mice incur greater myofiber membrane disruption in response to mechanical load compared with lean mice. *Obesity (Silver Spring)*. 2013;21(1):135-43.
9. Ma J, Yu S, Wang F et al. MicroRNA transcriptomes relate intermuscular adipose tissue to metabolic risk. *Int J Mol Sci*. 2013;14(4):8611-24.
10. Fink LN, Costford SR, Lee YS et al. Pro-inflammatory macrophages increase in skeletal muscle of high fat-fed mice and correlate with metabolic risk markers in humans. *Obesity (Silver Spring)*. 2014;22(3):747-57.

11. Akhmedov D, Berdeaux R. The effects of obesity on skeletal muscle regeneration. *Front Physiol*. 2013;4:371.
12. Brown LA, Lee DE, Patton JF et al. Diet-induced obesity alters anabolic signalling in mice at the onset of skeletal muscle regeneration. *Acta Physiol (Oxf)*. 2015;215(1):46-57.
13. Nguyen MH, Cheng M, Koh TJ. Impaired muscle regeneration in ob/ob and db/db mice. *ScientificWorldJournal*. 2011;11:1525-35.
14. D'Souza DM, Trajcevski KE, Al-Sajee D et al. Diet-induced obesity impairs muscle satellite cell activation and muscle repair through alterations in hepatocyte growth factor signaling. *Physiol Rep*. 2015;3(8).
15. Xu P, Werner JU, Milerski S et al. Diet-Induced Obesity Affects Muscle Regeneration After Murine Blunt Muscle Trauma-A Broad Spectrum Analysis. *Front Physiol*. 2018;9:674.
16. Fu X, Zhu M, Zhang S, Foretz M, Viollet B, Du M. Obesity Impairs Skeletal Muscle Regeneration Through Inhibition of AMPK. *Diabetes*. 2016;65(1):188-200.
17. Nosaka K, Newton M, Sacco P. Delayed-onset muscle soreness does not reflect the magnitude of eccentric exercise-induced muscle damage. *Scand J Med Sci Sports*. 2002;12(6):337-46.
18. Kim JY, Hickner RC, Cortright RL, Dohm GL, Houmard JA. Lipid oxidation is reduced in obese human skeletal muscle. *Am J Physiol Endocrinol Metab*. 2000;279(5):E1039-44.
19. Boyle KE, Zheng D, Anderson EJ, Neufer PD, Houmard JA. Mitochondrial lipid oxidation is impaired in cultured myotubes from obese humans. *Int J Obes (Lond)*. 2012;36(8):1025-31.
20. Aas V, Bakke SS, Feng YZ et al. Are cultured human myotubes far from home? *Cell Tissue Res*. 2013;354(3):671-82.
21. Gaster M, Rustan AC, Aas V, Beck-Nielsen H. Reduced lipid oxidation in skeletal muscle from type 2 diabetic subjects may be of genetic origin: evidence from cultured myotubes. *Diabetes*. 2004;53(3):542-8.
22. Gaster M. Insulin resistance and the mitochondrial link. Lessons from cultured human myotubes. *Biochim Biophys Acta*. 2007;1772(7):755-65.

23. Maples JM, Brault JJ, Shewchuk BM et al. Lipid exposure elicits differential responses in gene expression and DNA methylation in primary human skeletal muscle cells from severely obese women. *Physiol Genomics*. 2015;47(5):139-46.
24. Reyna SM, Ghosh S, Tantiwong P et al. Elevated toll-like receptor 4 expression and signaling in muscle from insulin-resistant subjects. *Diabetes*. 2008;57(10):2595-602.
25. Kargl CK, Nie Y, Evans S et al. Factors secreted from high glucose treated endothelial cells impair expansion and differentiation of human skeletal muscle satellite cells. *J Physiol*. 2019;597(20):5109-24.
26. Langone F, Cannata S, Fuoco C et al. Metformin protects skeletal muscle from cardiotoxin induced degeneration. *PLoS One*. 2014;9(12):e114018.
27. Tran L, Hanavan PD, Campbell LE et al. Prolonged Exposure of Primary Human Muscle Cells to Plasma Fatty Acids Associated with Obese Phenotype Induces Persistent Suppression of Muscle Mitochondrial ATP Synthase beta Subunit. *PLoS One*. 2016;11(8):e0160057.
28. A ISS, C AB, A JS. Changes in Plasma Free Fatty Acids Associated with Type-2 Diabetes. *Nutrients*. 2019;11(9).
29. Pike Winer LS, Wu M. Rapid analysis of glycolytic and oxidative substrate flux of cancer cells in a microplate. *PLoS One*. 2014;9(10):e109916.
30. Spector AA. Fatty acid binding to plasma albumin. *J Lipid Res*. 1975;16(3):165-79.
31. DeFronzo RA, Tripathy D. Skeletal muscle insulin resistance is the primary defect in type 2 diabetes. *Diabetes Care*. 2009;32 Suppl 2:S157-63.
32. Pedersen BK, Febbraio MA. Muscles, exercise and obesity: skeletal muscle as a secretory organ. *Nat Rev Endocrinol*. 2012;8(8):457-65.
33. Zhao Q, Yang ST, Wang JJ et al. TNF alpha inhibits myogenic differentiation of C2C12 cells through NF-kappaB activation and impairment of IGF-1 signaling pathway. *Biochem Biophys Res Commun*. 2015;458(4):790-5.
34. Nie Y, Sato Y, Garner RT et al. Skeletal muscle-derived exosomes regulate endothelial cell functions via reactive oxygen species-activated nuclear factor-kappaB signalling. *Exp Physiol*. 2019;104(8):1262-73.
35. Salic A, Mitchison TJ. A chemical method for fast and sensitive detection of DNA synthesis in vivo. *Proc Natl Acad Sci U S A*. 2008;105(7):2415-20.

36. Nie Y, Sato Y, Wang C, Yue F, Kuang S, Gavin TP. Impaired exercise tolerance, mitochondrial biogenesis, and muscle fiber maintenance in miR-133a-deficient mice. *FASEB J*. 2016;30(11):3745-58.
37. Wang HX, Lau SY, Huang SJ, Kwan CY, Wong TM. Cobra venom cardiotoxin induces perturbations of cytosolic calcium homeostasis and hypercontracture in adult rat ventricular myocytes. *J Mol Cell Cardiol*. 1997;29(10):2759-70.
38. Mendez I, Gutierrez JM, Angulo Y, Calvete JJ, Lomonte B. Comparative study of the cytolytic activity of snake venoms from African spitting cobras (Naja spp., Elapidae) and its neutralization by a polyspecific antivenom. *Toxicon*. 2011;58(6-7):558-64.
39. Ott M, Gogvadze V, Orrenius S, Zhivotovsky B. Mitochondria, oxidative stress and cell death. *Apoptosis*. 2007;12(5):913-22.
40. Rizzuto R, De Stefani D, Raffaello A, Mammucari C. Mitochondria as sensors and regulators of calcium signalling. *Nat Rev Mol Cell Biol*. 2012;13(9):566-78.
41. Macrae K, Stretton C, Lipina C et al. Defining the role of DAG, mitochondrial function, and lipid deposition in palmitate-induced proinflammatory signaling and its counter-modulation by palmitoleate. *Journal of Lipid Research*. 2013;54(9):2366-78.
42. Bergman BC, Hunerdosse DM, Kerege A, Playdon MC, Perreault L. Localisation and composition of skeletal muscle diacylglycerol predicts insulin resistance in humans. *Diabetologia*. 2012;55(4):1140-50.
43. Ly LD, Xu S, Choi S-K et al. Oxidative stress and calcium dysregulation by palmitate in type 2 diabetes. *Experimental & Molecular Medicine*. 2017;49(2):e291-e.
44. Andersson A, Nalsen C, Tengblad S, Vessby B. Fatty acid composition of skeletal muscle reflects dietary fat composition in humans. *Am J Clin Nutr*. 2002;76(6):1222-9.
45. Yuzefovych L, Wilson G, Rachek L. Different effects of oleate vs. palmitate on mitochondrial function, apoptosis, and insulin signaling in L6 skeletal muscle cells: role of oxidative stress. *Am J Physiol Endocrinol Metab*. 2010;299(6):E1096-105.
46. Sharples AP, Stewart CE, Seaborne RA. Does skeletal muscle have an 'epi'-memory? The role of epigenetics in nutritional programming, metabolic disease, aging and exercise. *Aging Cell*. 2016;15(4):603-616. doi:10.1111/acel.12486

47. Yoshida N, Yoshida S, Koishi K, Masuda K, Nabeshima Y. Cell heterogeneity upon myogenic differentiation: down-regulation of MyoD and Myf-5 generates 'reserve cells'. *J Cell Sci*. 1998;111 (Pt 6):769-79.
48. Baroffio A, Hamann M, Bernheim L, Bochaton-Piallat M-L, Gabbiani G, Bader CR. Identification of self-renewing myoblasts in the progeny of single human muscle satellite cells. *Differentiation*. 1996;60(1):47-57.
49. Paasuke R, Eimre M, Piirsoo A et al. Proliferation of Human Primary Myoblasts Is Associated with Altered Energy Metabolism in Dependence on Ageing In Vivo and In Vitro. *Oxid Med Cell Longev*. 2016;2016:8296150.
50. Yu M, Wang H, Xu Y et al. Insulin-like growth factor-1 (IGF-1) promotes myoblast proliferation and skeletal muscle growth of embryonic chickens via the PI3K/Akt signalling pathway. *Cell Biol Int*. 2015;39(8):910-22.

Table 4.1. Primers used for qRT-PCR.

Gene Name	Gene ID	Forward (5'-3')	Reverse (5'-3')
18s	106632259	GGCCCTGTAATTGGAATGAGTC	CCAAGATCCAACTACGAGCTT
SOD2	6648	GCTCCGGTTTTGGGGTATCTG	GCGTTGATGTGAGGTTCCAG
TFAM	7019	ATGGCGTTTCTCCGAAGCAT	TCCGCCCTATAAGCATCTTGA
Glut1	6513	GGCCAAGAGTGTGCTAAAGAA	ACAGCGTTGATGCCAGACAG
Glut4	6517	TGGGCGGCATGATTTCCTC	GCCAGGACATTGTTGACCAG
PPARα	5465	ATGGTGGACACGGAAAGCC	CGATGGATTGCGAAATCTCTTGG
MyoD	4654	CGCCATCCGCTATATCGAGG	CTGTAGTCCATCATGCCGTCG
MRF4	4618	GGAGCGCCATCAGCTATATTG	ATCCGCACCCTCAAGATTTTC
Myf5	4617	CTGCCAGTTCTCACCTTCTGA	AACTCGTCCCCAAATTCACCC
PCNA	5111	CCTGCTGGGATATTAGCTCCA	CAGCGGTAGGTGTCGAAGC
IGF-1	3479	GCTCTTCAGTTCGTGTGTGGA	GCCTCCTTAGATCACAGCTCC
Myostatin	2660	TCCTCAGTAAACTTCGTCTGGA	CTGCTGTCATCCCTCTGGA

Table 4.2. Subject Characteristics. BMI- body mass index. HOMA-IR- homeostasis model assessment for insulin resistance. HDL- high density lipoprotein. LDL- low density lipoprotein. *- Significantly different than lean. Mean ± SE.

Characteristics	Lean (n=7)	Obese (n=7)
Age (yr)	24.4 ± 2	27.1 ± 1.8
BMI (kg/m^2)	22.5 ± 1	*40.6 ± 2
Glucose (mg/dl)	93.7 ± 3.1	92.1 ± 3.9
Insulin (μU/ml)	8.1 ± 0.6	*33.1 ± 7.3
HOMA-IR	1.9 ± 0.1	*7.3 ± 1.6
Total Cholesterol (mg/dl)	165.6 ± 11.7	188.4 ± 14.7
HDL (mg/dl)	44.4 ± 2.6	45.0 ± 4.8
LDL (mg/dl)	101.3 ± 11.2	114.6 ± 15.2
Triglycerides (mg/dl)	100 ± 14.8	144.9 ± 22

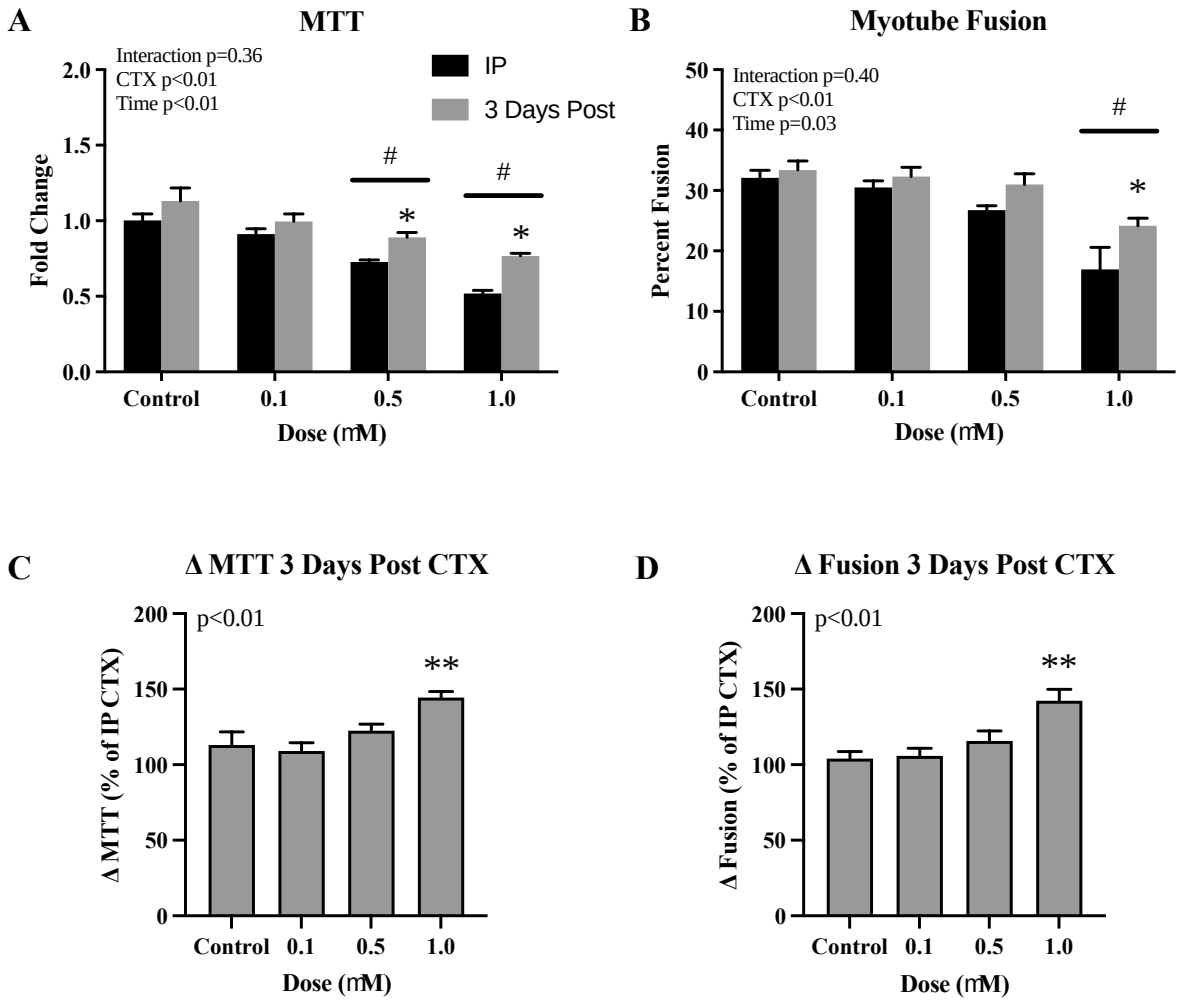

Figure 4.1. Cardiotoxin (CTX) reduces cell viability and myotube fusion in a dose dependent manner. Differentiated primary human myotubes from lean donors were exposed to cardiotoxin at various doses for 1 hr and either harvested immediately or placed in skeletal muscle growth media for 3 days to facilitate myotube recovery. (A) Cell viability measured via MTT assay and (B) myotube fusion immediately and 3 days after exposure to various doses of CTX for 1 hr. The change in (C) cell viability and (D) myotube fusion after 3 days of recovery in skeletal muscle growth media compared to immediately following CTX administration. Graphs A and B: Black bars – Immediately post (IP); grey bars – 3 Days Post. * - Significantly different than own IP ($P \leq 0.05$). # - Significantly different than control ($P \leq 0.05$). ** - Significantly different than all other groups ($P \leq 0.05$). Mean ± SE. n=4 - 7/group.

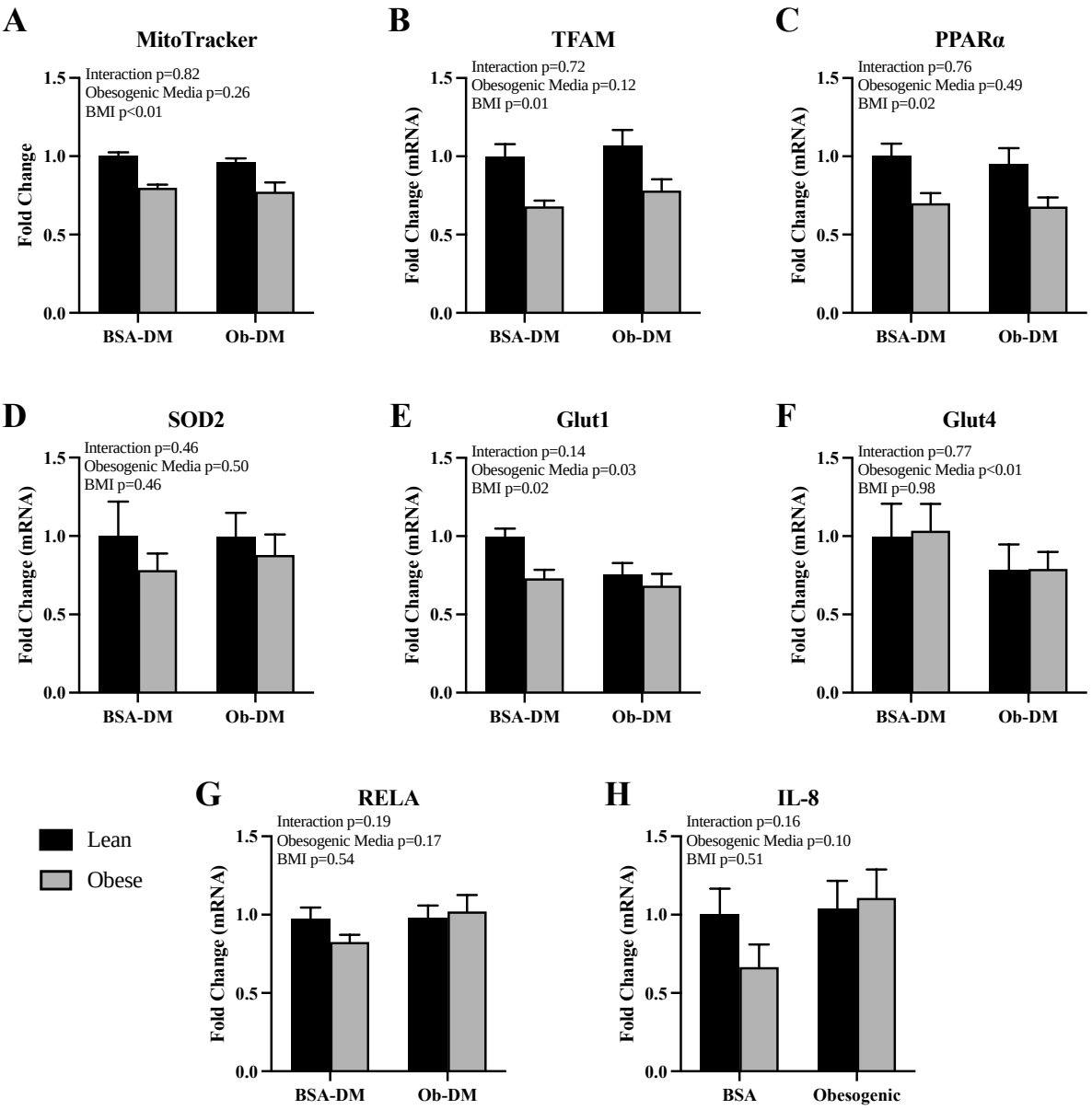

Figure 4.2. Obesogenic media reduces the expression of Glut 1 and Glut4 in primary human myotubes from lean and obese donors. (A) Mitochondrial content assessed fluorometrically via MitoTracker Green FM in primary human myotubes from lean and obese donors cultured in BSA (control) or obesogenic media. mRNA expression of (B) *TFAM*, (C) *PPARα,* (D) *SOD2*, (E) *Glut1*, (F) *Glut4*, (G) RELA and (H) IL-8 in primary human myotubes cultured in BSA (control) or obesogenic media media. Black bars – Lean; grey bars – Obese. Mean ± SE. n=6/group.

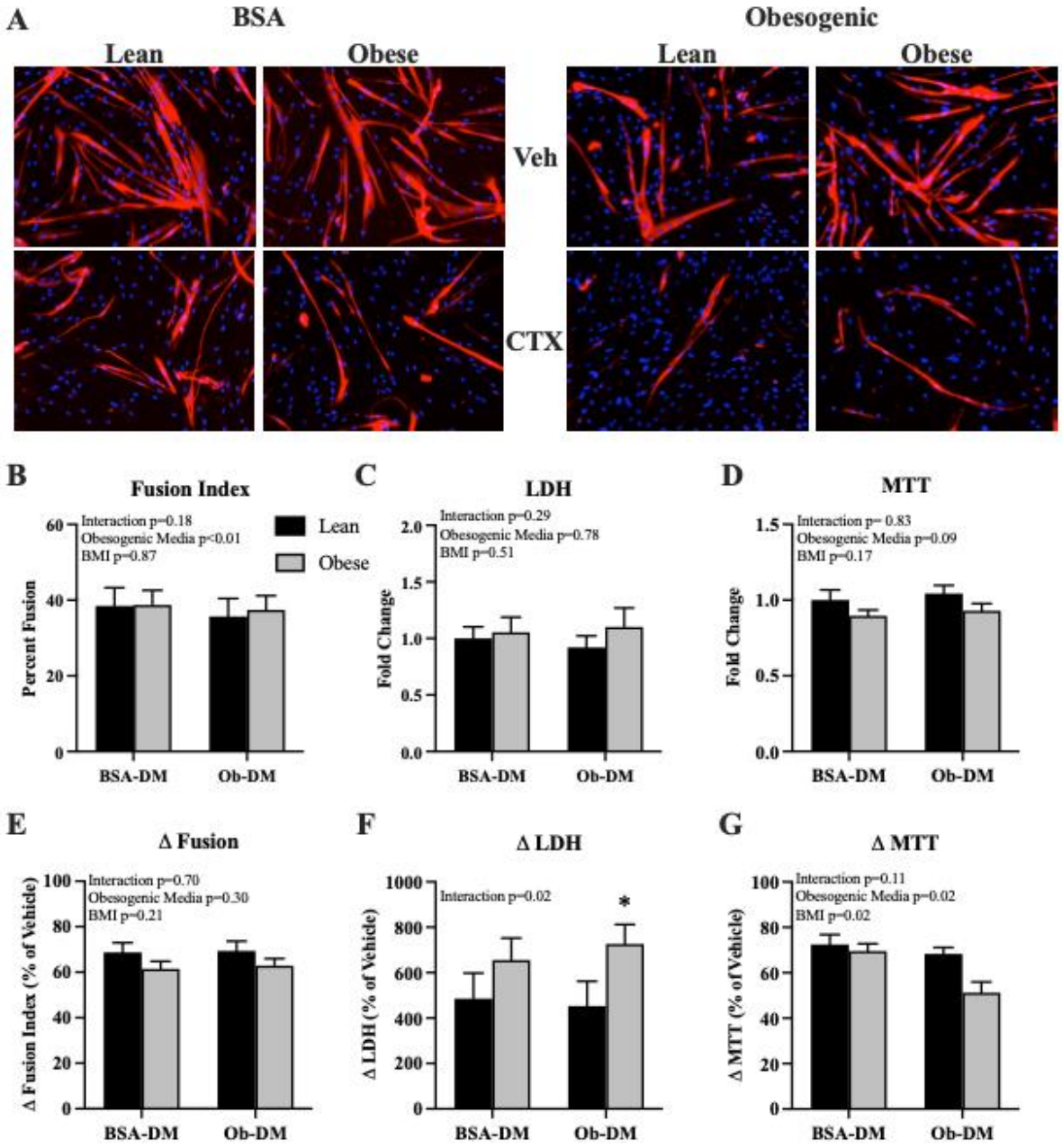

Figure 4.3. Obesogenic media reduces myotube fusion index and increases the extent of CTX-induced damage in myotubes from obese donors. (A) Representative images of lean and obese primary human myotubes cultured in BSA (control) or obesogenic media immediately after treatment with vehicle (control) or CTX and stained for myosin heavy chain (red) and DAPI (blue). (B) Quantification of myotube fusion, (D) media LDH activity, and (F) cell metabolic activity measured via MTT in lean and obese primary human myotubes cultured in BSA (control) or obesogenic media after vehicle treatment. (C) Quantification of the change in myotube fusion, (E) LDH activity, and (G) MTT following CTX administration in lean and obese primary human myotubes cultured in BSA (control or obesogenic media as a percent of vehicle control (Vehicle=100%). *- Significantly different than all other groups/types. Black bars – Lean; grey bars – Obese. Mean ± SE. n=7/group.

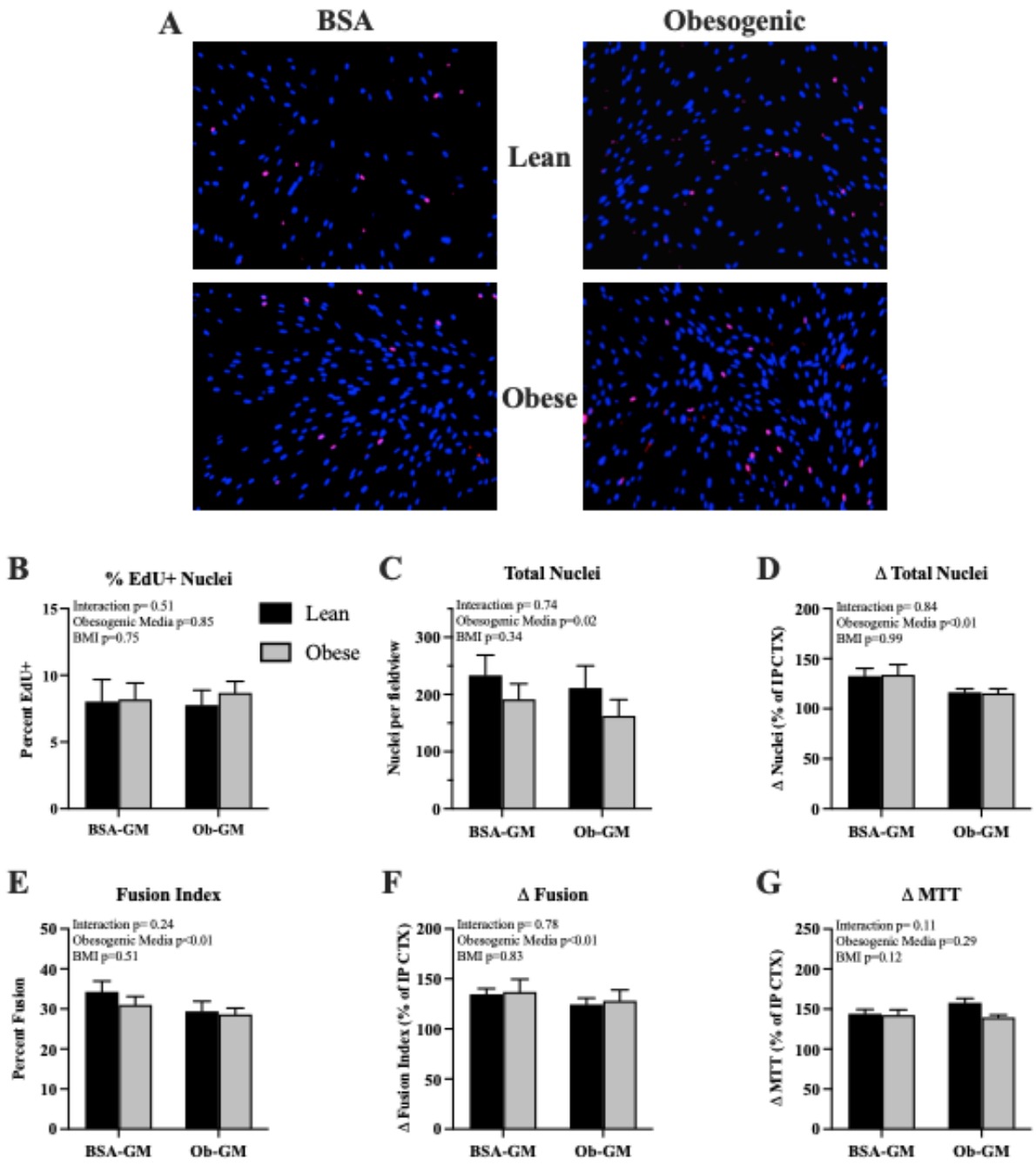

Figure 4.4. Obesogenic media limits the expansion of undifferentiated myoblasts and myotube fusion in lean and obese primary human myotubes during extended culture after CTX. (A) Representative image of lean and obese primary human myotubes incubated in BSA (control) or obesogenic media for 3 days after CTX administration and stained with EdU (red) and DAPI (blue). (B) Quantification of the percent EdU+ nuclei, (C) the total nuclei per field view and (E) the fusion index in lean and obese primary human myotubes incubated in BSA (control) or obesogenic media for 3 days after CTX administration. (D) Quantification of the change in nuclei, (F) myotube fusion index and (G) MTT 3 days following CTX treatment in lean and obese primary human myotubes grown in BSA (control) or obesogenic media. Black bars – Lean; grey bars – Obese. Mean ± SE. n=7/group.

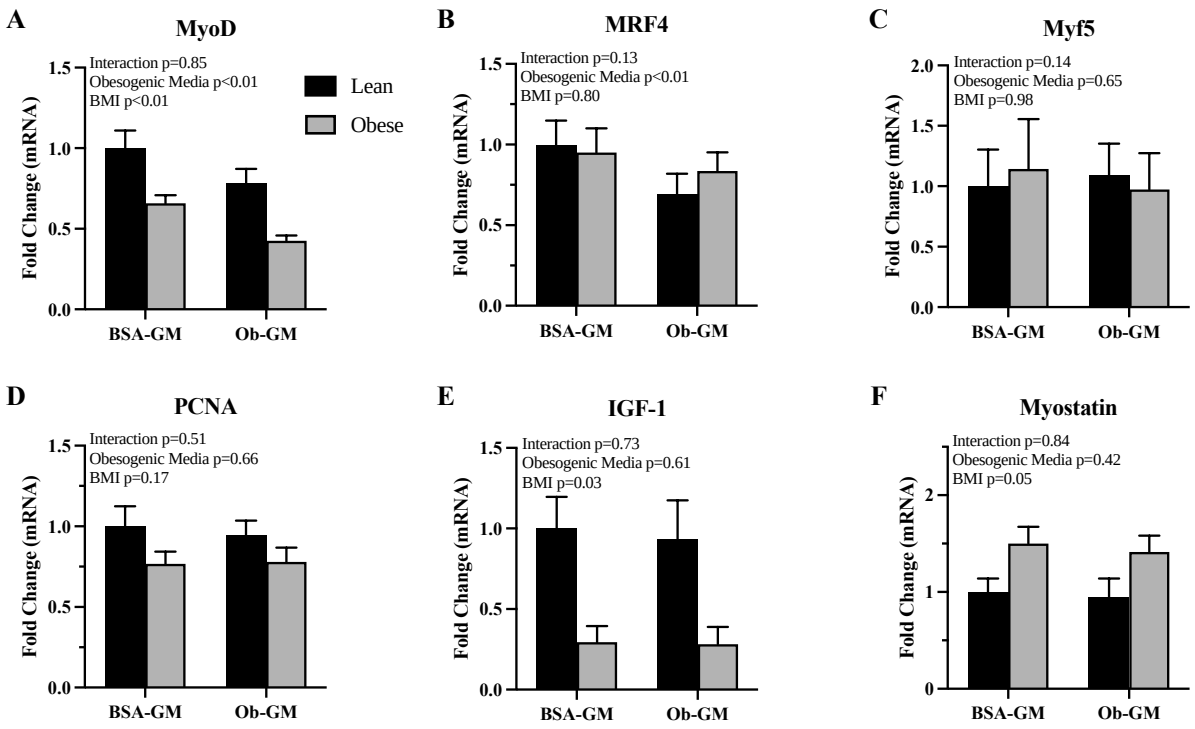

Figure 4.5. Obesity and obesogenic media independently alter the expression of genes associated with myogenesis. mRNA expression of (A) MyoD, (B) MRF4, (C) Myf5, (D) PCNA, (E) IGF-1 and (F) Myostatin in lean and obese primary human myotubes incubated in BSA (control) or obesogenic media for 3 days after CTX administration. Black bars – Lean; grey bars – Obese. Mean ± SE. n=7/group.

CHAPTER 5. CONCLUSION

The major goal of my dissertation studies has been to elucidate the mechanisms that lead to deficits in skeletal muscle integrity and regeneration in persons with obesity. Here we summarize the key findings of these studies and discuss the limitations and future directions.

Summary

Study 1.

Obesity alters the miR content of skeletal muscle EVs targeting the anabolic pathways IGF-1 and Wnt/β-Catenin. Consistent with our previous findings, skeletal muscle *IGF-1* and *Wnt* ligand mRNA were reduced in individuals with obesity. One week of concurrent aerobic and resistance exercise training altered skeletal muscle extracellular vesicle miRNA contents targeting inflammatory pathways IL-6 and IL-10. The alterations in EV content in individuals with and without obesity and before and after exercise training, indicates the importance of skeletal muscle EVs in tissue crosstalk during health and disease.

Study 2.

The overexpression of PGC-1α in primary human myotubes increases myotube fusion and reduces cardiotoxin induced damage. PGC-1α overexpression limits the ability of reserve cells to reenter the cell cycle and produce progeny. PGC-1α overexpression downregulates the gene expression of the myogenic regulatory factors, indicating that this is likely due to an increase in quiescence and not senescence.

Study 3.

Obesogenic media increases cardiotoxin induced damage in myotubes from obese but not lean donors and blunts the ability of undifferentiated myoblasts to proliferate and increase the fusion index after CTX administration. Our findings indicate that environmental and genetic factors interact with one another in the regulation of the susceptibility of muscle to damage.

Limitations and future directions.

Study 1.

Limitations for this study include: the timing of the final biopsy, the small n size of samples utilized for RNA Seq and the lack of control for cell origin in EV collection. The post training muscle biopsy was performed the day after the final training session and began around 12-14 hours after the final bout finished. There is conflicting evidence regarding if this long enough to avoid any acute effects of exercise. We did not control for EV origin in this study but isolated EVs from whole muscle which contains endothelial cells, satellite cells, neural cells, macrophages and pericytes. However, the contribution of EVs of non-muscular origin was likely minimal since approximately 80% of mapped reads were for muscle specific miRNA. Moving forward it would be interesting to explore how altered EV contents from skeletal muscle of individuals with obesity influence satellite cell function. Additionally, it would be very insightful to study the destination of *in vivo* produced skeletal muscle EVs in humans to better understand if these particles are capable of robust endocrine effects.

Study 2.

Limitations for this study include: the lack of direct measurements of senescence, calcium influx induced by cardiotoxin and the lack of characterization of undifferentiated myoblasts as a true Pax7+/MyoD- myogenic reserve cell population. Future directions for this project include examining if EVs secreted from myotubes overexpressing PGC-1α alter myoblast proliferation or differentiation. Research should be performed investigating the mechanism(s) through which PGC-1α reduces the expression of the myogenic regulatory factors.

Study 3.

Limitations for this study include not measuring the formation of DAG or ceramides, intracellular calcium flux after prolonged incubation in obesogenic media or after CTX administration and the lack of confirmation that our obesogenic media induced hall marks of metabolic dysfunction typically observed in individuals with obesity. The

next step for this project should be to explore what mechanisms are responsible for increased necrosis in obese but not lean myotubes cultured in obesogenic media. Additionally, examining the impact of exercise on skeletal muscle